Doctoral Thesis

Study of Electroweak Symmetry Breaking through Higgs and Gauge Boson Couplings

Satendra Kumar

A thesis

submitted for the degree of

Doctor of Philosophy

Supervisor:

Dr. Poulose Poulose

Department of Physics

Indian Institute of Technology Guwahati

Guwahati-781039, India

August 2015

Study of Electroweak Symmetry Breaking through Higgs and Gauge Boson Couplings

Satendra Kumar

A thesis
submitted for the degree of
Doctor of Philosophy

Supervisor:
Dr. Poulose Poulose

Department of Physics
Indian Institute of Technology Guwahati
Guwahati - 781 039, India

January 2015

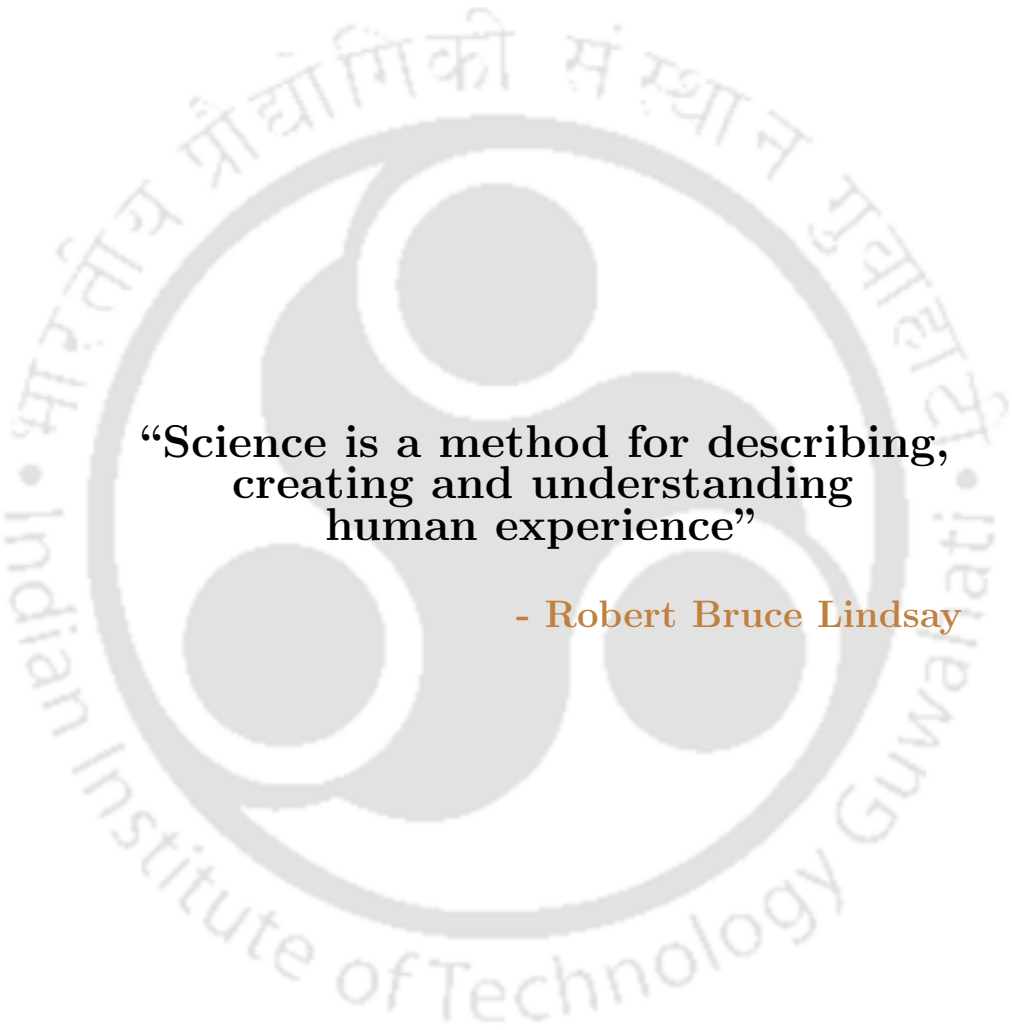

"Science is a method for describing, creating and understanding human experience"

- Robert Bruce Lindsay

Dr. Poulose Poulose
Department of Physics
Indian Institute of Technology Guwahati
Guwahati - 781039, INDIA
Email: poulose@iitg.ac.in

CERTIFICATE

This is to certify that the work contained in the thesis entitled ***"Study of Electroweak Symmetry Breaking through Higgs and Gauge Boson Couplings"*** by **Mr. Satendra Kumar**, a Ph.D student of the Department of Physics, Indian Institute of Technology Guwahati was carried out under my supervision and has not been submitted elsewhere for award of any degree.

The thesis, in my opinion, has reached the standard fulfilling the requirement for the award of degree of **Doctor of Philosophy** in accordance with the regulations of Indian Institute of Technology Guwahati.

Date:

Dr. POULOSE POULOSE
(Associate Professor)

This thesis is dedicated to
my parents,
and
my heavenly maternal grandparents,
who taught me
the merits of discipline
and
the rewards of education,
and
equally dedicated to
my loving heavenly cow "Shyama"

Declaration of Authorship

I, **Satendra Kumar**, declare that this thesis titled, "**Study of Electroweak Symmetry Breaking through Higgs and Gauge Boson Couplings**" and the work presented in it are my own. I confirm that:

- This work was done wholly or mainly while in candidature for a research degree at Indian Institute of Technology Guwahati.
- Where I have consulted the published work of others, this is always clearly attributed.
- Where I have quoted from the work of others, the source is always given. With the exception of such quotations, this thesis is entirely my own work.
- I have acknowledged all main sources of help.
- Where the thesis is based on work done by myself jointly with others, I have made clear exactly what was done by others and what I have contributed myself.

Date: January 23, 2015 **Satendra Kumar**

Acknowledgments

I am strongly indebted to my research supervisor Dr. Poulose Poulose for his guidance and constant support throughout my research work. He has motivated me to take this work as a challenge and without his help, it would have not been possible. I would like to thank him wholeheartedly for all the support, assistance, valuable suggestions and the opportunities to develop my character as well as research skill. I feel blessed to have him as my supervisor. My doctoral committee members: Dr. Bipul Bhuyan, Prof. G. S. Setlur and Dr. K. V. Krishna also deserve special thanks for their frank comments and encouragements.

I am very thankful to the former Head Prof. S. Ravi, and present Head Prof. Saurabh Basu, of Department of Physics for supplying the full support and facilities at their best. I extend my hearty thanks to all the faculty members and staff of the Department of Physics, who supported me in several ways during my research period, especially for their friendly behaviour. I am thankful to IIT Guwahati for providing me financial assistance during the research period. Apart from this, I extend my sincere thanks to Mr. Basab Purkayastha and Mr. Hemant Medhi for helping me to solve the computer related problems on many occasions.

I am thankful to my friends: Vipin Kumar, Indrajeet, Pathi Munendhar, Enamullah, Tikamani Beg, Suresh Babu, Anil Kumar, Shanu Shukla, Krishna Murari Awasthi, Mr. & Mrs. Sampat Mishra and all well wishers, and research fellows: Shibananda Sahoo, Subhasish Behera, Biswaranjan Das, Deepanwita Dutta, Deepanjali Goswami, Biswajit Karmakar for making pleasant atmosphere and their assistance time to time. My sincere thanks are also extends to my hostel mates: Kiran Kumar, Mukesh Singh, Rohit Tripathi, Rohit Singh, Mrityunjay Singh,

Manish Kamal, and seniors: Dr. Meera V, Mr. Himanshu Shekhar Jha, Dr. Aneesh, Dr. Jahir and many more colleagues for making my experience somewhat more intellectual and mostly for their understanding and co-operative behaviour. Really, I am fortunate to have such friends and juniors.

I express my gratitude towards the organizers of the workshops and schools which I participated during this period and has been very useful to me. Especially I would like to thank to the organizers of THINK TANK ON PHYSICS@LHC-2011, which really opened a new window to my research.

Really, my hearty thankful goes to the search engine GOOGLE, the libraries: arXiv, iNSPIRE-HEP and the owners and the developers of technical softwares: FORM, MATHEMATICA, CUBA, GNUPLOT, MADGRAPH. Undoubtedly, without all these things, the research work would not be possible to carry out within time window.

I am extremely indebted to my teachers: Mr. Mohan Lal Singh (faculty of physics), Mr. Kuldeep Singh (faculty of mathematics), Dr. O. P. Singh (faculty of mathematics) and Dr. Shripal Sharma (faculty of physics) for creating an interest in physics and as well as in mathematics, and their way of teaching which inspired me towards higher education. Without them I would not be able to qualify any of the national level tests and reach this position. I can never forget the strength and motivation I received from them during my graduation and post graduation times, which inspired me to achieve this goal. I always remain thankful to them. Apart from this, I am also very thankful to them, for their politeness, kindness and moral support. Also, I would like to express my hearty gratitude to all known and unknown people who inspired me somewhat in some directions.

I am not sure how would I thank my parents: Smt. Vimla Devi and Shri Shravan Kumar, without whom this PhD thesis would not have been possible. I am thankful for the support and care they have extended from the time I started my life. The depth of each of the words they have said to me whenever I was in need and the inspiration I got from it is unforgettable. I am also thankful to my

sweetheart Ms. Jyoti Pal and loving younger brothers: Bhupendra Kumar, Gyanendra Kumar, Shailendra Kumar, Abhinendra Kumar and all my well wishers for their constant love, support, unending patience with me during this crazy time, which inspiring me not only to pursue my PhD but also to dedicate myself and my works in the development of basic science and extra activities throughout the rest of my life. Really, I am fortunate enough to have them. I am wholeheartedly thankful to my supervisor's wife Mrs. Stavelin and their cute and sweet children Hasvid and Onella, especially for their moral support and time adjustment during busy days. Undoubtedly, I have stolen a lot of time from my supervisor's family timings, even from holidays.

Finally and foremost, I thank God for giving me the good times which I enjoyed and the bad times from which I learned many things. I remain thankful for the mental strength given to face the adverse situations.

Date: January 23, 2015 **Satendra Kumar**

Abstract

Recent discovery of a scalar resonance of mass about 126 GeV by the LHC has partially answered questions related to the origin of masses of elementary particles. It is now established that the necessary electroweak symmetry breaking (EWSB) is brought through the Higgs mechanism. Although most of the expected SM decay modes are observed by LHC, details of the couplings are yet to be established. Keeping in mind the issues related to the Standard Higgs mechanism, like the hierarchy problem, make one believe that the standard Higgs mechanism for EWSB could at the best be a method effective at the electroweak scale, which would require further explanation of the details through more fundamental models. In the light of present observation, which indicates a Higgs boson with properties compatible with that of the Standard Higgs boson, one may argue that the non-standard effects are sub-leading at the electroweak scale. Such effects are best probed through an effective Lagrangian framework, in which all the new physics effects are coded in effective interaction couplings of the standard model particles. We take this approach to understand the mechanism of EWSB. Apart from the Higgs self-couplings and Higgs couplings with the gauge bosons, the gauge boson self-couplings are also relevant in EWSB, as their longitudinal degrees of freedom arises from the scalar sector, which is responsible for the EWSB. In this work, we focus our attention on (i) the anomalous gauge couplings and (ii) anomalous Higgs couplings, and explore their effect in the phenomenology at the proposed International Linear Collider (ILC). The ILC is expected to be best suited for detailed precision studies, like the one being considered in this work, compared to a hadronic machine like LHC. Broadly, we have divided the entire thesis work into three projects.

In the first project, we investigate the effect of anomalous $WW\gamma$ couplings in the $e\gamma \to \nu W$ at an ILC. This process has the advantage that it is sensitive

only to the $WW\gamma$ triple gauge boson couplings, as against other processes like $e^+e^- \to WW$, which is sensitive to WWZ as well as $WW\gamma$. Our study is done within the narrow-width approximation, assuming that the W is produced on-shell, which is valid for center of mass energies of 500 GeV and above, considered here. Analyzing the decay of the W, a semi-analytical study of the secondary lepton energy-angle double distribution is considered. Utility of observables derived from this is demonstrated by considering the anomalous couplings, $\delta\kappa_\gamma$ and λ_γ. Results of our investigation for typical ILC machine considered at $\sqrt{s} = 500-1000$ GeV re-affirms potential of this collider as a precision machine. Our results show that the limits on the anomalous couplings can be improved by an order of magnitude compared to the LEP results, for moderate luminosity at ILC. Further, the dependence of $\delta\kappa_\gamma$ on the measurement of λ_γ and vice versa, are studied.

As mentioned earlier, the recent discovery of a Higgs boson at LHC, while establishing the Higgs mechanism as the way of electroweak symmetry breaking, started an era of precision measurements involving the Higgs boson. Precise knowledge of the trilinear and quartic self-couplings of the Higgs boson is an important input necessary to understand the mechanism of EWSB. In an effective Lagrangian framework, we consider the $e^+e^- \to Zhh$ process, at an ILC running at a center of mass energy of 800 GeV. This process is celebrated as the main way to obtain information on hhh coupling. We investigate the effect of the ZZh and $ZZhh$ couplings on the sensitivity of hhh coupling in this process. Our results show that the sensitivity of the trilinear Higgs self couplings on this process has somewhat strong dependence on the Higgs-gauge boson couplings. Single and two parameter reach of ILC with integrated luminosity of 1000 fb^{-1} are obtained on the effective couplings, $\bar{c}_6$ and $\bar{c}_H$, which are related to the hhh couplings. Further, it is shown how these limits are affected by the presence of anomalous ZZh and $ZZhh$ couplings. The kinematic distributions studied to understand the effect of the anomalous couplings, again, show strong influence of Z-h couplings on the dependence of these distributions on hhh coupling. Similar results are indicated in the case of the process, $e^+e^- \to \nu_e\bar{\nu}_e hh$, considered at a center of mass energy of 2 TeV, where the cross section is large enough. The effect of WWh and $WWhh$ couplings on the sensitivity of hhh coupling is clearly established through our analyses of this process.

In the third project, we extended the above study to understand the CP-violating parameters entering in the different couplings involved. Single and two

parameter reach of ILC with integrated luminosity of 300 fb^{-1} are obtained on the effective couplings, $\bar{c}_W$, $\bar{c}_B$, $\bar{c}_{HB}$, $\bar{c}_{HW}$ and $\tilde{c}_\gamma$, $\tilde{c}_{HB}$ and $\tilde{c}_{HW}$, which are related to the CP-conserving and CP-violating couplings, respectively. Here, we consider the $e^+e^- \to W^-\ W^+\ h$ process at an ILC running at a center of mass energy of 500 GeV to investigate the effect of the Higgs to gauge bosons couplings of this process. We have also made use of the kinematic distributions to understand the effect of the anomalous couplings on this process. Our study has established the strong correlation between different parameters, CP-conserving as well as CP-violating.

Precise knowledge of the Higgs self-couplings and Higgs couplings with gauge bosons, as well as the gauge boson self interactions are necessary to understand the mechanism of EWSB. In the thesis work, summarized above, we considered a study of processes which are suitable to measure the relevant couplings precisely. In case of the first project we have considered a process which is sensitive to only $WW\gamma$ coupling, which could therefore give more precise information regarding this coupling. In the latter two projects, we focused our attention on the hhh coupling and Higgs to gauge boson couplings. Our analysis has studied the correlation between different couplings affecting the process. We conclude that a precise knowledge knowledge of Higgs-gauge boson couplings is necessary to make precise measurement of the Higgs self-couplings.

Contents

List of Figures

List of Tables

Preface

This thesis describes my research activities carried out during the course of my PhD studies. I have a general interest in the phenomenology of both the Standard Model (SM) and physics Beyond the Standard Model (BSM). My research has been focused on Electroweak Symmetry Breaking (EWSB) through Higgs and gauge boson couplings. Discovery of the mechanism of EWSB used in nature is essential because it allows us to understand the origin of the masses of fundamental particles via Higgs mechanism. Since, with the recent discovery of Higgs boson of mass about 126 GeV by the ATLAS and the CMS collaborations at the Large Hadron Collider (LHC), the particle content of the standard model has been completed. So it is time to understand the interactions of Higgs to gauge bosons as well as with itself very precisely. In a perspective of precision Higgs physics, we devote this thesis to an effective Lagrangian approach to the Higgs phenomenology. We analyze the Higgs effective Lagrangian and give an estimate of the contribution of the dimension-six operators to the physical observables, putting in evidence that can give some information about the nature of the EWSB dynamics and the physics at the TeV scale. Moreover, we provide a collider analysis of the double Higgs production in the process $e^-e^+ \to Zhh$. Next we analyze the effect of CP-violating Higgs to gauge boson couplings in the Higgs sector through the process $e^-e^+ \to W^-W^+h$. Apart from this, we analyze the effect of anomalous $WW\gamma$ coupling through $W\nu$ production in the $e\gamma$ collisions in a model independent way within narrow width approximation.

This thesis is organized in five chapters as discussed below:

Chapter1 provides an introduction and motivation of my thesis work and a brief introduction of the standard model as well as its drawbacks. Thereafter, I discuss the standard mechanism of electroweak symmetry breaking in detail. Also it presents how the elementary particles (fermions and bosons) acquire their masses

through this mechanism. Further, it includes all the possible interaction vertices in the standard model. Next it concentrates on the framework of effective Lagrangian of anomalous gauge boson couplings as well as Higgs to gauge boson couplings, and provides constraints on various coupling parameters from different experiments. Finally, it moves to the present status of Higgs physics. Apart from this, we present a very brief introduction of the International Linear Collider (ILC).

Chapter2 focuses on the study of anomalous $WW\gamma$ coupling in electron-photon collisions at the ILC, where we start with detailed calculation of phase space of the process $e^-\gamma \to \nu_e W^- \to \nu_e \bar{\nu}_\mu \mu^-$. We carry out our study in a model independent framework and examine experimental observable quantities. We calculate their dependence on anomalous coupling parameters $\delta\kappa_\gamma$ and λ_γ, which are directly connected to the $WW\gamma$ coupling. We show that suitable combinations of the kinematic distributions can be used to disentangle different scenarios of $\delta\kappa_\gamma$ and λ_γ.

Chapter3 is devoted to the study of trilinear Higgs self couplings in the Zhh production as well as $\nu_e\bar{\nu}_e hh$ at ILC. It provides how the determination of Higgs self-couplings are influenced by the presence of Higgs to gauge boson couplings. This chapter presents the results of our study, carried out through single and two parameter analyses of hhh coupling parameters, and kinematic distributions at center of mass energy of 800 GeV along with an integrated luminosity of 1000 fb^{-1}. Main parameters related to other couplings influencing the process are studied.

Chapter4 begins with the brief discussion of CP-violating couplings in the Higgs sector. The WWh production at ILC will be considered for our study. We present the sensitivity of CP-violating coupling parameters through single and two parameter analyses. Apart from the total cross section against center of mass energy, we present various kinematic distributions like transverse momentum, angular, invariant mass distributions. Also we illustrate how the effect of CP-violating couplings can be extracted, and the influence of the presence of CP-conserving couplings on this is investigated.

Chapter5 provides the over all summary and conclusions of the thesis work.

Origin and Development of Particle Physics

A great Hindu sage and philosopher, Kashyapa (also called "Kanada"), is credited with having propounded the concept of an atom for the first time. According to legend, Kashyapa lived in the 6^{th} century B.C. near Dwaraka in Gujarat, India. It was Kanada who believed that the "Kana" ("parmanu", atom) was an indestructible particle of matter. According to him the material universe is made up of "Kana". When matter is divided and subdivided, we reach a stage beyond which no division is possible, the non divisible element of matter is Parmanu. Kanada explained that this indivisible, indestructibility cannot be sensed through any human organ. [source: en.wikipedia.org/wiki/kanada]

In the 5^{th} century B.C., Greek philosopher Democritus, introduced the idea that matter consisted of an infinite number of small, indivisible particles. He called these particles "atoms", which meant "unable to be divided".

The idea of the atom as indivisible persisted for centuries, until 1897, when J. J. Thomson discovered that the "cathode rays" emitted from hot filaments of wire were actually negatively charged particles with an extremely large charge-to-mass ratio. In fact, particles with the same charge-to-mass ratio were ejected from different atoms, leading Thomson to hypothesize these particles were of a single type. Today, we know this subatomic particle as the electron. Since atoms as a whole were known to be electrically neutral, the discovery of negatively charged components to the atom implied there must also be positively charged components to compensate. Since the negatively charged particles are so light, the positively charged component must carry most of the atom's mass.

Early in the 20^{th} century, Ernest Rutherford performed a scattering experiment where a beam of α-particles (ionized helium atoms) were fired at a thin

sheet of gold foil. Some of these α-particles scattered at large angles while most went through the foil without scattering at all. From this, Rutherford concluded that the positive charge and mass of an atom were concentrated at the atom's center and occupied very little of the atom's total volume – a nucleus. He named the nucleus of hydrogen, the lightest element, the proton, and in 1914 Niels Bohr proposed a hydrogen model, which consisted of a single electron orbiting this proton. However, the next heaviest atom, helium, weighed four times the mass of the hydrogen atom although it contains only two electrons and thus can have only two protons for the charge to balance. This mystery was solved in 1932, when Chadwick discovered the neutron, a heavy electrically neutral particle which also resides inside the nucleus.

Around the same time, other phenomena led to revolutions in the theory of light. Isaac Newton assumed light was a corpuscular object, but 19^{th} century physics had shown instead the wave-like nature of light. In 1900, Max Planck found a mathematical model for the black body radiation spectrum emitted by a hot object. He could only explain this spectrum by assuming that the radiation emitted by a black body was quantized, meaning the energy was always an integer multiple of some quantity. In 1905, Albert Einstein proposed the much more radical idea that this quantization was a property of light itself, returning to the classification of light as a particle. This particle, the quanta of light, is called the photon. The quantization of light led to an entirely new description of electromagnetism; classical electrodynamics described the interaction between two electrons, for example, as a consequence of the electric field around each electron. But in a quantum field theory, that interaction is a consequence of the exchange of particles, the field quanta, which is photons in the case of electromagnetic interactions. This realization paved the way for future descriptions of the subatomic world. One milestone of this description was its use by P. A. M. Dirac in 1930 to predict the existence of anti-matter, an opposite-charge counterpart to every matter particle. His theory was verified less than two years later when Anderson discovered a positively charged twin to the electron, dubbed the positron, in his study of cosmic rays. The simple view of the world as composed entirely of protons, neutrons, and electrons did not last long. In the $1930s$, there was no answer to the question of what held the positively charged protons in the nucleus together, gravity being too weak to overcome the electric repulsion. Initially, this force was simply called the "strong force." In 1934, Yukawa attempted to explain this strong force as a field between the proton and neutron in the nucleus; this field

must also be properly quantized, and Yukawa calculated the mass of this quanta to be about one-sixth the mass of the proton. In 1937, two independent groups studying the interactions of cosmic rays discovered a particle matching Yukawa's description. However, more detailed analysis of cosmic ray data showed this particle (later identified as the muon, a heavy version of the electron) interacted only very weakly with atomic nuclei. In 1947, another heavier particle (the pion) was discovered in the cosmic rays, and this proved to be the true Yukawa particle.

Also in the early 1930s, another puzzle presented itself in the form of nuclear beta decay. In beta decay, the radioactive nucleus transforms into a slightly lighter nucleus by emission of an electron. This seemed to be a straight-forward two-body decay; as such, the energies of the outgoing particles are kinematically determined in the center-of-mass frame. However, the energy spectrum of electrons in beta decay was found to be continuous, with the predicted energy serving as the upper limit to the spectrum. At first this anomaly appeared to be a non-conservation of energy. Wolfgang Pauli, however, postulated that the seeming two-body decay was really a three-body decay, and the third particle was a massless, electrically neutral, virtually undetectable new particle. This suggestion worked so well that it was generally accepted, even though the first neutrino, as this particle came to be called, was not experimentally observed until the mid-1950s.

As the study of cosmic rays continued, and were soon joined by the studies of particles produced by man-made nuclear reactors and particle accelerators, more and more new particles were discovered. By the 1960s, more than a hundred different particles had been identified, although some were later shown to be spurious. This proliferation led many physicists to wonder – could all of these particles truly be fundamental? In 1961, Murray Gell-Mann managed to organize many of these particles into geometrical patterns by their properties, similar to Mendeleev's ordering of chemical elements. Gell-Mann's patterns predicted one particle with specific properties which had not yet been observed, and in 1964, this missing particle (Ω^-) was indeed discovered. Starting from these patterns, Gell-Mann and Zweig were able to describe many of these particles as composed of more fundamental building blocks known as "quarks." Particles made of quarks were referred to as hadrons. There are two types of hadrons: mesons, which contain one quark and one anti–quark, and baryons, which contain three quarks or three anti–quarks. Gell-Mann and Zweig required three quarks to explain all the known hadrons. A fourth quark was predicted as early as 1964 to explain some

experimental observations, and a meson made of this fourth quark was finally seen in 1974. Since that time, two more quarks have also been discovered, the last one i.e. top quark found recently in 1995. On the other hand, the electron and the muon, along with neutrinos, are not made of quarks, but are fundamental particles called leptons. There is another lepton, called the tau, which was discovered in 1975. Experiments have shown that there are separate neutrinos corresponding to electrons, muons, and taus. These particles, and the forces that govern their interactions, make up the Standard Model of particle physics, which we use today to understand the dynamics of elementary particles.

High Energy Physics in the 21st Century

Particle physicists study the fundamental building blocks of matter, seeking to understand their origins and interactions. These particles exist on the smallest scales of time and length, making them impossible to "see" with any traditional microscope. Instead, we use high energy colliders as our microscopes for the sub-atomic world. In a collider, particles such as electrons or protons are accelerated to near the speed of light, and then made to collided with each other. The energy we give these particles by accelerating them, using Einstein's famous relation of $E^2 = m^2c^4 + p^2c^2$, allows us to probe their interactions at shorter distance scales; the higher the energy, the shorter the distance scale we can probe with these particle microscopes. Thus, this field of physics is known as high energy physics.

The Large Hadron Collider (LHC) is currently the world's highest energy hadron collider. It accelerates protons to 3 to 4 TeV and collides them to create a shower of particles. The electronvolt (eV) is a unit of energy commonly used in particle physics, and is equivalent to approximately 1.602×10^{-19} $Joules$. The particle collisions occur in the center of large detector complex which measure the properties of the particles created in the collisions. The data collected by these detectors is then used by physicists to reconstruct the collisions and understand the dynamics.

By studying particle collisions at higher and higher energies, physicists continue to test how particles interact and gain a better understanding of particle interactions at higher energies. The main attention of today's particle physics is to understand the new physics beyond the Standard Model.

Gauge Theories and Particle Interactions

The gauge theory is a special class of quantum field theory that introduces an invariance principle used to describe the interactions among all the fundamental constituents of matter. The interactions between the fundamental particles are dictated by symmetry principles, which are intimately connected with the ideas of conserved physical quantities. The connection between symmetries and conservation laws is described in the framework of Lagrangian field theory. The gauge symmetry of a physical system is realized through the invariance of the Lagrangian under gauge transformations, which are characterized by Lie group. Global-invariance (phase invariance) under gauge transformation leads to a conserved charge. The local gauge invariance (space-time dependence of parameter of the system) of the Lagrangian introduces a vector field, called gauge field, which governs the interaction. The quanta of the gauge fields are the gauge bosons, which mediate the particle interactions.

The Standard Model of Particle Physics

The Standard Model of particle physics is the most successful theory so far, it is based on quantum field theory of group $SU(3)_C \times SU(2)_L \times U(1)_Y$. This model summarizes the current knowledge in particle physics and describes the universe in terms of elementary particles and their interactions. In this model, all the matter and its interactions are characterized by three kinds of elementary particles: quarks, leptons, and the force mediators. The quarks and leptons are fermions having spin values, $S = \frac{\hbar}{2}$. These fermions interact with each other by exchange of the force mediators, which are called "gauge bosons" having spin values $S = \hbar$. All charge leptons carry one electronic charge, and are arranged in three families which are called electron (e), muon (μ) and tau (τ). The muons (μ) and taus (τ) are heavier versions of the electron (e), they have the same spin and electric charge as electron. Apart from these, there are neutral leptons so called neutrinos, and there is one associated with each lepton family. In the Model, lepton flavor is conserved by all interactions. The leptons are assigned a lepton number of $+1$, while the anti-matter leptons have a lepton number of -1. Recent observations have shown that neutrinos can oscillate from one lepton flavor to another. So far this is the only observed violation of lepton number conservation. The quarks also comes in six different flavors: up (u), down (d), charm (c), strange (s), top (t) and bottom (b) and have fractional charges $Q = +\frac{2}{3}, -\frac{1}{3}, +\frac{2}{3}, -\frac{1}{3}, +\frac{2}{3}$ and $-\frac{1}{3}$ respectively. The gauge fields in the SM describe the three interactions: the electromagnetic interaction, the strong interaction and the weak interaction. The

electromagnetic interaction is mediated by the photon (γ), the weak interaction is mediated by the weak vector bosons $W^{\pm}$ and Z^0 and strong interaction is mediated by the eight gluons (g_i). The gravitational interaction is supposed to be mediated by the graviton (spin 2 particle), still living away from the SM. This gravitational interaction is very weak compared to interactions at the energy scale being explored.

The fermions and the gauge bosons acquire masses via Higgs mechanism through spontaneous breaking of electroweak symmetry, $SU(3)_C \times SU(2)_L \times U(1)_Y \rightarrow SU(3)_C \times U(1)_{EM}$. In addition to providing the masses to the fermions and the $W^{\pm}$ and Z^0 gauge bosons, the Higgs mechanism predicts an additional electrically neutral scalar particle, called Higgs boson. A Higgs like state has recently been discovered at the LHC and its mass is measured to be about 126 GeV.

Furthermore, the idea of unification came into light in the 18^{th} century. It was believed that the electricity and the magnetism are two different physical entities. In 1861s, the Scottish physicist and mathematician James Clerk Maxwell came with his beautiful equations to describe how electric and magnetic fields are generated and altered by each other (by charges and currents). Later on these equations famous by his name as "Maxwell Equations". Today, we have a branch of physics as "Electromagnetism". It was a first step towards the unification. The next unification was carried out in the Standard Model by Sheldon Glashow's discovery in 1960 of a way to combine the electromagnetic and weak interactions.

Gauge theory of Electromagnetic Interaction

The electromagnetic interaction of particles is described by the Quantum ElectroDynamics (QED), where the global invariance of $U(1)$ in the QED introduces the conservation of the electric charge (Q) and the local gauge invariance of the gauge theory provides rise to the gauge field corresponding to a massless gauge boson, so called photon. This photon describes the interaction among all the fundamental electrically charged particles and also known as a quanta of electromagnetic interaction. The strength of the interaction between photon and the electrically charged matter constituents is characterized by coupling constant (α). At low energy, this constant is given by the fine structure constant , $\alpha = \frac{e^2}{4\pi\hbar c} = \frac{1}{137}$. Due to the abelian nature of the $U(1)$ symmetry group, photon do not exhibit charge and consequently does not interact with itself. The range of electromagnetic interaction is infinite.

Gauge theory of Electroweak Interaction

The unified description of electromagnetic and weak interaction was carried out in the Standard Model by Sheldon Glashow's discovery in 1960 of a way to combine the electromagnetic and weak interactions as electroweak interaction. Mathematically, it is described by gauge theory of the group $SU(2)_L \times U(1)_Y$, where the gauge field B_μ corresponds to the generator Y (also called weak hypercharge) of $U(1)_Y$ symmetry group and the three field $W^k_\mu, k = 1, 2, 3$ which corresponds to the generators $T_a(also\ called\ weak - isospin), a = 1, 2, 3$ of the $SU(2)_L$ group. Furthermore the fermions appear as left-handed doublet and right-handed singlets under the $SU(2)_L$, where the global gauge invariance leads to the conservation of the weak-isospin, T_a and the local gauge invariance of the Lagrangian of the system produces a weak-isospin triplet of the gauge fields, W^k_μ. The $SU(2)_L$ symmetry group is a non-abelian group which leads to the self-interactions of the gauge fields, where the global gauge invariance under the $U(1)_Y$ transformation leads to the conservation of weak hypercharge, Y and the local gauge invariance of $U(1)_Y$ exhibits a vector gauge field, B_μ. The weak-hypercharge, Y, third component of weak-isospin, T_3, and electric charge, Q are related by the Gell-Mann-Nishijima relation:

$$Q = T_3 + \frac{Y}{2} \tag{1}$$

These generators (T_a) of weak-isospin are in fact equivalent to the half of the non-commuting 2×2 Pauli matrices (σ_k) with the following commutation relations between these generators.

$$[T_a, T_b] = i f_{abc} T_c \tag{2}$$

where f_{abc} is anti-symmetric Levi-Civita tensor.

Gauge theory of Strong Interaction

The strong interaction in SM, described by Quantum ChromoDynamics (QCD) which is basically a group theory of $SU(3)_C$, where C refers to color and the digit of three represents the three possible color state of the quarks, namely red, green and blue. The color symmetry is exact so the QCD calculations are independent of the color of the quarks. In this theory the local invariance of the QCD Lagrangian introduces eight types the gluonic fields. These eight gluonic fields lead to the quanta of strong interaction, so called "gluon". QCD is a non-abelian theory, where the gluons carry both color and anti–color, in contrast to the photon in QED which does not carry the electric charge. Gluons interact with

each other directly and as strongly as they do with quarks. Due to this gluon-gluon interaction, the strong force increases with distance resulting in confinement of quarks. This means, the quarks do not exist freely in nature, but bind together by the strong force and form the mesons ($q\bar{q}$), which are composition of one quark and anti-quark, and the baryons (qqq), which are composition of three quarks such a way that the state remains colorless.

Sources: Introduction to Particle Physics by David J. Griffith, Wiley; Quraks & Leptons: An Introduction Course in Modern Particle Physics, by Francis Halzen and Alan D. Martin; An Introduction to Quantum Field Theory by Michael E. Peskin, Daniel V. Schroeder, Westview Press Inc; Modern Elementary Particle Physics by Gordan Kane, Perseus Publishing.

Chapter 1

Introduction

Particle physics is devoted to understand the universe in terms of elementary particles (constituents of matter and radiation) and their interactions. The framework of quantum field theory of the symmetry group $SU(3)_C \times SU(2)_L \times U(1)_Y$, where C, L and Y stand for "color", "left-handed" and "hypercharge", respectively, constructed by Sheldon Glashow, Steven Weinberg and Abdus Salam, describes the dynamics of known elementary particles as well as their interactions, and summarizes the current knowledge of particle physics. This description is known as the Standard Model (SM) [1, 2] of particle physics. $SU(3)_C$ corresponds to strong interaction, whereas $SU(2)_L \times U(1)_Y$ corresponds to the electroweak interactions. In the SM, all the elementary particles acquire their masses through the electroweak symmetry breaking (EWSB) [3, 4] via Higgs mechanism [5–7]. The particle content (see Fig.1.1) of this model has been completed with the recent discovery of the Higgs boson of mass of about 126 GeV by the ATLAS and the CMS collaborations at Large Hadron Collider (LHC) [8, 9]. So far, all the expected SM decays of the Higgs boson are observed at LHC. Similarly, mass of the Higgs boson and its spin-parity state [10–17] are also determined to be consistent with the SM Higgs boson. But still questions like "Are there more than one Higgs bosons ?" and "What is the exact nature of Higgs potential ?" need to be addressed. Albeit the SM has a great story of success and is widely accepted as the framework of contemporary high-energy physics, it suffers from several problems like hierarchy problem associated with the Higgs sector, absence of dark matter candidate, explanation for neutrino mass and matter-anti-matter asymmetry of the universe.

Many remedies for the above short-comings are proposed through several extensions of the SM, like the Two-Higgs Doublet Model (2HDM) [18–21], Minimal Supersymmetric Standard Model (MSSM) [22–24] and Next-to-Minimal Supersymmetric Standard Model (NMSSM) [25, 26] and Grand Unified Theory [27–31]. On the other hand, no direct evidence of the existence of new particles or other signatures of new physics has been observed so far. With this state of affairs, a practical way to investigate new physics could be a description based on an effective Lagrangian [32, 33] valid up to energy scale Λ lying around the TeV scale. In such a model-independent approach, the effective Lagrangian encodes new physics effects in deviations of the couplings of different particles in the SM. The mechanism of EWSB has seen renewed interest with recent discovery of the Higgs boson. Certainly it represents an important step forward in the exploration of the mechanism responsible for the EWSB. The properties of the Higgs boson, like its mass, spin and parity, couplings with other SM particles, self-couplings, etc. are important to establish the exact nature of EWSB mechanism. The associated couplings of gauge bosons are capable of throwing light on the EWSB. This arises from the fact that the longitudinal components of the gauge boson are basically the degrees of freedom of the Higgs gauge field. The study of trilinear gauge boson couplings (TGC) would, therefore, eventually tell us what the nature of Higgs potential and the mechanism of EWSB is. Further, precise knowledge of Higgs boson self couplings is very important and essential to establish the scalar potential responsible for the EWSB. Considering that the observation made by the LHC experiments is in remarkable agreement with the SM prediction, although within the current limited experimental precision, it is reasonable to assume that the Higgs is a CP-even scalar that forms an $SU(2)_L$ doublet together with the longitudinal polarizations of the W and Z, so that the $SU(2)_L \times U(1)_Y$ electroweak (EW) symmetry is linearly realized at high energies. Under these assumptions the effective Lagrangian can be expanded into a sum of operators with increasing dimensionality, where the leading new physics effects are given by dimension-six operators. The parametrization of the deviations of the Higgs couplings in terms of higher-dimensional operators started more than two decades ago. From a more detailed inspection of the effective Lagrangian, one can see that some operators are explicitly sensitive to the coupling strength of the new dynamics, and not simply on the energy scale of new physics. Hence, measuring the coefficient of the effective operators can shed light on the dynamics that controls the mechanism behind EWSB. In a perspective of precision Higgs physics, we devote this thesis to

the Higgs phenomenology through an effective Lagrangian approach, performed in the context of an International Linear Collider (ILC) [34–36]. Through suitably chose processes involving Higgs production associated with the gauge bosons, we investigate the Higgs effective Lagrangian and give an estimate of the sensitivity of the dimension-6 operators to the physical observables. In particular we shall focus on effective parameters affecting the Higgs self-couplings, Higgs boson couplings with the gauge bosons [37] as well as gauge boson self couplings. Undoubtedly photon collider options of ILC, like the $e\gamma$ and $\gamma\gamma$ collisions [38, 39] are well suited to the study of photon couplings with the other gauge bosons like γWW, $\gamma\gamma WW$, γZZ and $\gamma\gamma Z$ [40–44]. In the first work we shall take up a study of the process $e^-\gamma \to \nu_e W^-$. This process is sensitive to γWW coupling, anomalous nature of which will be probed through various suitably chosen observables. In the second work we consider the interplay of Higgs self-coupling and Higgs-gauge boson couplings [45]. For this we selected $e^-e^+ \to Zhh$ and $e^-e^+ \to \nu_e\bar{\nu}_e hh$ processes. The first process is sensitive to Zhh and $ZZhh$ couplings, while the second one is sensitive to WWh and $WWhh$, apart from hhh coupling [46, 47]. The main interest here is to understand how the Higgs-gauge boson couplings affect the measurement of hhh couplings, one of the essential information necessary to establish the Higgs potential. In the third work, we will deal with $e^-e^+ \to W^-W^+h$, which is sensitive to WWh, $WW\gamma$, WWZ and ZZh. Here we try to understand the interplay of the various couplings including their correlations obtained from various observables. We have included the possibility of CP-violation, and tried to understand the extend to which the relevant couplings can be probed.

In the next section, we will explain the standard mechanism of electroweak symmetry breaking.

1.1 The Standard Higgs Mechanism

All the fundamental particles in the SM acquire their masses through the Higgs mechanism of electroweak symmetry breaking, which was introduced by three independent groups: by Robert Brout and François Englert [7]; by Peter Higgs [5, 6]; and by Gerald Guralnik, C. R. Hagen, and Tom Kibble [48]. After the experimental confirmation of scalar particle by the ATLAS and the CMS collaborations [8, 9, 49–52] at the LHC, Peter Higgs and François Englert were awarded the 2013 Nobel Prize in Physics for the theoretical development of the mechanism.

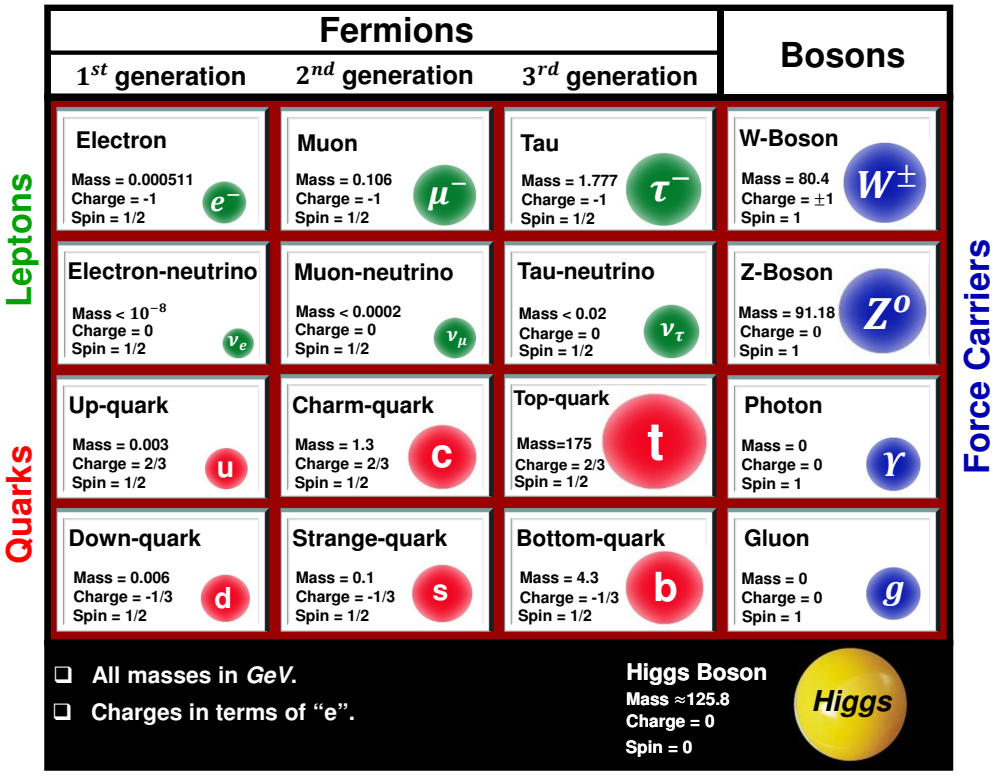

FIGURE 1.1: Chart showing the particle content of the standard model.

In the following we shall briefly describe how the Higgs mechanism is employed to generate masses for elementary particles.

In the SM, we need to generate masses for the three gauge bosons, two of them charged gauge bosons $W^{\pm}$ and third one is electrically neutral Z boson. But at the same time photon should remains massless, so that QED must stay an exact symmetry. Therefore, we need at least three degrees of freedom for the scalar fields. The simplest choice must be a complex $SU(2)_L$ doublet of scalar field Φ.

$$\Phi = \begin{pmatrix} \phi^+ \\ \phi^0 \end{pmatrix} \qquad \text{with hypercharge} \quad Y_\Phi = +1 \tag{1.1}$$

In the Standard Model, the part of the Lagrangian involving the scalar field relevant to the present discussion is given by

$$\mathcal{L}_{Scalar} = (D^\mu \Phi)^\dagger (D_\mu \Phi) - \mu^2 |\Phi^\dagger \Phi| - \lambda |\Phi^\dagger \Phi|^2, \tag{1.2}$$

where the covariant derivative

$$D_\mu = \partial_\mu + ig\frac{\tau^k}{2}W_\mu^k + ig'\frac{Y}{2}B_\mu$$

with W_μ^k $(k = 1, 2, 3)$ denoting the three massless $SU(2)_L$ gauge bosons, B_μ the massless $U(1)_Y$ gauge boson while g and g' are the respective gauge coupling constant. For a choice of $\mu^2 < 0$ and $\lambda > 0$, the minimum energy configuration of Φ, obtained by minimizing the potential, is given by $|\Phi^\dagger\Phi| = -\frac{\mu^2}{2\lambda} \equiv \frac{v^2}{2}$ (see Fig.1.2). The scalar field thus develops a non-vanishing vacuum expectation value (VEV), which is degenerate. A single value of the VEV can be chosen, which is essentially a choice of a preferred "direction" in the Higgs-doublet space. The VEV should be chosen so that it preserves $U(1)_{QED}$. The usual choice is

$$\Phi(x) = \frac{1}{\sqrt{2}}\begin{bmatrix} 0 \\ v + h(x) \end{bmatrix}, \tag{1.3}$$

where $h(x)$ is a physical scalar field. The choice of this new ground state "spon-

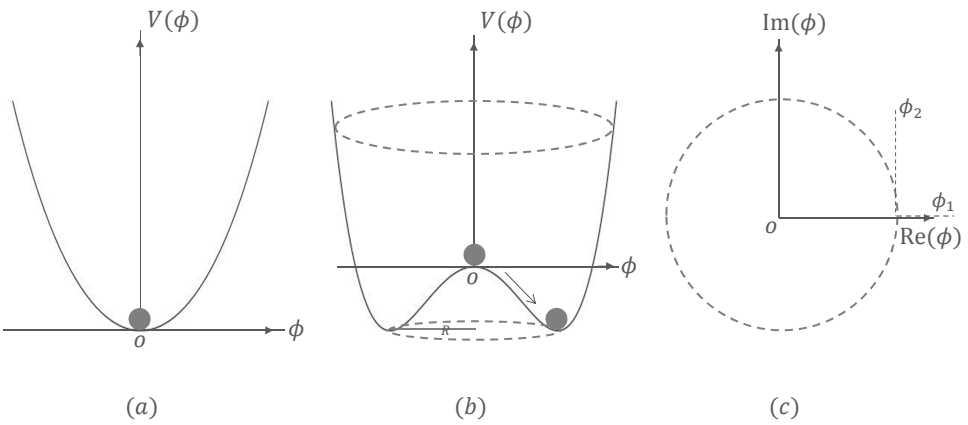

FIGURE 1.2: An illustration of the Higgs potential (Eq. 1.2) : (a) case of $\mu^2 > 0$, while (b) case of $\mu^2 < 0$, the minimum is at $|\Phi|^2 = -\frac{\mu^2}{2\lambda}$, where figure (c) shows the top view of figure (b).

taneously" breaks the $SU(2)_L \times U(1)_Y$ symmetries to $U(1)_{QED}$, while maintaining the renormalizability and unitarity of the theory. As the $U(1)_Y$ gauge symmetry remains unbroken in this transformation, the associated gauge boson, the photon, remains massless. However, three of the degrees of freedom of the scalar doublet (corresponding to the would be Goldstone bosons) are "eaten by" or transformed into the longitudinal polarization components of the weak-isospin triplet of $W^\mp$

and Z^0 bosons, giving them masses of $m_W = \frac{vg}{2}$ and $m_{Z^0} = \frac{v}{2}\sqrt{g^2+g'^2}$, respectively [53]. The mass eigenstates are expressed in terms of the gauge eigenstates as bellow:

$$W_\mu^\pm = \frac{1}{\sqrt{2}}(W_\mu^1 \mp iW_\mu^2)$$
$$Z_\mu^0 = W_\mu^3 \cos\theta_W - B_\mu \sin\theta_W$$
$$A_\mu = W_\mu^3 \sin\theta_W - B_\mu \cos\theta_W, \tag{1.4}$$

where A_μ is the gauge field of the electromagnetic interaction, and θ_W is the Weinberg mixing angle. The remaining degree of freedom of the scalar field Φ corresponds to a massive neutral scalar particle, the Higgs boson, h. The mass of this scalar is given by $m_h^2 = 2v^2\lambda$.

The Higgs mechanism also provides masses to the fermions (leptons and quarks, except neutrinos) through Yukawa interaction terms in the Lagrangian. The $SU(2)_L \times U(1)_Y$ gauge invariant terms in the Lagrangian for the first generation leptons and quarks is given by

$$\mathcal{L}_{Lepton} = -g_e \left[\begin{pmatrix} \bar{\nu}_e & \bar{e} \end{pmatrix}_L \begin{pmatrix} \phi^+ \\ \phi^0 \end{pmatrix} e_R + \bar{e}_R \begin{pmatrix} \bar{\phi}^- & \bar{\phi}^0 \end{pmatrix}_L \begin{pmatrix} \nu_e \\ e \end{pmatrix} \right]$$
$$\mathcal{L}_{Quark} = -g_d \begin{pmatrix} \bar{u} & \bar{d} \end{pmatrix}_L \begin{pmatrix} \phi^+ \\ \phi^0 \end{pmatrix} d_R - g_u \begin{pmatrix} \bar{u} & \bar{d} \end{pmatrix}_L \begin{pmatrix} -\phi^0 \\ \phi^- \end{pmatrix} u_R + h.c., \tag{1.5}$$

where g_e, g_u, g_d are the corresponding Yukawa coupling constants. After the Spontaneous Symmetry Breaking (SSB) as discussed above, the Higgs field picks up a VEV generating the mass term, and an interaction term (with the Higgs boson) of the fermions .

$$\mathcal{L}_{Lepton} = -m_e \bar{e}e - \frac{m_e}{v}\bar{e}eh^0$$
$$\mathcal{L}_{Quarks} = -m_d \bar{d}d - m_u \bar{u}u - \frac{m_d}{v}\bar{d}dh^0 - \frac{m_u}{v}\bar{u}uh^0, \tag{1.6}$$

where

$$m_e = \frac{g_e v}{\sqrt{2}}, \qquad m_u = \frac{g_u v}{\sqrt{2}}, \qquad m_d = \frac{g_d v}{\sqrt{2}}. \tag{1.7}$$

Similarly the other generations of fermions receive their masses through Yukawa interactions, which can be expressed as

$$m_\mu = \frac{g_\mu v}{\sqrt{2}}, \qquad m_c = \frac{g_c v}{\sqrt{2}}, \qquad m_s = \frac{g_s v}{\sqrt{2}},$$

$$m_\tau = \frac{g_\tau v}{\sqrt{2}}, \qquad m_t = \frac{g_t v}{\sqrt{2}}, \qquad m_b = \frac{g_b v}{\sqrt{2}}. \tag{1.8}$$

The couplings of the Higgs boson with the fermions is now fixed in terms of the mass of the fermion and the VEV, as

$$g_{\bar{e}eh} = i\frac{m_e}{v}, \qquad g_{\bar{u}uh} = i\frac{m_u}{v}, \qquad g_{\bar{d}dh} = i\frac{m_d}{v}, \tag{1.9}$$

$$g_{\bar{\mu}\mu h} = i\frac{m_\mu}{v}, \qquad g_{\bar{c}ch} = i\frac{m_c}{v}, \qquad g_{\bar{s}sh} = i\frac{m_s}{v},$$
$$g_{\bar{\tau}\tau h} = i\frac{m_\tau}{v}, \qquad g_{\bar{t}th} = i\frac{m_t}{v}, \qquad g_{\bar{b}bh} = i\frac{m_b}{v}. \tag{1.10}$$

Coming to the Higgs mass term and the self-interaction terms, the scalar potential $V(\Phi) = \mu^2\Phi^\dagger\Phi + \lambda(\Phi^\dagger\Phi)^2$ when written in terms of the physical fields is given by

$$V(\Phi) = \frac{\mu^2}{2}\begin{pmatrix}0 & v+h(x)\end{pmatrix}\begin{pmatrix}0\\ v+h(x)\end{pmatrix} + \frac{\lambda}{4}\left[\begin{pmatrix}0 & v+h(x)\end{pmatrix}\begin{pmatrix}0\\ v+h(x)\end{pmatrix}\right]^2 \tag{1.11}$$

This leads to the the Lagrangian of the Higgs sector as

$$\mathcal{L}_h = \frac{1}{2}(\partial_\mu h)^2 - \lambda v^2 h^2 - \lambda v h^3 - \frac{\lambda}{4}h^4. \tag{1.12}$$

The mass and the self-couplings of the Higgs boson derived from the above scalar part of the Lagrangian are

$$m_h^2 = 2\lambda v^2 = -2\mu^2, \quad g_{hhh} = i\frac{m_h^2}{2v}, \qquad g_{hhhh} = i\frac{m_h^2}{8v^2} \tag{1.13}$$

The Higgs couplings with the gauge bosons arises through the covariant kinetic term of the scalar field $(D^\mu\Phi)^\dagger (D_\mu\Phi)$, which are given by

$$g_{hWW} = 2i\frac{m_W^2}{v}, \qquad g_{hZZ} = i\frac{m_Z^2}{v}$$
$$g_{hhWW} = i\frac{m_Z^2}{v^2}, \qquad g_{hhZZ} = i\frac{m_Z^2}{2v^2} \tag{1.14}$$

The Feynman rules for the couplings in the SM are given in figures 1.3 and 1.4.

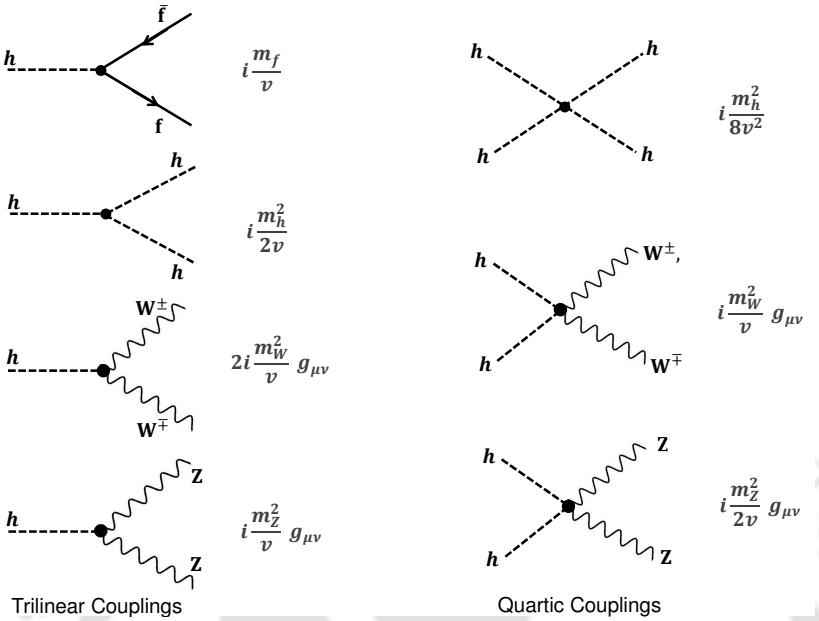

FIGURE 1.3: Feynman rules for Yukawa couplings, and Higgs to gauge boson couplings along with the Higgs trilinear and quartic self couplings.

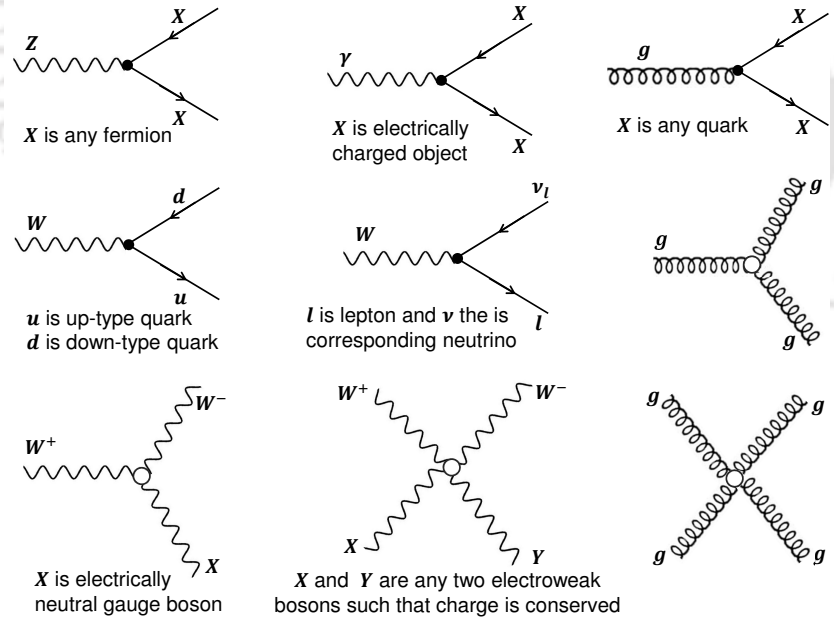

FIGURE 1.4: The tree level vertices involving gauge bosons and fermions in the standard model.

1.2 Drawbacks of the SM

While highly successful, surviving very stringent experimental tests, the SM has left many things unexplained, giving reasons to believe that it needs to be modified at higher energies. This section briefly provides some of the main drawbacks of the SM.

1.2.1 Hierarchy problem

The fact that gravity is much weaker than all other forces implies the existence of two vastly different scales of energy: $\Lambda_{Planck} \sim 10^{19}\ GeV$ where gravity gets strong, and the electroweak scale: $\Lambda_{EW} \sim \mathcal{O}(100\ GeV)$. If the SM is a complete theory and holds all the way up to the Planck scale, then this leads to a difficult situation in the computation of mass of the Higgs boson. It has recently been measured that the Higgs boson has a mass of about 126 GeV. On the other hand, unlike gauge boson mass, the scalar particle mass is not protected by any symmetry consideration. Thus, it is seen that the quantum corrections involving higher-order fermionic loops are quadratically divergent. The physical Higgs mass m_h can be defined as

$$m_h^2 = m_0^2 + \Delta m_{rad}^2 \tag{1.15}$$

where m_0 denotes bare mass (parameter appearing the Lagrangian) and Δm_{rad}^2 is

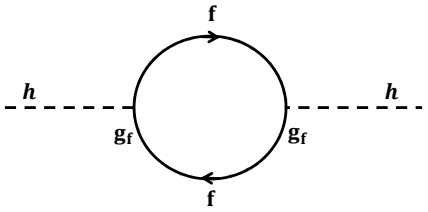

FIGURE 1.5: One loop correction to the Higgs squared mass m_h^2, where f and g_f denote the fermionic field and the Yukawa coupling constant respectively.

the radiative correction to the Higgs mass squre. Fig. 1.5 alone gives the largest correction to the Higgs mass,

$$\Delta m_{rad}^2 = -\frac{g_f^2}{8\pi^2}\left[\Lambda_{UV}^2 - 3m_f^2\ \ln(\tfrac{\Lambda_{UV}}{m_f})\right] \tag{1.16}$$

which is quadratically divergent to the scale where new physics is believed to occur (Λ_{UV}). The dominant contribution comes from the top quark in the loop since it has the largest Yukawa coupling to the Higgs boson. If the SM is a complete theory that is valid all the way up to the Planck scale ($\Lambda_{UV} = \Lambda_{Planck}$), then it implies that in order to obtain a physical Higgs mass $m_h \simeq \Lambda_{EW}$, m_0 must be of the order Λ_{Planck}. Since the ratio of square of electroweak scale to the square of Planck scale (10^{-34}), is so small the cancellation must be extremely precise.

1.2.2 Dark Matter

There is ample evidence from observations like the rotation curve of galaxies, that luminous matter in the universe accounts for only a small fraction of the total matter-energy density. The unknown matter content of the universe is called

FIGURE 1.6: The composition of visible matter, dark matter and dark energy of the present universe.

the dark matter (DM) [54–57]. It accounts for about 26.8% of the total energy density of the observable universe, while the ordinary matter accounts for only 4.9%, with the remainder being attributed to dark energy. The SM does not have a viable candidate for DM particles. However, there are extension of SM including supersymmetric models, which contain viable candidates for DM. The Fig. 1.6 indicates this classification of the content of the universe.

1.2.3 Matter and Anti-Matter Asymmetry

It is well observed that the universe made up of protons, neutrons and electrons. According to astrophysical observations, the density of protons and neutrons, constitute the bulk of the mass of visible matter, as the baryon content of the universe.

There is enough evidence to show that there are no large regions of anti-matter at any distance scales observed so far [58], albeit some small domains of anti-matter in the matter-dominated universe are not ruled out by observations [59–61]. At the same time, according to the SM, matter is created in particle-anti-particle pairs during the very early times of the universe. The SM does not propose a way to reach the presently observed baryon asymmetric universe starting from such a symmetric situation.

1.2.4 Neutrino's Mass

Neutrinos, initially thought to be massless is now proved to have small mass. The SM cannot construct a renormalizable mass term for the neutrinos. So in order to introduce a neutrino mass one must either extend the particle content of the model or abandon gauge invariance and/or renormalizability [62, 63].

So far, we have described the problems in the SM, and the standard mechanism of EWSB. Now it is very obvious how the couplings of the Higgs to gauge bosons as well as with itself can be useful in order to understand the nature of EWSB potential. In the next section, we will discuss current status of Higgs physics and some details of effective theories.

1.3 Theoretical Framework and Motivation

With the recent LHC discovery of the Higgs boson and associated measurements, the details of Electroweak Symmetry Breaking is expected to be explored in detail in the near future experiments. In the absence of any direct observation of new physics effects in the form of new particles, and with the measurements so far indicating a picture very close to that of the SM case, it is natural to consider the detailed study of various couplings involved in a model independent framework under effective field theories [64–67]. In the rest of this section we shall first briefly discuss the status of Higgs boson discovery and related measurements, followed by a detailed description of the effective Lagrangian employed in the thesis work.

1.3.1 Production mechanisms at hadron colliders

The main production mechanisms at the Tevatron and the LHC are gluon fusion, weak-boson fusion, associated production with a gauge boson and associated production with top quarks. Here Fig. 1.7 depicts representative diagrams for these dominant Higgs production processes.

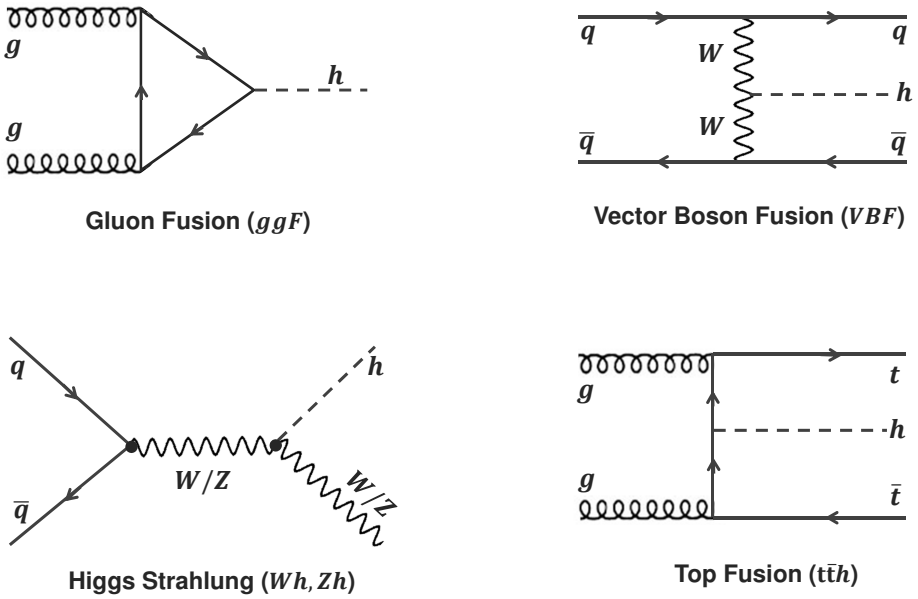

FIGURE 1.7: Generic Feynman diagrams contributing to the Higgs production.

Table 1.1 showing the cross sections for the production of a SM Higgs boson at the center of mass energy ($\sqrt{s}$) of 7 TeV and 8 TeV respectively, in pp collisions as given Ref. [68].

$\sqrt{s}$ $[TeV]$	m_h $[GeV]$	ggF $[pb]$	VBF $[pb]$	Wh $[pb]$	Zh $[pb]$	tth $[pb]$	Total $[pb]$
7	125	15.13	12.22	0.5785	0.3351	0.0863	17.35
	126	14.89	12.11	0.5629	0.3267	0.0843	17.08
8	125	19.27	1.578	0.7046	0.4153	0.1293	22.10
	126	18.97	1.568	0.6860	0.4050	0.1262	21.76

TABLE 1.1: The SM Higgs boson production cross section in pp collisions at the center of mass energy ($\sqrt{s}$) of 7 TeV and 8 TeV.

1.3.2 Status of the Higgs Boson

The ATLAS and the CMS presented the results on five main decay modes[1]: $h \to \gamma\gamma$, $h \to ZZ \to 4l$, $h \to WW \to l\nu l\nu$, $h \to \tau\tau$ and $h \to bb$ channels, with an integrated luminosities of up to 5 fb^{-1} at $\sqrt{s} = 7\ TeV$ and up to 21 fb^{-1} at $\sqrt{s} = 8\ TeV$. The $h \to \gamma\gamma$ and $h \to ZZ \to 4l$ channels allow to measure the mass of the boson with very high precision. ATLAS measures a mass of $125.5 \pm 0.2(stat.)^{+0.5}_{-0.6}(syst.)\ GeV$ [69], CMS measures a mass of $125.7 \pm 0.3\ (stat.) \pm 0.3\ (syst.)\ GeV$ [70]. Figures 1.8 and 1.9 are showing the signal strength μ (ratio of the measured value divided by the SM value) for the various decay channels for ATLAS and CMS. For ATLAS the combined signal strength is determined to be $\mu = 1.17 \pm 0.27$ at the measured mass value [52]. For CMS the combined signal strength is determined to be $\mu = 1.14^{+0.26}_{-0.23}$ at the measured mass value [51].

1.3.3 Effective Lagrangian: For two Charged and a Neutral Vector Gauge Bosons

In the CP conserving case $WW\gamma$ anomalous coupling is commonly parametrized in terms of two parameters, $\delta\kappa_\gamma$ and λ_γ [65]. Although bounds on these parameters can be extracted from high precision low energy measurements and measurements at the Z^0 pole [71], there are some ambiguities and model dependencies in the

[1] In Fig. 1.8, 1.9 and 1.10, H is used instead of h to denote the SM Higgs boson.

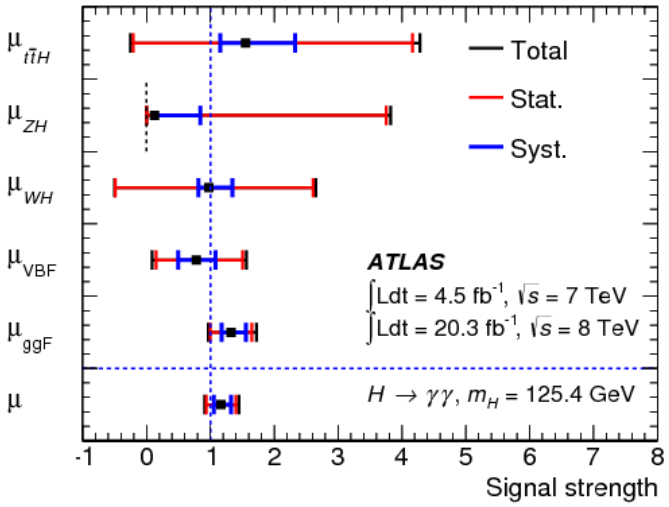

FIGURE 1.8: The signal strength for the individual channel and their combination. The values of μ are given for $M_h = 125.5\ GeV$ for ATLAS. The plot is adopted from Ref. [52].

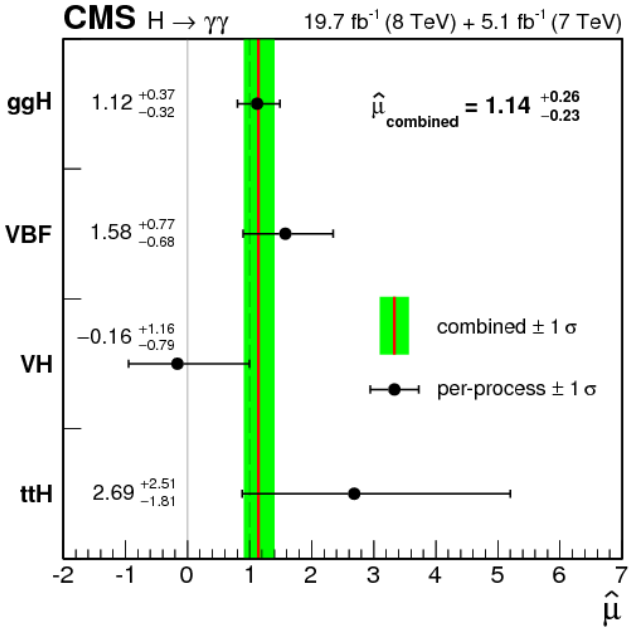

FIGURE 1.9: Showing the signal strength for the individual channel and their combination. The value of μ is given for $M_h = 125.5\ GeV$ for CMS. The plot is adopted from Ref. [51].

results [72]. So far the direct measurement of these parameters come from the CDF and $D0$ collaborations at the Fermilab $p\bar{p}$ [73–75] and the LEP experiment [76].

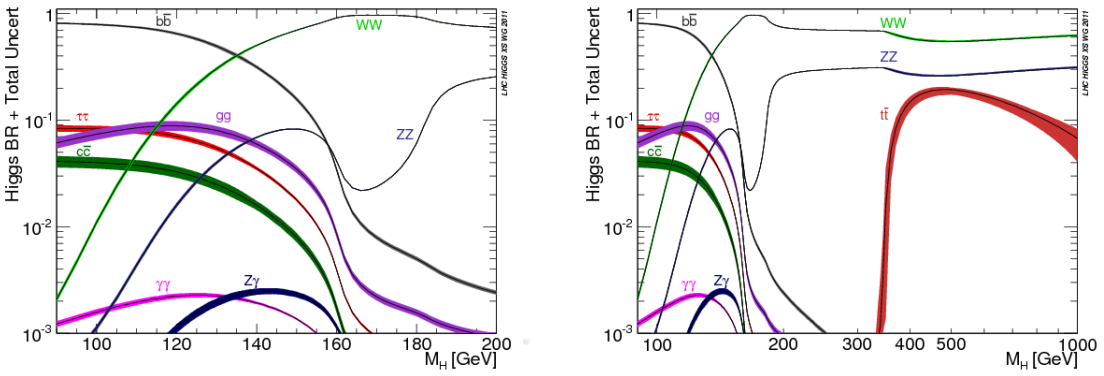

FIGURE 1.10: Showing the Higgs branching ratios and their uncertainties for the low mass range (left) and for the full mass range (right). These plots adopted from Ref. [68]

The most general coupling of two charged vector bosons with a neutral vector bosons can be derived from the following effective Lagrangian [65]:

$$\begin{aligned}\mathcal{L}_{VWW} \;=\; & ig_V\Bigg[g_1^V\Big([W^\dagger_{\mu\nu}W^\mu V^\nu - W^\dagger_\mu V_\nu W^{\mu\nu}\Big) + \kappa_V W^\dagger_\mu W_\nu V^{\mu\nu} \\ & + \frac{\lambda_V}{m_W^2}\, W^\dagger_{\lambda\mu}W^\mu_\nu V^{\nu\lambda} - g_4^V W^\dagger_\mu W_\nu\Big(\partial^\mu V^\nu + \partial^\nu V^\mu\Big) \\ & - ig_5^V\,\epsilon^{\mu\nu\rho\sigma}\Big(W^\dagger_\mu \overleftrightarrow{\partial}_\rho W_\nu V_\sigma\Big) + \tilde{\kappa}_V W^\dagger_\mu W_\nu \tilde{V}^{\mu\nu} \\ & + \frac{\tilde{\lambda}_V}{m_W^2} W^\dagger_{\lambda\mu}W^\mu_\nu \tilde{V}^{\nu\lambda}\Bigg], \end{aligned} \tag{1.17}$$

where V stands for neutral gauge bosons, either Z or γ, $\tilde{V}_{\mu\nu} = \frac{1}{2}\epsilon_{\mu\nu\rho\sigma}V^{\rho\sigma}$ and $\big(A\overleftrightarrow{\partial}_\mu B\big) = A(\partial_\mu B) - (\partial_\mu A)B$. The effective $WW\gamma$ vertex pictured in Fig.1.11

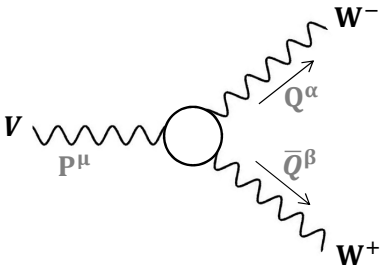

FIGURE 1.11: The general WWV vertex, where $V \equiv Z$ or γ.

can be written considering most general Lorentz structure for the W satisfying

$\partial_\mu W^\mu = 0$, as

$$
\begin{aligned}
i\Gamma_V^{\alpha\beta\mu}(Q,\bar{Q},P) \;=\; & ig_V\Bigg[f_1^V\big(Q-\bar{Q}\big)^\mu g^{\alpha\beta} - \frac{f_2^V}{m_W^2}\big(Q-\bar{Q}\big)^\mu P^\alpha P^\beta \\
& + f_3^V\Big(P^\alpha g^{\mu\beta} - P^\beta g^{\mu\alpha}\Big) + if_4^V\Big(P^\alpha g^{\mu\beta} + P^\beta g^{\mu\alpha}\Big) \\
& + if_5^V\,\epsilon^{\mu\alpha\beta\rho}\big(Q-\bar{Q}\big)_\rho - f_6^V\,\epsilon^{\mu\alpha\beta\rho}P_\rho \\
& - \frac{f_7^V}{m_W^2}\big(Q-\bar{Q}\big)^\mu\epsilon^{\alpha\beta\rho\sigma}P_\rho\big(Q-\bar{Q}\big)_\sigma\Bigg].
\end{aligned}
\tag{1.18}
$$

The condition of $\partial_\mu W^\mu = 0$ is automatically satisfied by on-shell $W^\mp$ for both real and virtual photons. All the form factors f_i^V are dimensionless functions of P^2, Q^2 and $\bar{Q}^2$. To lowest order, the form factors are related to the Lagrangian parameters via

$$
\begin{aligned}
f_1^V &= g_1^V + \frac{P^2}{2m_W^2}\lambda_V, & f_2^V &= \lambda_V, \\
f_3^V &= g_1^V + \kappa_V + \frac{Q^2+\bar{Q}^2}{2m_W^2}\lambda_V, & & \\
f_4^V &= g_4^V - \frac{Q^2-\bar{Q}^2}{2m_W^2}i\lambda_V, & f_5^V &= g_5^V + \frac{Q^2-\bar{Q}^2}{2m_W^2}i\tilde{\lambda}_V, \\
f_6^V &= \tilde{\kappa}_V - \frac{Q^2+\bar{Q}^2}{2m_W^2}\tilde{\lambda}_V, & f_7^V &= -\frac{1}{2}\tilde{\lambda}_V.
\end{aligned}
\tag{1.19}
$$

Contribution from the higher dimensional operators in the Lagrangian give P^2, Q^2 and $\bar{Q}^2$ dependence to the form factor. Now without lose of generality, the overall coupling constants could be taken as

$$
g_\gamma = -e, \qquad\qquad g_Z = -e\,\cot\theta_W, \tag{1.20}
$$

where $-e$ is the charge of the electron and θ_W is the weak mixing angle. The electric charge of the W boson determines $g_1^\gamma = 1$. The coupling parameters κ_V and λ_V are connected to the magnetic dipole moment μ_W and electric quadrupole moment Q_W of the W^+ as

$$
\mu_W = \frac{e}{2m_W}\big(1+\kappa_V+\lambda_V\big), \qquad\qquad Q_W = -\frac{e}{m_W^2}\big(\kappa_V-\lambda_V\big). \tag{1.21}
$$

These three coupling parameters g_1^V, κ_V and λ_V are invariant under both C and P transformation.

Parameter	ALEPH	DELPHI	L3	OPAL	Combined 95% CL	SM
g_1^Z	$0.996^{+0.030}_{-0.028}$	$0.975^{+0.035}_{-0.032}$	$0.965^{+0.038}_{-0.037}$	$0.985^{+0.035}_{-0.034}$	[0.946, 1.021]	1
κ_γ	$0.983^{+0.060}_{-0.060}$	$1.022^{+0.082}_{-0.084}$	$1.020^{+0.075}_{-0.069}$	$0.899^{+0.090}_{-0.084}$	[0.901, 1.066]	1
λ_γ	$-0.014^{+0.029}_{-0.029}$	$0.001^{+0.036}_{-0.035}$	$-0.023^{+0.042}_{-0.039}$	$-0.061^{+0.037}_{-0.036}$	$[-0.059, 0.017]$	0

TABLE 1.2: The measured central value and one standard deviation errors obtained by the four *LEP* experiments for the charged TGC parameters.

The parameters, $\tilde{\kappa}_V$ and $\tilde{\lambda}_V$, conserve C but violate P. These parameters are related to the electric dipole moment d_W and the magnetic quadrupole moment $\tilde{Q}_W$ of the W^+ as

$$d_W = \frac{e}{2m_W}\left(\tilde{\kappa}_V + \tilde{\lambda}_V\right), \qquad \tilde{Q}_W = -\frac{e}{m_W^2}\left(\tilde{\kappa}_V - \tilde{\lambda}_V\right) \tag{1.22}$$

The remaining two couplings of Eq.2.1, g_4 and g_5 violating the charge conjugation C, while g_4 respects P whereas g_5 violates P.

The individual analysis and experimental results for the charged gauge bosons couplings are described in Refs. [77–81]. The results of single parameter fits from each experiment are shown in Table 1.2, where the errors including both statistical and systematic effects. Apart from this, the results form the combination are given in the same table. In each case the TGC parameter listed is varied while the remaining two are fixed to their SM values. The experimental bounds on other parameters can be found in Ref. [76].

1.3.4 Effective Lagrangian for a Light Higgs Doublet

The ignorance of the EWSB sector can be parametrized in terms of an effective Lagrangian for the gauge bosons as well as the Higgs boson. The most general $SU(3)_C \times SU(2)_L \times U(1)_Y$ invariant Lagrangian for a weak Higgs doublet at the level of dimension-6 operators was first classified in a systematic way in Refs. [82–85]. Generally, in the effective field theory based approach an effective Lagrangian is constructed including higher-dimensional operators to the SM Lagrangian ($\mathcal{L}_{SM}$), that parametrize the possible effects of non-observed states expected to appear in the spectrum at higher energies compared to the energies

being explored. This low energy effective scale is identified with the W-boson mass m_W or equivalently with the VEV of the Higgs field v. The effective Lagrangian including upto dimension six operators is given by [32, 82–84, 86, 87]

$$\mathcal{L} = \mathcal{L}_{SM} + \sum_i \bar{c}_i \mathcal{O}_i = \mathcal{L}_{SILH} + \mathcal{L}_{CP} + \mathcal{L}_{F_1} + \mathcal{L}_{F_2} + \mathcal{L}_G, \tag{1.23}$$

where $\mathcal{O}_i$ are the effective operators, and $\bar{c}_i$ are the corresponding coefficients. The above Lagrangian assumes baryon and lepton number conservation. Following the Refs. [85, 85, 87] the effective Lagrangian involving the Higgs doublet (Φ) is presented below.

$$\begin{aligned}
\mathcal{L}_{SILH} \;=\; & \frac{\bar{c}_H}{2v^2}\partial^\mu\big(\Phi^\dagger\Phi\big)\partial_\mu\big(\Phi^\dagger\Phi\big) + \frac{\bar{c}_T}{2v^2}\big(\Phi^\dagger \overleftrightarrow{D}^\mu \Phi\big)\big(\Phi^\dagger \overleftrightarrow{D}_\mu \Phi\big) - \frac{\bar{c}_6\lambda}{v^2}\big(\Phi^\dagger\Phi\big)^3 \\
& - \left[\frac{\bar{c}_u}{v^2} y_u \Phi^\dagger\Phi\ \Phi^\dagger\cdot\bar{Q}_L u_R + \frac{\bar{c}_d}{v^2} y_d \Phi^\dagger\Phi\ \Phi\bar{Q}_L d_R + \frac{\bar{c}_l}{v^2} y_l \Phi^\dagger\Phi\ \Phi\bar{L}_L e_R\right] \\
& + \frac{ig\bar{c}_W}{m_W^2}\big(\Phi^\dagger T_{2k} \overleftrightarrow{D}^\mu \Phi\big) D^\nu W^k_{\mu\nu} + \frac{ig'\bar{c}_B}{2m_W^2}\big(\Phi^\dagger \overleftrightarrow{D}^\mu \Phi\big)\partial^\nu B_{\mu\nu} \\
& + \frac{2ig\bar{c}_{HW}}{m_W^2}\big(D^\mu\Phi^\dagger T_{2k} D^\nu\Phi\big) W^k_{\mu\nu} + \frac{ig'\bar{c}_{HB}}{m_W^2}\big(D^\mu\Phi^\dagger D^\nu\Phi\big) B_{\mu\nu} \\
& + \frac{g'^2\bar{c}_\gamma}{m_W^2}\Phi^\dagger\Phi B_{\mu\nu}B^{\mu\nu} + \frac{g_s^2\bar{c}_g}{m_W^2}\Phi^\dagger\Phi G^a_{\mu\nu}G_a^{\mu\nu}
\end{aligned} \tag{1.24}$$

where λ is the Higgs quartic coupling, y_u, y_d and y_l are the 3×3 Yukawa coupling matrices in flavor space, and g_s, g and g' are coupling constants corresponding to $SU(3)_C, SU(2)_L$ and $U(1)_Y$, respectively. The $SU(2)_L$ generators are taken to be $T_{2k} = \frac{\sigma_k}{2}$, where σ_k are Pauli matrices. In the above expression, $\overleftrightarrow{D}_\mu$ is defined as

$$\Phi^\dagger \overleftrightarrow{D}_\mu \Phi = \Phi^\dagger(D_\mu\Phi) - (D_\mu\Phi^\dagger)\Phi, \tag{1.25}$$

The $SU(2)_L$ doublets are explicitly given as

$$Q_L = \begin{pmatrix} u_L \\ d_L \end{pmatrix}, \quad L_L = \begin{pmatrix} \nu_L \\ l_L \end{pmatrix}, \quad \Phi = \begin{pmatrix} -iG^+ \\ \frac{1}{\sqrt{2}}\big[v + h + iG^0\big] \end{pmatrix} \tag{1.26}$$

where, $l = e,\ \mu,\ \tau$ and ν represent the corresponding neutrino. The $SU(2)_L$ invariant products written with the help of the rank two anti-symmetric tensor ϵ_{ij}, with $\epsilon_{12} = 1$ and $\epsilon^{12} = -1$, is given as

$$Q_L\cdot\Phi = \epsilon_{ij}Q_L^i\Phi^j \quad \textit{and} \quad \Phi^\dagger\cdot\bar{Q}_L = \epsilon^{ij}\Phi_i^\dagger\bar{Q}_L j, \tag{1.27}$$

The field strength tensors and the gauge covariant derivatives are given by

$$\begin{aligned} B_{\mu\nu} &= \partial_\mu B_\nu - \partial_\nu B_\nu \\ W^k_{\mu\nu} &= \partial_\mu W^k_\nu - \partial_\nu W^k_\mu + g\epsilon_{ij}^{\ k} W^i_\mu W^j_\nu \\ G^a_{\mu\nu} &= \partial_\mu G^a_\nu - \partial_\nu G^a_\mu + g_s f_{bc}^{\ a} G^b_\mu G^c_\nu \\ D_\mu\Phi &= \partial_\mu\Phi - \frac{1}{2}ig' B_\mu\Phi - igT_{2k}W^k_\mu\Phi, \end{aligned} \tag{1.28}$$

where $\epsilon_{ij}^{\ k}$ and $f_{bc}^{\ a}$ are the structure constants of $SU(2)_L$ and $SU(3)_C$, respectively. The second piece in Eq. 1.23 involving CP-violating operators is given by

$$\begin{aligned} \mathcal{L}_{CP} &= \frac{ig\tilde{c}_{HW}}{m_W^2} D^\mu\Phi^\dagger T_{2k} D^\nu\Phi\tilde{W}^k_{\mu\nu} + \frac{ig'\tilde{c}_{HB}}{m_W^2} D^\mu\Phi^\dagger D^\nu\Phi\tilde{B}_{\mu\nu} + \frac{g'^2\tilde{c}_\gamma}{m_W^2}\Phi^\dagger\Phi B_{\mu\nu}\tilde{B}_{\mu\nu} \\ &+ \frac{g_s^2\tilde{c}_g}{m_W^2}\Phi^\dagger\Phi G^a_{\mu\nu}\tilde{G}^a_{\mu\nu} + \frac{g^3\tilde{c}_{3W}}{m_W^2}\epsilon_{ijk}W^i_{\mu\nu}W^{\nu j}_\rho\tilde{W}^{\rho\mu k} \\ &+ \frac{g_s^3\tilde{c}_{3G}}{m_W^2} f_{abc}G^a_{\mu\nu}G^{\nu b}_\rho\tilde{G}^{\rho\mu c} \end{aligned} \tag{1.29}$$

where the dual field strength tensors are defined as

$$\tilde{B}_{\mu\nu} = \frac{1}{2}\epsilon_{\mu\nu\rho\sigma}B^{\rho\sigma}, \quad \tilde{W}^k_{\mu\nu} = \frac{1}{2}\epsilon_{\mu\nu\rho\sigma}W^{\rho\sigma k}, \quad \tilde{G}^a_{\mu\nu} = \frac{1}{2}\epsilon_{\mu\nu\rho\sigma}G^{\rho\sigma a} \tag{1.30}$$

The fermionic interaction part of the Lagrangian, with two Higgs bosons ($\mathcal{L}_{F_1}$), and one Higgs boson and gauge boson ($\mathcal{L}_{F_2}$) are given by

$$\begin{aligned} \mathcal{L}_{F_1} &= \frac{i\bar{c}_{HQ}}{v^2}\big(\bar{Q}_L\gamma^\mu Q_L\big)\big(\Phi^\dagger\overleftrightarrow{D}_\mu\Phi\big) + \frac{4i\bar{c}'_{HQ}}{v^2}\big(\bar{Q}_L\gamma^\mu T_{2k}Q_L\big)\big(\Phi^\dagger T_2^k\overleftrightarrow{D}_\mu\Phi\big) \\ &+ \frac{i\bar{c}_{Hu}}{v^2}\big(\bar{u}_R\gamma^\mu u_R\big)\big(\Phi^\dagger\overleftrightarrow{D}_\mu\Phi\big) + \frac{i\bar{c}_{Hd}}{v^2}\big[\bar{d}_R\gamma^\mu d_R\big]\big(\Phi^\dagger\overleftrightarrow{D}_\mu\Phi\big) \\ &- \left[\frac{i\bar{c}_{Hud}}{v^2}\big(\bar{u}_R\gamma^\mu d_R\big)\big(\Phi^\dagger\cdot\overleftrightarrow{D}_\mu\Phi\big) + h.c.\right] \\ &+ \frac{i\bar{c}_{HL}}{v^2}\big(\bar{L}_L\gamma^\mu L_L\big)\big(\Phi^\dagger\overleftrightarrow{D}_\mu\Phi\big) + \frac{4i\bar{c}'_{HL}}{v^2}\big(\bar{L}_L\gamma^\mu T_{2k}L_L\big)\big(\Phi^\dagger T_2^k\overleftrightarrow{D}_\mu\Phi\big) \\ &+ \frac{i\bar{c}_{He}}{v^2}\big(\bar{e}_R\gamma^\mu e_R\big)\big(\Phi^\dagger\overleftrightarrow{D}_\mu\Phi\big), \end{aligned} \tag{1.31}$$

$$\begin{aligned}\mathcal{L}_{F_2} &= \Bigg[\frac{-2g'\bar{c}_{uB}}{m_W^2}y_u\Phi^\dagger\cdot\bar{Q}_L\gamma^{\mu\nu}u_R B_{\mu\nu} - \frac{4g\bar{c}_{uW}}{m_W^2}y_u\Phi^\dagger\cdot(\bar{Q}_L T_{2k})\gamma^{\mu\nu}u_R W^k_{\mu\nu} \\ &\quad -\frac{4g_s\bar{c}_{uG}}{m_W^2}y_u\Phi^\dagger\cdot\bar{Q}_L\gamma^{\mu\nu}T_a u_R G^a_{\mu\nu} + \frac{2g'\bar{c}_{dB}}{m_W^2}y_d\Phi\bar{Q}_L\gamma^{\mu\nu}d_R B_{\mu\nu} \\ &\quad +\frac{4g\bar{c}_{dW}}{m_W^2}y_d\Phi(\bar{Q}_L T_{2k})\gamma^{\mu\nu}d_R W^k_{\mu\nu} + \frac{4g_s\bar{c}_{dG}}{m_W^2}y_u\Phi\bar{Q}_L\gamma^{\mu\nu}T_a d_R G^a_{\mu\nu} \\ &\quad +\frac{2g'\bar{c}_{eB}}{m_W^2}y_l\Phi\bar{L}_L\gamma^{\mu\nu}e_R B_{\mu\nu} + \frac{4g\bar{c}_{eW}}{m_W^2}y_l\Phi(\bar{L}_L T_{2k})\gamma^{\mu\nu}e_R W^k_{\mu\nu} + h.c.\Bigg] \quad (1.32)\end{aligned}$$

where T_a are the generators of the $SU(3)_C$ symmetry group in the fundamental representation and $\gamma^{\mu\nu}$ is defined as $\gamma^{\mu\nu} = \frac{i}{4}\big[\gamma^\mu,\ \gamma^\nu\big]$. The last term of Eq.(1.23) involving gauge boson self-interactions refers to operators which are not directly related to Higgs physics. We include them for completeness.

$$\begin{aligned}\mathcal{L}_G &= \frac{g^3\bar{c}_{3W}}{m_W^2}\epsilon_{ijk}W^i_{\mu\nu}W^{\nu j}_{\rho}W^{\rho\mu k} + \frac{g_s^3\bar{c}_{3G}}{m_W^2}f_{abc}G^a_{\mu\nu}G^{\nu b}_{\rho}G^{\rho\mu c} + \frac{\bar{c}_{2W}}{m_W^2}D^\mu W^k_{\mu\nu}D_\rho W^{\rho\nu}_k \\ &\quad +\frac{\bar{c}_{2B}}{m_W^2}\partial^\mu B_{\mu\nu}\partial_\rho B^{\rho\nu} + \frac{\bar{c}_{2G}}{m_W^2}D^\mu G^a_{\mu\nu}D_\rho G^{\rho\nu}_a. \quad (1.33)\end{aligned}$$

1.3.4.1 Effective Lagrangian in the Mass Eigen-Basis: For a Light Higgs Doublet

We shall present the parts of the Lagrangian presented above, relevant to this thesis, given in the physical basis.[2] Firstly, the $\mathcal{O}_H$ operator leads to an additional contribution to kinetic terms of the Higgs boson (h) given as

$$\mathcal{O}_H = \frac{\bar{c}_H}{2v^2}\partial^\mu\big(\Phi^\dagger\Phi\big)\partial_\mu\big(\Phi^\dagger\Phi\big) \Rightarrow \frac{\bar{c}_H}{2}\partial^\mu h\ \partial_\mu h. \quad (1.34)$$

The Lagrangian involving the Higgs interaction terms, split according to the number of physical states involved, are written schematically as

$$\mathcal{L}_{Higgs} = \mathcal{L}_3 + \mathcal{L}_4, \quad (1.35)$$

[2]The Higgs mechanism in the context of dimension-six operators is described in Appendix-C.

The three-point interaction Lagrangian is given by

$$\begin{aligned}
\mathcal{L}_3 \;=\; & -v\lambda g^1_{hhh}h^3 + \frac{1}{2}g^2_{hhh}h\;\partial_\mu h\;\partial^\mu h \\
& + \frac{1}{4}g_{hgg}G^a_{\mu\nu}G^{\mu\nu}_a h - \frac{1}{4}\tilde{g}_{hgg}G^a_{\mu\nu}\tilde{G}^{\mu\nu}_a h - \frac{1}{4}g_{h\gamma\gamma}F_{\mu\nu}F^{\mu\nu}h - \frac{1}{4}\tilde{g}_{h\gamma\gamma}\tilde{F}_{\mu\nu}F^{\mu\nu}h \\
& - \frac{1}{4}g^1_{hZZ}Z_{\mu\nu}Z^{\mu\nu}h - g^2_{hZZ}Z_\nu\partial_\mu Z^{\mu\nu}h + \frac{1}{2}g^3_{hZZ}Z_\mu Z^\mu h - \frac{1}{4}\tilde{g}_{hZZ}Z_{\mu\nu}\tilde{Z}^{\mu\nu}h \\
& - \frac{1}{2}g^1_{h\gamma Z}Z_{\mu\nu}F^{\mu\nu}h - \frac{1}{2}\tilde{g}_{h\gamma Z}Z_{\mu\nu}\tilde{F}^{\mu\nu}h - g^2_{h\gamma Z}Z_\nu\partial_\mu F^{\mu\nu}h \\
& - \frac{1}{2}g^1_{hWW}W^{\mu\nu}W^\dagger_{\mu\nu}h - \Big[g^2_{hWW}W^\nu\partial^\mu W^\dagger_{\mu\nu}h + h.c.\Big] \\
& + gm_W W^\dagger_\mu W^\mu h - \frac{1}{2}\tilde{g}_{hWW}W^{\mu\nu}\tilde{W}^\dagger_{\mu\nu}h \\
& - \left[\tilde{y}_u\frac{1}{\sqrt{2}}\big(\bar{u}P_R u\big)h + \tilde{y}_d\frac{1}{\sqrt{2}}\big(\bar{d}P_R d\big)h + \tilde{y}_l\frac{1}{\sqrt{2}}\big(\bar{l}P_R l\big)h + h.c.\right],
\end{aligned} \tag{1.36}$$

where $W_{\mu\nu}, Z_{\mu\nu}$ and $F_{\mu\nu}$ are field strength tensors of W-boson, Z-boson and photon, respectively. The Lagrangian with four-point interactions are split into two sets, $\mathcal{L}^{(1)}_4$ containing interaction of the Higgs boson with the gauge bosons, and $\mathcal{L}^{(2)}_4$ involving Higgs boson interaction with fermions and gauge bosons, as given below.

$$\begin{aligned}
\mathcal{L}^{(1)}_4 \;=\; & -\frac{\lambda}{4}g^1_{hhhh}h^4 + \frac{1}{2}g^2_{hhhh}h^2\partial_\mu h\partial^\mu h - \frac{1}{8}g_{hhgg}G^a_{\mu\nu}G^{\mu\nu}_a h^2 - \frac{1}{8}\tilde{g}_{hhgg}G^a_{\mu\nu}\tilde{G}^{\mu\nu}_a h^2 \\
& - \frac{1}{8}g^2_{hh\gamma\gamma}F_{\mu\nu}F^{\mu\nu}h^2 - \frac{1}{8}\tilde{g}^2_{hh\gamma\gamma}F_{\mu\nu}\tilde{F}^{\mu\nu}h^2 \\
& - \frac{1}{8}g^1_{hhZZ}Z_{\mu\nu}Z^{\mu\nu}h^2 - \frac{1}{8}\tilde{g}_{hhZZ}Z_{\mu\nu}\tilde{Z}^{\mu\nu}h^2 \\
& - \frac{1}{2}g^2_{hhZZ}Z_\nu\partial_\mu Z^{\mu\nu}h^2 + \frac{1}{4}g^3_{hhZZ}Z_\mu Z^\mu h^2 \\
& - \frac{1}{4}g^1_{hh\gamma Z}Z_{\mu\nu}F^{\mu\nu}h^2 - \frac{1}{4}\tilde{g}_{hh\gamma Z}Z_{\mu\nu}\tilde{F}^{\mu\nu}h^2 \\
& - \frac{1}{2}g^2_{hh\gamma Z}Z_\nu\partial_\mu F^{\mu\nu}h^2 - \frac{1}{4}g^1_{hhWW}W_{\mu\nu}W^\dagger_{\mu\nu}h^2 - \frac{1}{4}\tilde{g}_{hhWW}W_{\mu\nu}\tilde{W}^\dagger_{\mu\nu}h^2 \\
& - \frac{1}{2}\Big[g^2_{hhWW}W_\nu\partial^\mu W^\dagger_{\mu\nu}h^2 + h.c.\Big] + \frac{1}{4}g^2W^\dagger_\mu W^\mu h^2 - ig^1_{h\gamma WW}F^{\mu\nu}W_\mu W^\dagger_\nu h \\
& + \Big[ig^2_{h\gamma WW}W_{\mu\nu}A^\mu W^\dagger_\nu h + h.c.\Big] + ig^3_{h\gamma WW}A_\mu W_\nu W^\dagger_\rho\Big[\eta^{\mu\rho}\partial^\nu h - \eta^{\mu\nu}\partial^\rho h\Big] \\
& + i\tilde{g}^1_{h\gamma WW}\tilde{F}^{\mu\nu}W_\mu W^\dagger_\nu h + \Big[i\tilde{g}^2_{h\gamma WW}\tilde{W}^{\mu\nu}A_\mu W^\dagger_\nu h + h.c.\Big] \\
& - ig^1_{hZWW}Z^{\mu\nu}W_\mu W^\dagger_\nu h + \Big[ig^2_{hZWW}W^{\mu\nu}Z_\mu W^\dagger_\nu h + h.c.\Big] \\
& + i\tilde{g}^1_{hZWW}\tilde{Z}^{\mu\nu}W_\mu W^\dagger_\nu h - \Big[i\tilde{g}^2_{hZWW}\tilde{W}^{\mu\nu}Z_\mu W^\dagger_\nu h + h.c.\Big] \\
& - ig^3_{hZWW}Z_\mu W_\nu W^\dagger_\rho\Big[\eta^{\mu\rho}\partial^\nu h - \eta^{\mu\nu}\partial^\rho h\Big]
\end{aligned} \tag{1.37}$$

$$
\begin{aligned}
\mathcal{L}_4^{(2)} &= -\Big[\bar{y}_u\frac{1}{\sqrt{2}}(\bar{u}P_R u)h^2 + \bar{y}_d\frac{1}{\sqrt{2}}(\bar{d}P_R d)h^2 + \Big[\bar{y}_l\frac{1}{\sqrt{2}}(\bar{l}P_R l)h^2 + h.c.\Big] \\
&-\bar{u}\gamma^\mu\Big[g^L_{hZuu}P_L + g^R_{hZuu}P_R\Big]uZ_\mu h - \bar{d}\gamma^\mu\Big[g^L_{hZdd}P_L + g^R_{hZdd}P_R\Big]d\ Z_\mu h \\
&-\bar{l}\gamma^\mu\Big(g^L_{hZll}P_L + g^R_{hZll}P_R\Big)lZ_\mu h - \bar{\nu}\gamma^\mu\Big(g^L_{hZ\nu\nu}P_L\Big)\nu\ Z_\mu h \\
&-\Big[\bar{u}\gamma^\mu\Big(g^L_{hWud}P_L + g^R_{hWud}P_R\Big)d\ W_\mu h + \bar{\nu}\gamma^\mu\Big(g_{hW\nu l}P_L\Big)lW_\mu h + h.c.\Big] \\
&-\Big[g^{(\partial)}_{h\gamma uu}\Big(\bar{u}\gamma^{\mu\nu}P_R u\Big) + g^{(\partial)}_{h\gamma dd}\Big(\bar{d}\gamma^{\mu\nu}P_R d\Big) + g^{(\partial)}_{h\gamma ll}\Big(\bar{l}\gamma^{\mu\nu}P_R l\Big) + h.c.\Big]F_{\mu\nu}h \\
&-\Big[g^{(\partial)}_{hZuu}\Big(\bar{u}\gamma^{\mu\nu}P_R u\Big) + g^{(\partial)}_{hZdd}\Big(\bar{d}\gamma^{\mu\nu}P_R d\Big) + g^{(\partial)}_{hZll}\Big(\bar{l}\gamma^{\mu\nu}P_R l\Big) + h.c.\Big]Z_{\mu\nu}h \\
&-\Big[\bar{u}\gamma^{\mu\nu}\Big(g^{\partial L}_{hWud}P_L + g^{\partial R}_{hWud}P_R\Big)dW_{\mu\nu} + g^{\partial}_{hW\nu l}\bar{\nu}\gamma^{\mu\nu}P_R lW_{\mu\nu} + h.c.\Big]h \\
&-\Big[g^{(\partial)}_{hguu}\Big(\bar{u}T_a\gamma^{\mu\nu}P_R u\Big) + g^{(\partial)}_{hgdd}\Big(\bar{d}T_a\gamma^{\mu\nu}P_R d\Big) + h.c.\Big]G^a_{\mu\nu}h, \qquad (1.38)
\end{aligned}
$$

The part of the Lagrangian involving only the gauge bosons is given below in $\mathcal{L}_{3V}$ (trilinear couplings) and $\mathcal{L}_{4V}$ (quartic couplings).

$$
\begin{aligned}
\mathcal{L}_{3V} &= \Big[ig^1_{\gamma ww}W^\dagger_{\mu\nu}A^\mu W^\nu + h.c.\Big] + ig^2_{\gamma ww}F_{\mu\nu}W^\mu W^{\nu\dagger} \\
&+ \Big[ig^1_{zww}W^\dagger_{\mu\nu}Z^\mu W^\nu + h.c.\Big] + ig^2_{zww}Z_{\mu\nu}W^\mu W^{\nu\dagger} \qquad (1.39)
\end{aligned}
$$

$$
\begin{aligned}
\mathcal{L}_{4V} &= g_{wwww}\Big[W_\mu W^\mu W^\dagger_\nu W^{\nu\dagger} - W_\mu W^\nu W^\dagger_\nu W^{\mu\dagger}\Big] \\
&+ g_{\gamma\gamma ww}\Big[A_\mu A^\mu W^\dagger_\nu W^\nu - A_\mu A^\nu W^\dagger_\nu W^\mu\Big] \\
&+ g_{zzww}\Big[Z_\mu Z^\mu W^\dagger_\nu W^\nu - Z_\mu Z^\nu W^\dagger_\nu W^\mu\Big] \\
&+ g_{\gamma zww}\Big[A_\mu Z^\mu W^\dagger_\nu W^\nu - A_\mu Z^\nu W^\dagger_\nu W^\mu\Big] \qquad (1.40)
\end{aligned}
$$

The physical coupling expressed in terms of the coefficients of the effective operators in Eq. 1.23 are given in Tables (1.3, 1.4, 1.5 and 1.6).

Coupling	Parametrization
g^1_{hhh}	$1+\frac{5}{2}\bar{c}_6$
g^2_{hhh}	$\frac{g}{m_W}\bar{c}_H$
g^1_{hhhh}	$1+\frac{15}{2}\bar{c}_6$
g^2_{hhhh}	$\frac{g^2}{4m_W^2}\bar{c}_H$

TABLE 1.3: CP-conserving trilinear and quartic couplings strength of the interactions of a Higgs boson with itself.

1.3.4.2 Experimental Constraints on Dimension-6 Effective Operators

An impact of the coefficient associated with the dimension-six operators on the physical observables can be naively computed by a simple power counting. In this way, each power of Φ leads to a $g_{NP}/M \equiv 1/f$ suppression factor, where M is the typical mass scale of the new physics sector and g_{NP} the coupling strength of the new states to the Higgs field. This means that, for strongly coupled systems with $g_{NP} \gg 1$, the scale at which the new physics effects will be seen (f) can be much smaller than M. This power counting leads to the constraints [32]

$$\bar{c}_H, \bar{c}_T, \bar{c}_6, \bar{c}_\psi \sim \mathcal{O}\left(\frac{g_{NP}^2 v^2}{M^2}\right), \qquad \bar{c}_W, \bar{c}_B \sim \mathcal{O}\left(\frac{m_W^2}{M^2}\right)$$
$$\bar{c}_{HW}, \bar{c}_{HB}, \bar{c}_\gamma, \bar{c}_g \sim \mathcal{O}\left(\frac{m_W^2}{16\pi^2 f^2}\right) \tag{1.41}$$

Experimental constraints on the coefficients arising from measurements including electroweak precision data are presented in [85, 88]. Constraints on couplings relevant to this thesis, arising from electroweak precision measurements are

$$\bar{c}_T(m_Z) \in \left[-1.5, 2.2\right] \times 10^{-3}, \qquad \left[\bar{c}_W(m_Z) + \bar{c}_B(m_Z)\right] \in \left[-1.4, 1.9\right] \times 10^{-3} \tag{1.42}$$

Here $\bar{c}_T$ can be neglected, and will not be considered in our further analyses. Note that, $\bar{c}_W$ and $\bar{c}_B$ are not independently constrained, leaving possibility of having large values with cancellation between them as per the above constraint. $\bar{c}_W$ itself, along with $\bar{c}_{HW}$ and $\bar{c}_{HB}$ is constrained from LHC observations on associated

Coupling	Parametrization
g^1_{hgg}	$g_H - \frac{4\bar{c}_g g_s^2 v}{m_W^2}$
$g^1_{h\gamma\gamma}$	$a_H - \frac{8g\bar{c}_\gamma s_W^2 v}{m_W}$
g^1_{hZZ}	$\frac{2g}{c_W^2 m_W}\left[\bar{c}_{HB}s_W^2 - 4\bar{c}_\gamma s_W^4 + c_W^2\bar{c}_{HW}\right]$
g^2_{hZZ}	$\frac{g}{c_W^2 m_W}\left[(\bar{c}_{HW}+\bar{c}_W)c_W^2 + (\bar{c}_B+\bar{c}_{HB})s_W^2\right]$
g^3_{hZZ}	$\frac{gm_Z}{c_W}\left[1-2\bar{c}_T\right]$
$g^1_{h\gamma Z}$	$\frac{gs_W}{c_W m_W}\left[\bar{c}_{HW} - \bar{c}_{HB} + 8\bar{c}_\gamma s_W^2\right]$
$g^2_{h\gamma Z}$	$\frac{gs_W}{c_W m_W}\left[\bar{c}_{HW} - \bar{c}_{HB} - \bar{c}_B + \bar{c}_W\right]$
g^1_{hWW}	$\frac{2g}{m_W}\bar{c}_{HW}$
g^2_{hWW}	$\frac{g}{2m_W}\left[\bar{c}_W + \bar{c}_{HW}\right]$
$(g^1_{hhZZ}, g^2_{hhZZ}, g^2_{hh\gamma Z}, g^1_{hhWW}, g^2_{hhWW})$	$\frac{g}{2m_W}(g^1_{hZZ}, g^2_{hZZ}, g^2_{h\gamma Z}, g^1_{hWW}, g^2_{hWW})$
g^3_{hhZZ}	$\frac{g^2}{2c_W^2}\left[1-6\bar{c}_T\right]$
$g^1_{h\gamma WW}$	$\frac{g^2 s_W}{m_W}\left[2\bar{c}_W + \bar{c}_{HB} + \bar{c}_{HW}\right]$
$g^2_{h\gamma WW}$	$\frac{2g^2 s_W}{m_W}\bar{c}_W$
$g^3_{h\gamma WW}$	$\frac{g^2 s_W}{m_W}\left[\bar{c}_W + \bar{c}_{HW}\right]$
g^1_{hZWW}	$\frac{g^2}{c_W m_W}\left[\bar{c}_{HW}c_W^2 - \bar{c}_{HB}s_W^2 + \bar{c}_W(3-2s_W^2)\right]$
g^2_{hZWW}	$\frac{g^2}{c_W m_W}\left[\bar{c}_{HW} + \bar{c}_W(3-2s_W^2)\right]$
g^3_{hZWW}	$\frac{g^2}{c_W m_W}\left[\bar{c}_{HW} + \bar{c}_W\right]s_W^2$
$g_{hh\gamma\gamma}$	$-\frac{4\bar{c}_\gamma g^2 s_W^2}{m_W^2}$
g_{hhgg}	$-\frac{4\bar{c}_g g_s^2}{m_W^2}$

TABLE 1.4: CP-conserving trilinear and quartic couplings strength of the interactions of a Higgs boson with vector bosons. a_H and g_H are the effective photon and gluon couplings to the Higgs boson in the SM, respectively. $s_W = \sin\theta_W$ and $c_W = \cos\theta_W$, where θ_W is the weak mixing angle.

Coupling	Parametrization
$\tilde{g}_{hgg}$	$-\frac{4\ \tilde{c}_g\ g_s^2}{m_W^2}$
$\tilde{g}_{h\gamma\gamma}$	$-\frac{8\ g\ \tilde{c}_\gamma\ s_W^2}{m_W}$
$\tilde{g}_{hZZ}$	$\frac{2g}{c_W^2 m_W}\left[\tilde{c}_{HB}s_W^2 - 4\tilde{c}_\gamma s_W^4 + c_W^2\tilde{c}_{HW}\right]$
$\tilde{g}_{h\gamma Z}$	$\frac{g s_W}{c_W m_W}\left[\tilde{c}_{HW} - \tilde{c}_{HB} + 8\tilde{c}_\gamma s_W^2\right]$
$\tilde{g}_{hWW}$	$\frac{2\ g}{m_W}\tilde{c}_{HW}$
$\tilde{g}^1_{h\gamma WW}$	$\frac{g^2\ s_W}{m_W}\left[\tilde{c}_{HW} - \tilde{c}_{HB}\right]$
$\tilde{g}^2_{h\gamma WW}$	$\frac{g^2\ s_W}{m_W}\tilde{c}_{HW}$
$\tilde{g}_{hhgg}$	$\frac{-4\tilde{c}_g\ g_s^2}{m_W^2}$
$\tilde{g}^1_{hzWW}$	$\frac{g^2}{c_W m_W}\left[\tilde{c}_{HW}(2 - s_W^2) + \tilde{c}_{HB}s_W^2\right]$
$\tilde{g}^2_{hzWW}$	$\frac{2\ g^2\ c_W}{m_W}\tilde{c}_{HW}$

TABLE 1.5: CP-violating trilinear and quartic couplings strength of the interactions of a Higgs boson with vector bosons.

production of Higgs along with W in Ref. [89]. Consideration of the Higgs associated production along with W, ATLAS and CMS along with D0 put a limit of $\bar{c}_W \in \big[-0.05, 0.04\big]$, when all other parameters are set to zero. A global fit using various information from ATLAS and CMS, including signal-srength information constrains the region in $\bar{c}_W - \bar{c}_{HW}$ plane, leading to a slightly more relaxed limit on $\bar{c}_W$, and a limit of about $\bar{c}_{HW} \in \big[-0.1, 0.06\big]$. The limit on $\bar{c}_{HB}$ estimated using a global fit in Ref. [89] is about $\bar{c}_{HB} \in [-0.05, 0.05]$ with a one parameter fit.

Coupling	Parametrization
$g^1_{\gamma ww}$	$e\left[1-2\bar{c}_W\right]$
$g^2_{\gamma ww}$	$e\left[1-2\bar{c}_W-\bar{c}_{HB}-\bar{c}_{HW}\right]$
g^1_{zww}	$\frac{g}{c_W}\left[c^2_W-\bar{c}_{HW}+(2s^2_W-3)\bar{c}_W\right]$
g^2_{zww}	$\frac{g}{c_W}\left[c^2_W(1-\bar{c}_{HW})+s^2_W\bar{c}_{HB}+(2s^2_W-3)\bar{c}_W\right]$
g_{wwww}	$\frac{g^2}{2}\left[1-2\bar{c}_{HW}-4\bar{c}_W\right]$
$g_{\gamma\gamma ww}$	$e^2\left[2\bar{c}_W-1\right]$
g_{zzww}	$g^2\left[2(2-s^2_W)\bar{c}_W+2\bar{c}_{HW}-c^2_W\right]$
$g_{\gamma zww}$	$\frac{2ge}{c_W}\left[(3-2s^2_W)\bar{c}_W+\bar{c}_{HW}-c^2_W\right]$

TABLE 1.6: Trilinear and quartic gauge boson couplings in terms of the coefficients of effective operators.

1.3.5 Production mechanisms at e^-e^+ colliders

The main Higgs boson production cross-sections at an e^-e^+ collider are the Higgs-strahlung process $e^-e^+ \to Zh$ [90, 91], and the WW fusion process [92–94] $e^-e^+ \to \bar{\nu}_e\nu_e W^*W^* \to \bar{\nu}_e\nu_e h$. As the center-of-mass energy ($\sqrt{s}$) is increased, the cross-section for the Higgs-strahlung process decreases as $\frac{1}{s}$ and is dominant at low energies, while the cross-section for the WW fusion process grows as $\ln(\frac{s}{m_h^2})$ and dominates at high energies. The ZZ fusion mechanism, $e^-e^+ \to e^-e^+Z^*Z^* \to e^-e^+h$, also contributes to Higgs boson production, with a cross-section suppressed by an order of magnitude with respect to that of WW fusion. The process $e^-e^+ \to t\bar{t}h$ [66, 67, 95] becomes relevant for large $\sqrt{s} \geq 500\ GeV$. For more detail see Refs. [35, 96–98].

1.4 The International Linear Collider (ILC)

The ILC [99–103] is a proposed linear particle accelerator, which would be the largest linear collider across the globe, and is intended as a precision machine. It is planned to have a collision energy of 500 GeV initially, with the possibility for a later upgrade to 1000 GeV. Further, its potential can be enhanced by considering options for high energy photon-photon collisions as well as electron-photon collisions. The ILC in principle could be upgraded to very high energies of a few TeV's. The details of such possibility is especially studied in the context of a Compact Linear Collider (CLIC) [104]. Following graphic is showing the dimensions of the ILC machine along with the some detail.

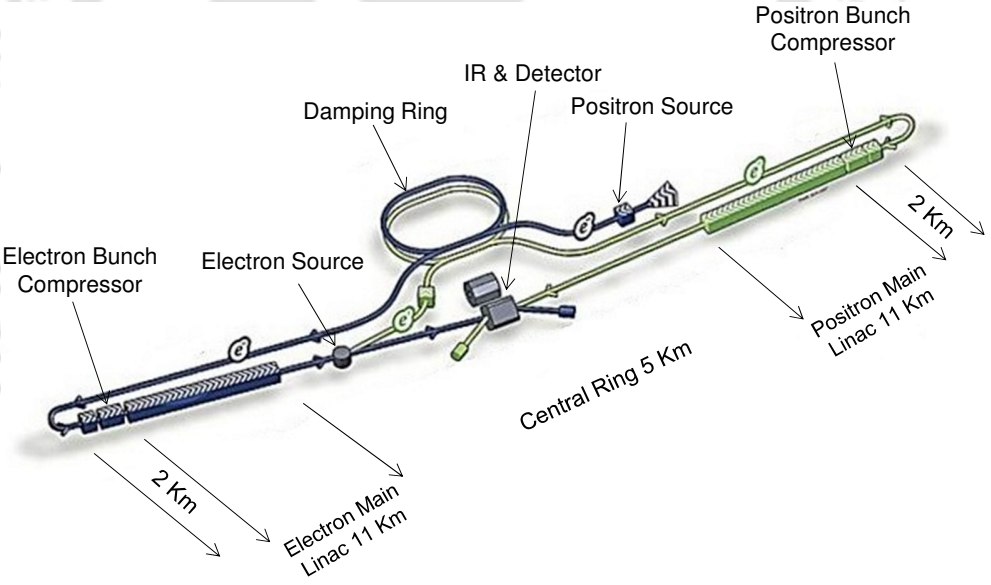

FIGURE 1.12: An overview graphic of the planned ILC based on the accelerator design of the Technical Design Report.

There are many advantages that leptonic colliders have over the hadronic colliders. Having elementary initial states, the energy of the initial state can be controlled precisely, unlike the case of hadron colliders, where the actual initial state for any interaction consists of partons of varying energies. Apart from this, additional features like beam polarization are of great advantage in exploring physics in many cases. Leptonic colliders are expected to be much cleaner machines compared to the hadronic machines. The environment for electron-positron collisions is much more benign. At LHC energies, the proton-proton total cross section is

roughly 100 mb. In the current scheme for running the LHC, proton-proton bunch collisions occur every 50 $nsec$, each bunch crossing leads to about 30 proton-proton collisions, and each of these produces hundreds of energetic particles. At the ILC, the most important chronic background source comes from photon-photon collisions, for which the cross section is hundreds of nb. The difference between hadron-hadron and e^+e^- collisions has profound implications for the detectors and for experimentation.

At a proton-proton collider, one creates collisions at a fixed center of mass energy, relying on the energy distribution of partons in the proton to sample a range of collisions energies for elementary processes. At a circular e^+e^- collider, the maximum energy is preset by the size of the ring, and typically the performance of the accelerator is best just near this maximum energy. An e^+e^- linear collider is more forgiving in terms of operating at different energies and in different running conditions. In principle, it is possible to run at any energy up to the energy set by the length of the machine, with a penalty in luminosity roughly proportional to the reduction in the energy. This flexibility has let the designers of the ILC to envision an experimental programs at series of energies well adapted to individual physics goals.

The ILC machine offers many opportunities for measurements that will address the most important current problems of particle physics. It will give unique views of the Higgs boson, the top quark, and possible new particles relevant to the mysteries of the matter content of the universe. The collider enables measurements of very high precision. The ILC is thus an essential tool that will advance our understanding of the basic laws of nature. On the other hand, extended Higgs bosons have pair-production cross sections that are as substantial as those for other particles with electroweak charges. The comprehensive search for extended Higgs bosons and the precision measurement of the properties of all accessible Higgs particles is thus an important goal for the ILC.

So far, we have discussed the standard mechanism of electroweak symmetry breaking, drawbacks of the SM, the importance of effective Lagrangian theories, obtained constraints on anomalous couplings parameters form various experiments and the current status of Higgs boson. Apart from this, also we have talked about the functioning and the mission of international linear collider (ILC) machine. Next move to the outline of working chapters.

1.4.1 Outline

The thesis is organized into five chapters. The first chapter deals with introduction. The brief description of working chapters are the following.

1.4.1.1 Chapter 2

This chapter concentrates on the study of anomalous $WW\gamma$ coupling in electron-photon collisions at the ILC, where we start with detailed calculation of phase space of considered process $e^-\gamma \to \nu_e W^- \to \nu_e \bar{\nu}_\mu \mu^-$. We carry out our study in a model independent framework under the consideration of narrow width approximation (NWA). Moreover we show how the suitably chosen observables in the center of mass frame connected with the laboratory frame. Next we examine which quantities are experimentally observable, estimate the accuracy with which they can be measured, and calculate their dependence on anomalous coupling parameters $\delta\kappa_\gamma$ and λ_γ which are directly connected to the $WW\gamma$ coupling. Finally, we present the effect of angular and muon energy cuts on chosen observables and their deviations from the SM for all the possible combinations of anomalous coupling parameter. Apart from all these, we present forward-backward asymmetry in the angular distributions and its deviation from the SM.

1.4.1.2 Chapter 3

This chapter starts with the discussion of trilinear Higgs self coupling in the Zhh production as well as $\nu_e \bar{\nu}_e hh$ at ILC, and its role, in order to understand the mechanism of electroweak symmetry breaking. Next we move to the framework of Higgs effective Lagrangian which involves dimension-six operators. After that we discuss the obtained bounds from various experiments, on CP-conserving couplings parameters. Finally we present the influence of Higgs to gauge bosons couplings on determination of hhh coupling through the single parameter analyses as well as kinematic distributions like angular, transverse momentum, energy, and invariant mass distributions. Also we present the correlation between parameters which are directly connected to the Higgs self coupling.

1.4.1.3 Chapter 4

This begins with the brief discussion of CP-violating couplings in the Higgs sector. The WWh production at ILC will be considered for our study. We present the sensitivity of CP-violating couplings parameters trough single and two parameter analyses. Apart from the total cross section against center of mass energy ($\sqrt{s}$), we present various kinematic distributions like transverse momentum, angular, invariant mass distributions. Also we illustrate how the effect of CP-violating couplings influenced in the presence of CP-conserving couplings. Next we deals with forward-backward asymmetry in the angular distribution and a table summarizes its deviation from the SM.

1.4.1.4 Chapter 5

This chapter provides the over all summary and conclusions.

Chapter 2

Anomalous $WW\gamma$ Coupling

This chapter is devoted to the study of anomalous $WW\gamma$ coupling in $e^{-}\gamma$ collisions at the ILC. It starts with introduction of problem and its formulation in effective Lagrangian framework, and then moves to the general set-up and analysis of the process being considered. This will be followed by a discussion of the numerical results of the study, and finally summary and conclusion of the work.

2.1 Introduction

With the recent discovery of the Higgs boson by the LHC [8, 9, 49, 50], the Standard Model (SM) has reaffirmed itself as the theoretical explanation of elementary particle dynamics, including presenting a plausible picture of Electroweak Symmetry Breaking (EWSB) [3, 4] through the Higgs mechanism. While this is so, and not withstanding the fact that SM has been extensively tested very successfully by many different experiments [1], it is widely believed that the SM is an effective theory, which needs to incorporate suitable modifications at large energies. Many expect that this large energy scale could be as small as a few TeV, which is being explored at the LHC. Apart from direct measurements of the properties of the Higgs boson, like its interaction couplings with itself, as well as with gauge bosons and fermions, signature of EWSB could be probed by understanding the structure and values of gauge-boson self interactions. This is so, because the longitudinal degrees of freedom of the gauge bosons arise from the Higgs sector. The discovery of Higgs boson of about 126 GeV mass, while establishing the Higgs mechanism

as the method of EWSB, has opened an era of Higgs precision studies. Being a hadronic machine, LHC has limitations to undertake precision studies. The ILC proposed to collide high energy, high luminosity electrons and positrons has the mission of studying the SM at high precision and to look for signals beyond the standard model [34, 35]. Such a machine is well suited to an in-depth analysis of the gauge boson interactions, within and beyond the SM. A large number of physics studies establish the fact that the potential of ILC is further enhanced by considering high energy photon-photon collisions as well as electron-photon collisions, apart from the electron-positron collisions.

It is obvious that, the $e\gamma$ and $\gamma\gamma$ colliders are better suited to study the photon couplings with other gauge bosons like the γWW, $\gamma\gamma WW$, γZZ and $\gamma\gamma Z$ [105]. In this chapter, we will focus on $e\gamma \to \nu W$ with $W \to l\bar{\nu}$. Signature of such an event is a single lepton with large missing energy. This process is sensitive to new physics effects including anomalous γWW [106–108], composite fermion models [37], etc. In the case of anomalous γWW couplings, this process has the advantage over $e^+e^- \to W^+W^-$ [109], which is sensitive to both γWW and WWZ couplings. Again, $\gamma\gamma \to W^+W^-$ [40, 110] is sensitive to γWW, $\gamma\gamma WW$ and $\gamma\gamma Z$ couplings, revealing the edge of $e\gamma$ collider to study γWW. In most of the previous studies, observables at the production level of the single W are investigated, with the exception of Ref. [107, 108], where the authors considered angular spectrum of the secondary leptons, also including the effect of off-shell W. Our main aim of this work is to study the possibility to exploit the secondary lepton spectrum including the energy and angular distributions to probe relevant new physics signals arising in anomalous γWW coupling.

In many models beyond the SM the quartic and triple-gauge boson couplings including $\gamma WW$are altered from their SM values. In a model independent approach, an effective Lagrangian with terms additional to the SM Lagrangian is considered in phenomenological and experimental studies [65]. Relevant to the process considered here, the effective γWW vertex is commonly parametrized in terms of $\delta\kappa_\gamma$ and λ_γ, in the absence of CP-violation (with vanishing SM values). LEP constraints in single-parameter analysis (taking one parameter at a time, keeping the others at their SM values) gives bounds of $-0.099 < \delta\kappa_\gamma < +0.066$ and $-0.059 < \lambda_\gamma < +0.017$ and two-parameter analysis limits their values to $-0.072 < \delta\kappa_\gamma < +0.127$ and $-0.068 < \lambda_\gamma < +0.023$ [76, 111] at 95% C.L. Tevatron constraints from $W\gamma$ process are not contaminated by other couplings, but are more

Process	Advantages	Disadvantages
$e^-e^+ \to W^-W^+$	1- The interference terms are more significant and therefore more sensitive to the couplings. 2- Well defined initial polarization state could be made use of.	1- Relatively smaller cross-section. 2- Both $WW\gamma$ and WWZ are involved.
$e^-\gamma \to W^-\nu_e$	1- Large cross-section which does not fall with $\sqrt{s}$. 2- Relatively simple final states, without much background. 3- Involve only $WW\gamma$ couplings.	1- W can not be reconstructed in case of leptonic decays. 2- Requires photon beam option at ILC.
$\gamma\gamma \to W^-W^+$	1- Larger cross-section which saturates with $\sqrt{s}$. 2- Couplings enter twice in the amplitude, making it more sensitive.	1- Sensitive to $Z\gamma\gamma$ and $WW\gamma\gamma$coupling. 2- Requires photon beam option at ILC.

TABLE 2.1: Advantages and disadvantages of chosen process of $e\gamma$ collisions over e^-e^+ and $\gamma\gamma$ collisions.

relaxed compared to the LEP constraints giving limits of $-0.51 < \delta\kappa_\gamma < +0.51$ and $-0.12 < \lambda_\gamma < +0.13$ [112]. The CMS constraints [9] from $W\gamma$ process are also more relaxed compared to the LEP constraints.

Phenomenology of anomalous γWW coupling in the context of LHC as well as ILC has been carried out in a number of recent publications [64, 106–108, 110, 113–116]. In particular, [107, 108] has analyzed single W production with its leptonic decay to probe the effect of anomalous couplings in $e\gamma$ collision. In this work we exploit the full potential of the secondary lepton spectrum to study the effect of γWW coupling in $e\gamma \to \nu W \to \nu(l\bar{\nu})$ with $\delta\kappa_\gamma$ and λ_γ deviating from its SM value.

The main reason to choose the process $e^-\gamma \to \nu_e W^-$ instead of $e^-e^+ \to W^-W^+$, $\gamma\gamma \to W^-W^+$ for the study of $WW\gamma$ processes is summarized in Table 2.1. In the next section we provide some details of the process and the observables used. In Section 3 we present our numerical results, and finally summarize the study and present our conclusions in the last section.

2.2 General Setup and Analysis

The most general CP-conserving γWW coupling within a Lorentz invariant effective Lagrangian can be written in the following form [65].

$$\mathcal{L}_{\gamma WW} = -ie\left[W^{\dagger}_{\mu\nu}W^{\mu}A^{\nu} - W^{\dagger}_{\mu}A_{\nu}W^{\mu\nu} + (1+\delta\kappa_{\gamma})\, W^{\dagger}_{\mu}W_{\nu}F^{\mu\nu} + \frac{\lambda_{\gamma}}{m_W^2}\, W^{\dagger}_{\lambda\mu}W^{\mu}_{\ \nu}\, F^{\lambda\nu}\right] \tag{2.1}$$

Here we have assumed an on-shell W boson. In the SM, the gauge structure $SU(2)_L \times U(1)_Y$ dictates the γWW couplings, with vanishing $\delta\kappa_{\gamma}$ and λ_{γ} at tree level. Therefore, precise measurements of these couplings will test the gauge sector of the electroweak interactions. Fig. 2.1 shows the Feynman diagrams for the process along with the momentum labels.

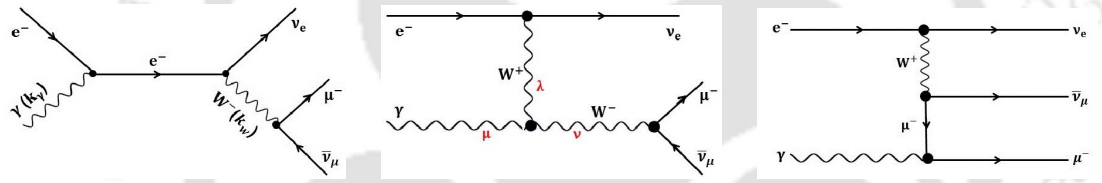

FIGURE 2.1: Feynman diagrams for the process $e\gamma \to \nu W \to \nu(\mu\bar{\nu})$. First diagram shows the momenta used and second diagram shows the indices used in the vertex in Eq. 2.2

With the effective Lagrangian given by Eq. 2.1, the γWW vertex for the process under study (Fig. 2.1) takes the form:

$$\begin{aligned}\Gamma^{\mu\nu\lambda} \;=\; & ie\left[2k_w^{\mu}\, g^{\nu\lambda} + 2k_{\gamma}^{\nu}\, g^{\mu\lambda} - (k_{\gamma}+k_w)^{\lambda}\, g^{\mu\nu}\right. \\ & +(\delta\kappa_{\gamma}-\lambda_{\gamma})\,(k_{\gamma}^{\nu}\, g^{\mu\lambda} - k_{\gamma}^{\lambda}\, g^{\mu\nu}) \\ & \left.+\frac{\lambda_{\gamma}}{m_W^2}(k_{\gamma}+k_w)^{\lambda}(k_w^{\mu}k_{\gamma}^{\nu} - (k_{\gamma}\cdot k_w)g^{\mu\nu})\right]\end{aligned} \tag{2.2}$$

The effective Lagrangian in Eq. 2.1 should be considered as a low energy approximation of some fundamental theory, which is expected to emerge at some high energy scale, Λ. To control unitarity violation at high energy, when this Lagrangian is used, we consider the anomalous couplings as form factors according

to the following [107]

$$A = \frac{A_0}{\left[\left(1+\frac{|k_w^2|}{\Lambda^2}\right)\left(1+\frac{|(k_\gamma - k_w)^2|}{\Lambda^2}\right)\right]}, \tag{2.3}$$

where $A_0 \equiv \delta\kappa_\gamma,\ \lambda_\gamma$.

2.2.1 Phase Space

The differential cross-section is written in terms of the phase space factor (dQ') and the Lorentz invariant amplitude (M) as,

$$d\sigma = \frac{dQ'}{F}\,|M|^2 \tag{2.4}$$

where F is the flux factor, which is equal to $2\sqrt{\hat{s}}$ in center of mass frame. We perform our computation in the Narrow-Width Approximation (NWA) in which the W-propagator is approximated to get

$$\frac{1}{|k_w^2 - m_W^2|^2} = \frac{\pi}{m_W \Gamma_W}\,\delta(k_w^2 - m_W^2), \tag{2.5}$$

where m_W is the mass and Γ_W is the total width of the W boson. Thus the propagator factor, $\frac{1}{|k_w^2 - m_W^2|^2}$ is removed from the invariant amplitude, and joined with the phase space factor, dQ' so that,

$$d\sigma = \frac{dQ}{F}\,|M_r|^2 \tag{2.6}$$

where $dQ = \frac{1}{(k_w^2 - m_W^2)^2}\,dQ'$ and $|M|^2 = \frac{1}{(k_w^2 - m_W^2)^2}\,|M_r|^2$.

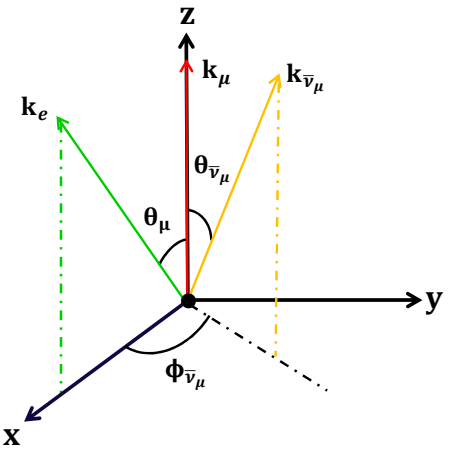

FIGURE 2.2: Reference frame defining different angles used in Eq. 2.7.

To perform phase space integrations we fix our reference frame as the center of mass frame (CMF) of the colliding electron and photon system. z-axis is taken along $\vec{k_\mu}$, which is the momentum of the outgoing lepton (considered as muon in the further discussion) as pictured in Fig. 2.2. y-axis is defined as $\vec{k_\mu} \times \vec{k_e}$, where $\vec{k_e}$ is the momentum of the colliding electron. The $\bar{\nu}_\mu$ comes out at a polar angle $\theta_{\bar{\nu}_\mu}$ and azimuthal angle $\phi_{\bar{\nu}_\mu}$. Explicitly, the momenta of initial and final particles in the process being considered, $e^-(k_e)\ \gamma(k_\gamma) \to \nu_e\ W^-(k_w) \to \nu_e(k_{\nu_e})\ \bar{\nu}_\mu(k_{\bar{\nu}_\mu})\ \mu^-(k_\mu)$ are given as

$$\begin{aligned}
k_e &= \frac{\sqrt{\hat{s}}}{2}\Big(1,\quad \sin\theta_\mu,\quad 0,\quad \cos\theta_\mu\Big) \\
k_\gamma &= \frac{\sqrt{\hat{s}}}{2}\Big(1,\quad -\sin\theta_\mu,\quad 0,\quad -\cos\theta_\mu\Big) \\
k_\mu &= E_\mu\ \Big(1,\quad 0,\quad 0,\quad 1\Big) \\
k_{\bar{\nu}_\mu} &= E_{\bar{\nu}_\mu}\Big(1,\quad \sin\theta_{\bar{\nu}_\mu}\cos\phi_{\bar{\nu}_\mu},\quad \sin\theta_{\bar{\nu}_\mu}\sin\phi_{\bar{\nu}_\mu},\quad \cos\theta_{\bar{\nu}_\mu}\Big) \\
k_w &= k_\mu + k_{\bar{\nu}_\mu}
\end{aligned} \tag{2.7}$$

where $\sqrt{\hat{s}}$ is the center of mass energy of $e^-\gamma$ system. The phase space factor is then,

$$\begin{aligned}
dQ &= \frac{d^3\vec{k}_{\nu_e}}{(2\pi)^3\ 2E_{\nu_e}}\ \frac{d^3\vec{k}_\mu}{(2\pi)^3\ 2E_\mu}\ \frac{d^3\vec{k}_{\bar{\nu}_\mu}}{(2\pi)^3\ 2E_{\bar{\nu}_\mu}}\ (2\pi)^4\ \delta^4(k_e + k_\gamma - k_{\nu_e} - k_\mu - k_{\bar{\nu}_\mu}) \\
&\quad \times \frac{1}{|k_w^2 - m_W^2|^2},
\end{aligned} \tag{2.8}$$

Applying the NWA, and using the integral identity,

$$\int \frac{d^3\vec{k}_{\nu_e}}{(2\pi)^3} = \int d^4k_{\nu_e}\Theta(E_{\nu_e})\delta(k^2_{\nu_e}) \tag{2.9}$$

Eq. 2.8 takes the form

$$\begin{aligned} dQ &= \frac{d^3\vec{k}_\mu\ d^3\vec{k}_{\bar{\nu}_\mu}}{(2\pi)^5\ 4\ E_\mu E_{\bar{\nu}_\mu}} \frac{\pi}{m_W\Gamma_W}\delta(k_w^2 - m_W^2) \\ &\quad \times\delta^4(k_e + k_\gamma - k_{\nu_e} - k_\mu - k_{\bar{\nu}_\mu})\ d^4k_{\nu_e}\ \Theta(E_{\nu_e})\ \delta(k^2_{\nu_e}) \\ &= \frac{\pi\ d^3\vec{k}_\mu\ E^2_{\bar{\nu}_\mu}\ d\cos\theta_{\bar{\nu}_\mu}}{(2\pi)^5\ 4\ E_\mu E_{\bar{\nu}_\mu}\ m_W\Gamma_W}\ d\phi_{\bar{\nu}_\mu}\ \Theta(E_{\nu_e})\ \delta(k^2_{\nu_e})\ \delta(k_w^2 - m_W^2), \end{aligned} \tag{2.10}$$

where the second line is obtained after performing the k_{ν_e} integration, resulting in the relation $k_{\nu_e} = k_e + k_\gamma - k_\mu - k_{\bar{\nu}_\mu}$. This also leads to the relations,

$$k^2_{\nu_e} = \hat{s} - 2\sqrt{\hat{s}}(E_\mu + E_{\bar{\nu}_\mu}) + m_W^2 \tag{2.11}$$

and

$$\left(k_w^2 = m_W^2\right) = \left(k_\mu + k_{\bar{\nu}_\mu}\right)^2 = 2\ E_\mu E_{\bar{\nu}_\mu}(1 - \cos\theta_{\bar{\nu}_\mu}). \tag{2.12}$$

After using Eq. 2.7, 2.11 and 2.12, phase space factor takes the following form,

$$dQ = \frac{\pi\ d^3\vec{k}_\mu\ d\phi_{\bar{\nu}_\mu}\ dE_{\bar{\nu}_\mu}}{(2\pi)^5\ 16\ \sqrt{\hat{s}}\ E_\mu^2\ \Gamma_W\ m_W}\delta\left(\frac{\hat{s} - 2\sqrt{\hat{s}}\ E_\mu + m_W^2}{2\ \sqrt{\hat{s}}} - E_{\bar{\nu}_\mu}\right)\Theta(E_{\nu_e})$$

along with the relation

$$\cos\theta_{\bar{\nu}_\mu} = \frac{2E_\mu E_{\bar{\nu}_\mu} - m_W^2}{2E_\mu E_{\bar{\nu}_\mu}} \tag{2.13}$$

Now after integrating over $dE_{\bar{\nu}_\mu}$, we are left with,

$$dQ = \frac{\pi\ d^3\vec{k}_\mu\ d\phi_{\bar{\nu}_\mu}}{(2\pi)^5\ 16\ \sqrt{\hat{s}}\ E_\mu^2\ \Gamma_W\ m_W}\Theta(E_{\nu_e})$$

along with the relation

$$E_{\bar{\nu}_\mu} = \frac{(\hat{s} - 2\sqrt{\hat{s}}\ E_\mu + m_W^2)}{2\ \sqrt{\hat{s}}}. \tag{2.14}$$

In order to identify with the experimental set up, we shall now rotate the reference frame so as to coincide the z-axis with the direction of electron beam, by a rotation about the y-axis. This leads to $d^3\vec{k_\mu} = |\vec{k_\mu}|^2\ d|\vec{k_\mu}|\ d\cos\theta_\mu\ d\phi_\mu =$

$E_\mu^2\ dE_\mu\ d\cos\theta_\mu\ d\phi_\mu$, and the Eq. 2.14 becomes,

$$dQ \;=\; \frac{\pi\ E_\mu^2\ dE_\mu\ d\cos\theta_\mu\ d\phi_\mu\ d\phi'_{\bar{\nu}_\mu}}{(2\pi)^5\ 16\ m_W\ \Gamma_W\ E_\mu^2\ \sqrt{\hat{s}}}\ \Theta(E_{\nu_e}). \tag{2.15}$$

Since, in the present case, the invariant amplitude does not depend on the azimuthal angle of muon, the ϕ_μ integration becomes trivial to give a factor of 2π. Defining the dimensionless parameter $x_\mu = \frac{2E_\mu}{\sqrt{\hat{s}}}$, the Eq. 2.15 now takes the form

$$dQ \;=\; \frac{dx_\mu\ d\cos\theta_\mu\ d\phi'_{\bar{\nu}_\mu}}{(2\pi)^3\ 64\ m_W\ \Gamma_W}.$$

The step function $\Theta(E_{\nu_e})$ is removed, with the understanding that the condition $E_{\nu_e} > 0$ is imposed in the computations. With this phase space factor one obtains the differential cross-section

$$\frac{d\sigma}{dx_\mu\ d\cos\theta_\mu\ d\phi'_{\bar{\nu}_\mu}} = \frac{x_\mu}{(2\pi)^3\ 128\ m_W\ \Gamma_W}|M_r|^2. \tag{2.16}$$

$|M_r|^2$ is obtained using FORM computational package [117]. After integrating the unobservable $\phi'_{\bar{\nu}_\mu}$, we get the double distribution of energy and polar angle of the secondary muon in the center of mass frame of the colliding particles with the electron momentum now taken along the redefined z-axis. Notice that the muon energy in the CMF is bounded by $\frac{m_W^2}{2\sqrt{\hat{s}}} \le E_\mu \le \frac{\sqrt{\hat{s}}}{2}$. To obtain the distribution in the lab frame, we need to boost the above differential cross-section appropriately. For an electron beam energy of E_e and photon energy of $\omega_\gamma = x\ E_e$, we have the following relation between the variables in the CMF and the laboratory frame.

$$\hat{s} = x\ 4E_e^2, \qquad E_\mu = E_\mu^{lab}\ \gamma\ \left(1 - \beta\ \cos\theta_\mu^{lab}\right), \qquad \cos\theta_\mu = \frac{\cos\theta_\mu^{lab} - \beta}{1 - \beta\ \cos\theta_\mu^{lab}} \tag{2.17}$$

where β is the speed of the CMF compared to the lab frame, and $\gamma = \frac{1}{\sqrt{1-\beta^2}}$. Notice that the limits of E_μ^{lab} integration depends on $\cos\theta_\mu^{lab}$, keeping it within the bound

$$\frac{m_W^2}{4\sqrt{x}E_e}\frac{1}{\gamma\left(1-\beta\cos\theta_\mu^{lab}\right)} \le E_\mu^{lab} \le \frac{\sqrt{x}E_e}{\gamma\left(1-\beta\cos\theta_\mu^{lab}\right)}. \tag{2.18}$$

Finally we need to fold the cross-section with the appropriate photon distribution function, $f_{\gamma/e}(x)$, an expression for which is provided in the Appendix-A, so that

the total cross-section in the lab frame is given by

$$\sigma = \int f_{\gamma/e}(x)\ \sigma(\hat{s})\ dx. \tag{2.19}$$

The photon beam polarization effects are neglected as described in Appendix-A.2. We use Eqs. 2.16, 2.17, 2.19 to obtain the total cross-section, the muon angular distribution $\frac{d\sigma}{d\cos\theta_\mu^{lab}}$, the scaled muon energy distribution $\frac{d\sigma}{dx_\mu^{lab}}$, and the energy-angle distribution of the muons $\frac{d\sigma}{dx_\mu^{lab}\ d\cos\theta_\mu^{lab}}$ in the lab frame. Integrations over the photon distribution variable x, the scaled muon energy x_μ^{lab} and the muon angular variable $\cos\theta_\mu^{lab}$ in appropriate cases are performed numerically using the `Cuhre` routines under the `CUBA` package [118]. From now on we will drop the superscript *lab* from the variables, and use x_μ and $\cos\theta_\mu$ to denote the corresponding quantities in the lab frame.

Phenomenological analysis of $e\gamma \to \nu W$ is considered in the literature in the past [106–108]. Most of the studies limit their analysis at the production level. Experimentally it is more useful to understand the effect on the final state particles arising from W decay. This is all the more important in the case of leptonic decay, as it is not possible to reconstruct the W in such case. In Ref. [107], analysis including decay spectrum is presented, where detailed study of the secondary lepton angular distribution is considered along with other reconstructed observables concerning the W production. In the analysis presented here, we demonstrate the usefulness of the combined energy-angle distribution of the secondary leptons in extracting information on the anomalous γWW couplings. While Ref. [107] takes into account the contribution due to off-shell W along with the on-shell production, our work is in the NWA assuming on-shell W production. At the same time, as note above, the effect of off-shell contribution, mainly arising through the diagram with muon propagator, is negligible, while our analysis with energy-angle double distributions, along with combinations of the angular and energy distributions give a handle on disentangling the effect of $\delta\kappa_\gamma$ and λ_γ, to certain extend.

2.2.2 Calculation Scheme

We have used FORM [117] program which is widely used to simplify the algebraic expressions. We used the FORM particularly to simplify the Dirac algebra. The FORM code used in our study can be seen in the Appendix-B. Ultimately, it provides simplified expression of invariant amplitude square which is used in a

FORTRAN code incorporating the CUBA package (a library for multi-dimensional integration) [118], in order to get the suitably chosen kinematic distributions. Finally, the data is analyzed and the plotted using Gnuplot [119]. The flow chart of the computation scheme can be seen in Fig. 2.3.

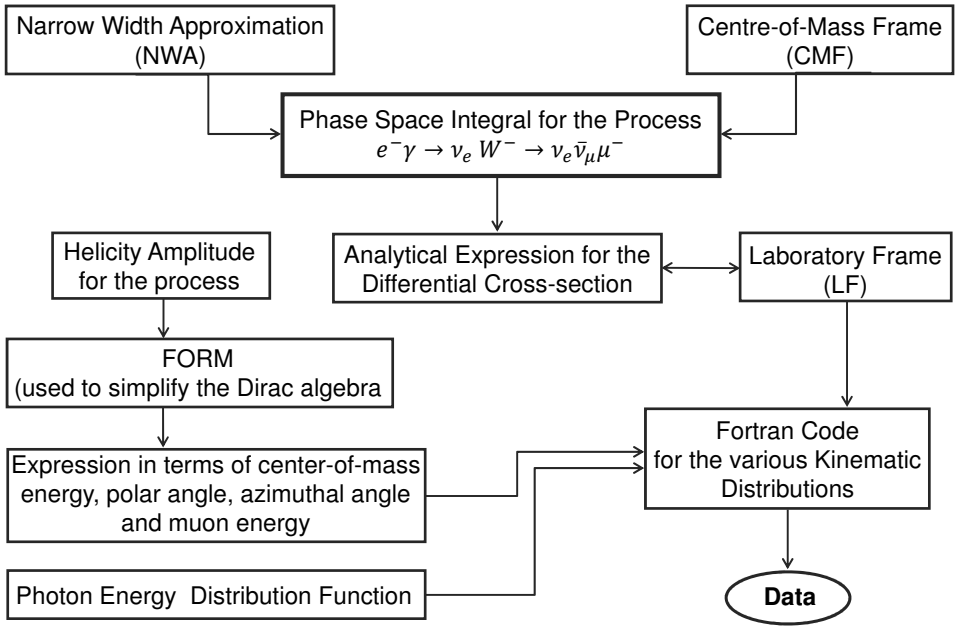

FIGURE 2.3: Flow chart for the calculation scheme used in the analyses of the considered process $e^-\gamma \to \nu_e W^-$.

2.3 Numerical Results and Discussion

For our numerical analysis we consider an ILC of center of mass energy of 500 GeV and 1000 GeV, with the option of $e\gamma$ collision using backscattered laser photons, and with unpolarized electron beams. It may be noted that as the process being considered is a purely a weak interaction process, only left-handed electrons will take part. Therefore, the left-polarized electron beam would enhance the cross-section, without presenting any additional advantage. We shall present all our analysis for unpolarized beam, without losing any generality.

Firstly, we consider the total cross-section. Fig. 2.4, shows the total cross-section against the center of mass energy of the e^-e^- system (denoted as $\sqrt{s}$), one of which Compton-scatters on the laser beam to produce the high energy photon

beam. In order to be more quantitative, in Table 2.2, we have presented the cross-sections for the limiting values of the couplings for two selected center of mass energy values, $\sqrt{s} = 500\ GeV$ and $1000\ GeV$. Taking individually separately, the effect of λ_γ is negligible, with a maximum of about 7% for negative values at $1000\ GeV$ center of mass energy. On the other hand, the effect of $\delta\kappa_\gamma$ is at about 10% level at both $500\ GeV$ as well as $1000\ GeV$. It may be noted that the effect is sensitive to the sign of the parameter, indicating that the interference term is dominant, as expected. At $500\ GeV$, one can ignore the effects of λ_γ even when considering along with $\delta\kappa_\gamma$, whereas at $1000\ GeV$, the presence of λ_γ can either nullify or enhance considerably the effect of $\delta\kappa_\gamma$. Largest effect is seen when $\delta\kappa_\gamma$ is positive and λ_γ is negative, with about 20% deviation in the total cross-section at $1000\ GeV$.

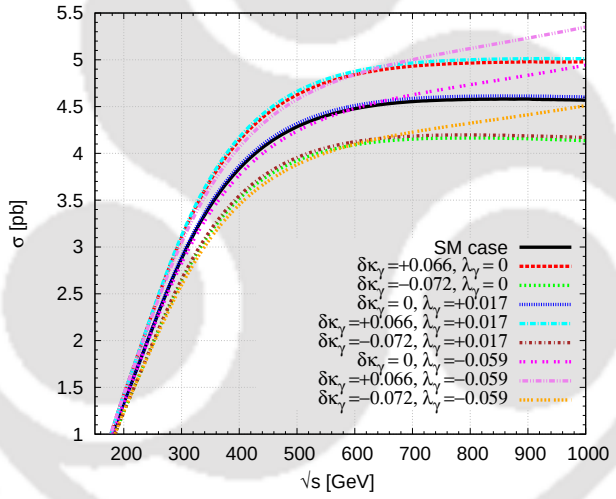

FIGURE 2.4: Total cross-section against $\sqrt{s} = 2E_e$, where E_e is the electron beam energy, for different anomalous couplings, along with the SM case.

In the surface plots shown in Fig.2.5, variation of the cross-section with $\delta\kappa_\gamma$ and λ_γ at center-of-mass energy of $500\ GeV$ and $1000\ GeV$ are presented. The cross-section looks more pronounced for positive values of $\delta\kappa_\gamma$ for any value of λ_γ within its allowed domain. The two-parameter bound showing the allowed region in the $\delta\kappa_\gamma - \lambda_\gamma$ plane is presented in Fig.2.6, at center-of-mass energy of $500\ GeV$ with an integrated luminosity of $100\ fb^{-1}$. We remind the reader that, when cross-section is considered as a function of anomalous coupling parameters $\delta\kappa_\gamma$ and λ_γ, the result is a second order polynomial in these two parameters. With this, the 3σ limit of the cross-section with an integrated luminosity of $100\ fb{-}1$ leads to an elliptic equation corresponding to the relation between these two parameters.

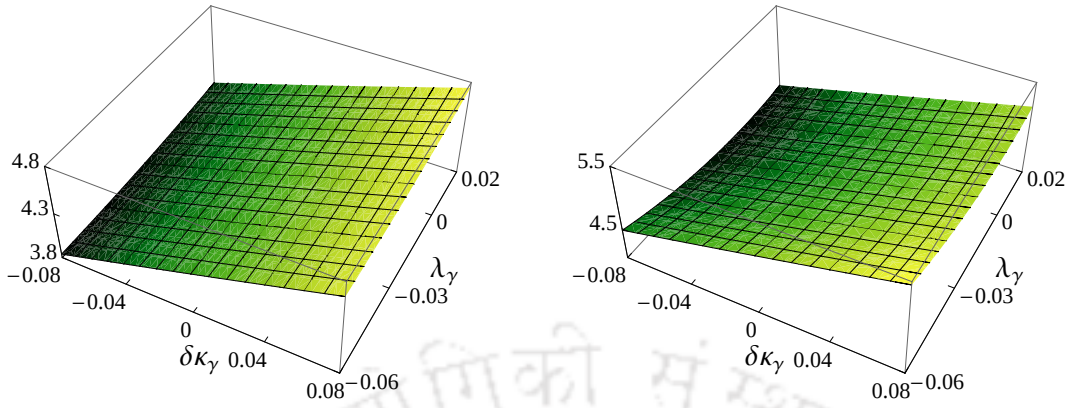

FIGURE 2.5: The surface plots showing the total cross-section against $\delta\kappa_\gamma$ and λ_γ for the center-of-mass energy ($\sqrt{s}$) of 500 GeV (left) and 1000 GeV (right), where cross-section in pb is along the vertical axis.

This results in an elliptic band in the $\delta\kappa_\gamma - \lambda_\gamma$ plane respecting the 3σ limit of the cross-section. Very strong bound on $\delta\kappa_\gamma$ can be derived for any assumed value of λ_γ. On the other hand, for small values of $\delta\kappa_\gamma$ the sensitivity of cross-section on λ_γ is comparatively smaller. At the same time, the relative sign of the parameters is preferred to be opposite to each other.

$\delta\kappa_\gamma$,	λ_γ	σ [pb]	
		$\sqrt{s} = 500$ GeV	1000 GeV
SM case		4.3	4.6
+0.066,	0	4.6	5.0
-0.072,	0	3.9	4.1
0,	+0.017	4.3	4.6
0,	-0.059	4.2	4.9
+0.066,	+0.017	4.7	5.0
+0.066,	-0.059	4.6	5.4
-0.072,	+0.017	4.0	4.2
-0.072,	-0.059	3.9	4.5

TABLE 2.2: Total cross-section for different combinations of TGC parameters at $\sqrt{s} = 500$ GeV and 1000 GeV.

Moving on to the single parameter, sensitivity of cross-section on one parameter, while the other one is fixed is presented in Fig. 2.7, for center of mass energies of 500 GeV and 1000 GeV. The green band shows the 3σ region of the SM value of the cross-section, considering an integrated luminosity of 100 fb^{-1}. The cross-section has a linear dependence on $\delta\kappa_\gamma$, showing that the contribution proportional

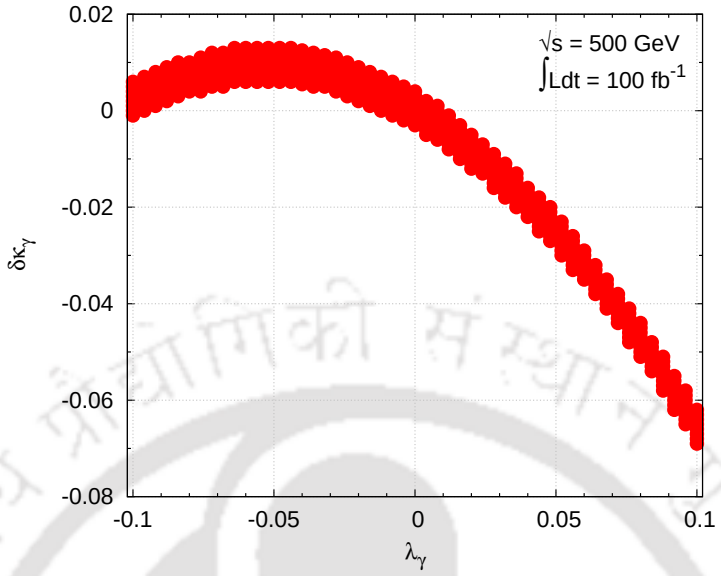

FIGURE 2.6: The shaded region corresponds to values of $\delta\kappa_\gamma - \lambda_\gamma$ with the total cross-section within the 3σ limit, for an integrated luminosity of 100 fb^{-1} at a center of mass energy of 500 GeV.

to the quadratic term is negligible. The 3σ allowed range of $\delta\kappa_\gamma$ shifts with the value of λ_γ. Although, as Table 2.2 suggests, the effect of λ_γ is small compared to that of large $\delta\kappa_\gamma$ values, the influence is significant for derivable limits as can be read from Fig. 2.7. For example, at 500 GeV center of mass energy, assuming $\lambda_\gamma = 0$, one obtain a 3σ limit of $-0.004 \leq \delta\kappa_\gamma \leq +0.004$, which is moved to about $-0.008 \leq \delta\kappa_\gamma \leq 0$ for $\lambda_\gamma = 0.01$, or moved to $0 \leq \delta\kappa_\gamma \leq +0.008$ for $\lambda_\gamma = -0.014$. We shall see later that, a combined analysis including kinematic distributions of the muon can remove this ambiguity to a great extend. A similar story, although different in nature, can be seen in the case of limit derivable for λ_γ as well.

We next consider the angular distribution of the secondary muons plotted in Fig. 2.8 for different combinations of $\delta\kappa_\gamma$ and λ_γ, at center of mass energies of 500 GeV and 1000 GeV. As can be seen, the effect is more pronounced at smaller $\cos\theta_\mu$ values, while most of the events are gathered in the forward direction. With high luminosity, one can expect high statistics for single W production at $e\gamma$ collider. In such case the tail region could also perhaps be probed. The effect is analyzed for all the combinations of TGC parameters. In Table 2.3 the deviation from SM case is illustrated by considering a bin of $-0.90 \leq \cos\theta_\mu \leq -0.85$ with an integrated luminosity of 100 fb^{-1}. Clearly the deviations are magnified when

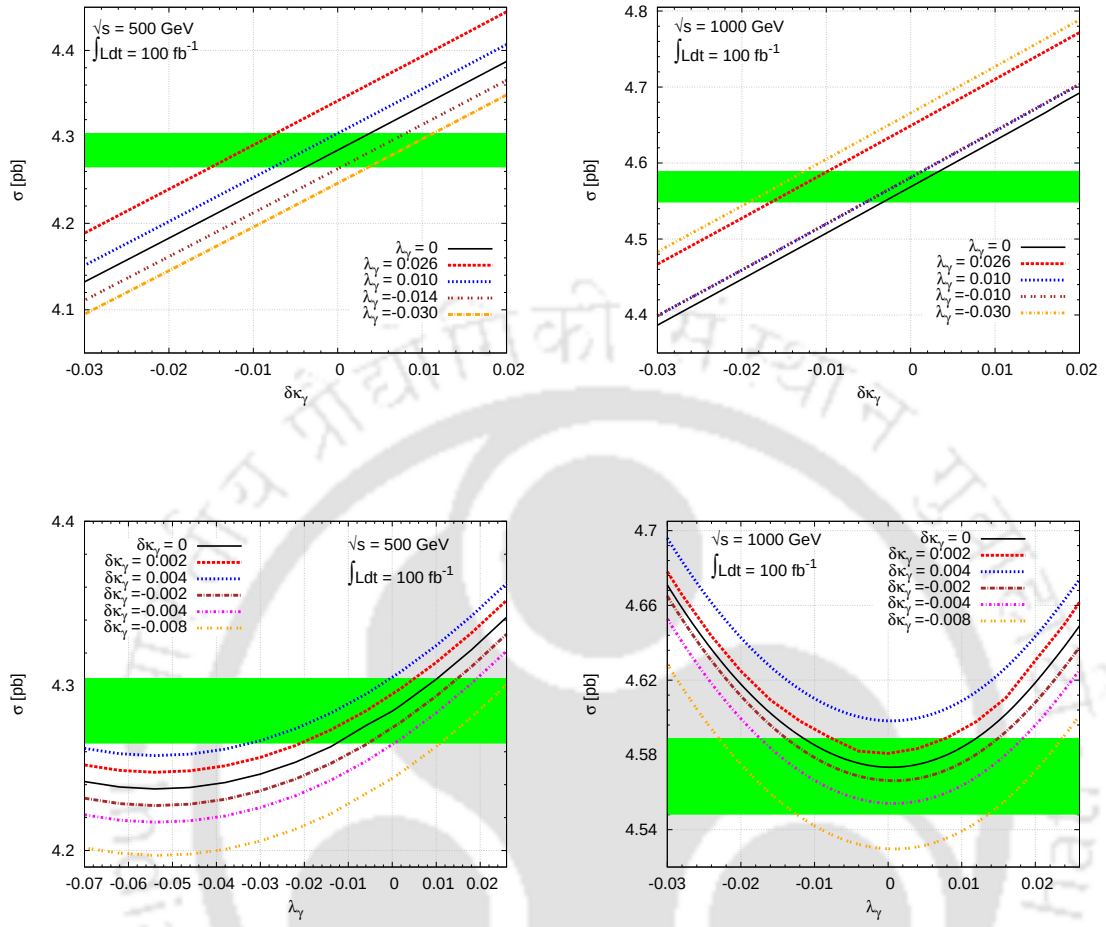

FIGURE 2.7: Cross section against $\delta\kappa_\gamma$ (top row) and λ_γ (bottom row), when the other parameter assume typical values. The center of mass energies considered are $\sqrt{s} = 500\ GeV$ (left column) and $1000\ GeV$ (right column). The green band indicates the 3σ limit of the SM cross-section, with integrated luminosity of 100 fb^{-1}.

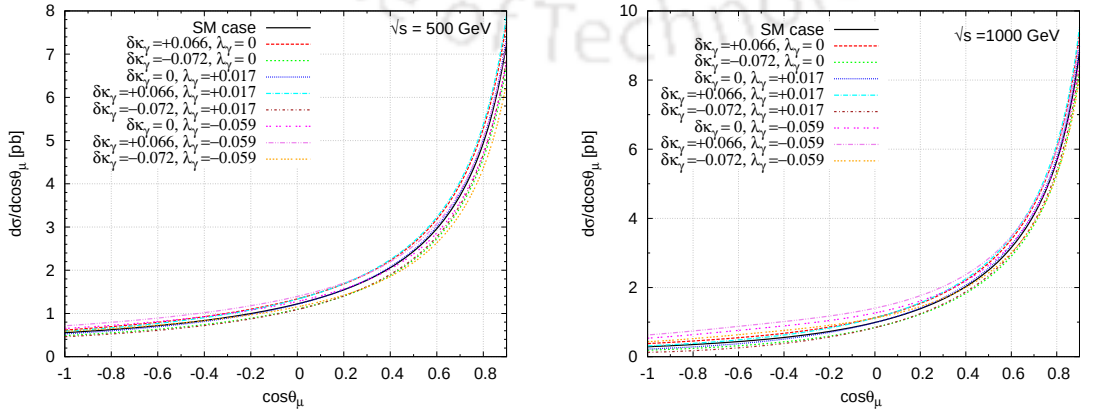

FIGURE 2.8: The angular distribution for different combinations of $\delta\kappa_\gamma$ and λ_γ for the two different values of $\sqrt{s} = 500\ GeV$ (left) and $1000\ GeV$ (right).

Sl. No.	$\delta\kappa_\gamma$	λ_γ	$\sqrt{s} = 500\ GeV$		$1000\ GeV$	
			N_{events}	Δ [%]	N_{events}	Δ [%]
1	SM case		2900	0	1600	0
2	0.066	0	3250	12	2100	31
3	-0.072	0	2600	−10	1100	−31
4	0	0.017	2800	−3	1250	−22
5	0	-0.059	3400	17	2850	78
6	0.066	0.017	3100	7	1700	6
7	0.066	-0.059	3750	30	3900	144
8	-0.072	0.017	2400	−17	750	−53
9	-0.072	-0.059	3050	5	2350	43

TABLE 2.3: The number of events within $-0.90 \leq \cos\theta_\mu \leq -0.85$ for different combinations of $\delta\kappa_\gamma$ and λ_γ at $\sqrt{s} = 500\ GeV$ and $1000\ GeV$, along with the corresponding deviation from the SM case. An integrated luminosity of 100 fb^{-1} is considered.

specific angular regions are considered, compared to the integrated total cross-section. This is more so in the case of $1000\ GeV$, compared to $500\ GeV$. For certain combinations of the parameter values, the forward-backward asymmetry, defined as

$$A_{FB} = \left[\frac{\int_{-1}^{0} \frac{d\sigma}{d\cos\theta_\mu} d\cos\theta_\mu - \int_{0}^{1} \frac{d\sigma}{d\cos\theta_\mu} d\cos\theta_\mu}{\int_{-1}^{0} \frac{d\sigma}{d\cos\theta_\mu} d\cos\theta_\mu + \int_{0}^{1} \frac{d\sigma}{d\cos\theta_\mu} d\cos\theta_\mu}\right] \tag{2.20}$$

$$\Delta A_{FB}(\%) = \frac{\left|A_{FB}^{Ano.} - A_{FB}^{SM}\right|}{A_{FB}^{SM}} \times 100. \tag{2.21}$$

is considerably different compared to that of the SM case. In Fig. 2.9, this asymmetry is presented for different combinations of the parameter values. The green band shows the region falls within 10% deviation from the SM values. While the A_{FB} alone does not seems to be very important, a combination of the cross-section measurement (total or in a particular angular bin) along with the measurements of the asymmetry may constrain the possible $\delta\kappa_\gamma$-λ_γ combinations. For example, about 30-40 % increase in the cross-section in angular region $-0.90 \leq \cos\theta_\mu \leq -0.85$ could be due to cases 2, 5, 7 or 9 shown in Table 2.3. Among these, case 2 correspond to positive $\delta\kappa_\gamma$, which could be ruled out in case of more than 10% A_{FB}. A more thorough and complete such analysis could constrain the allowed combinations more effectively.

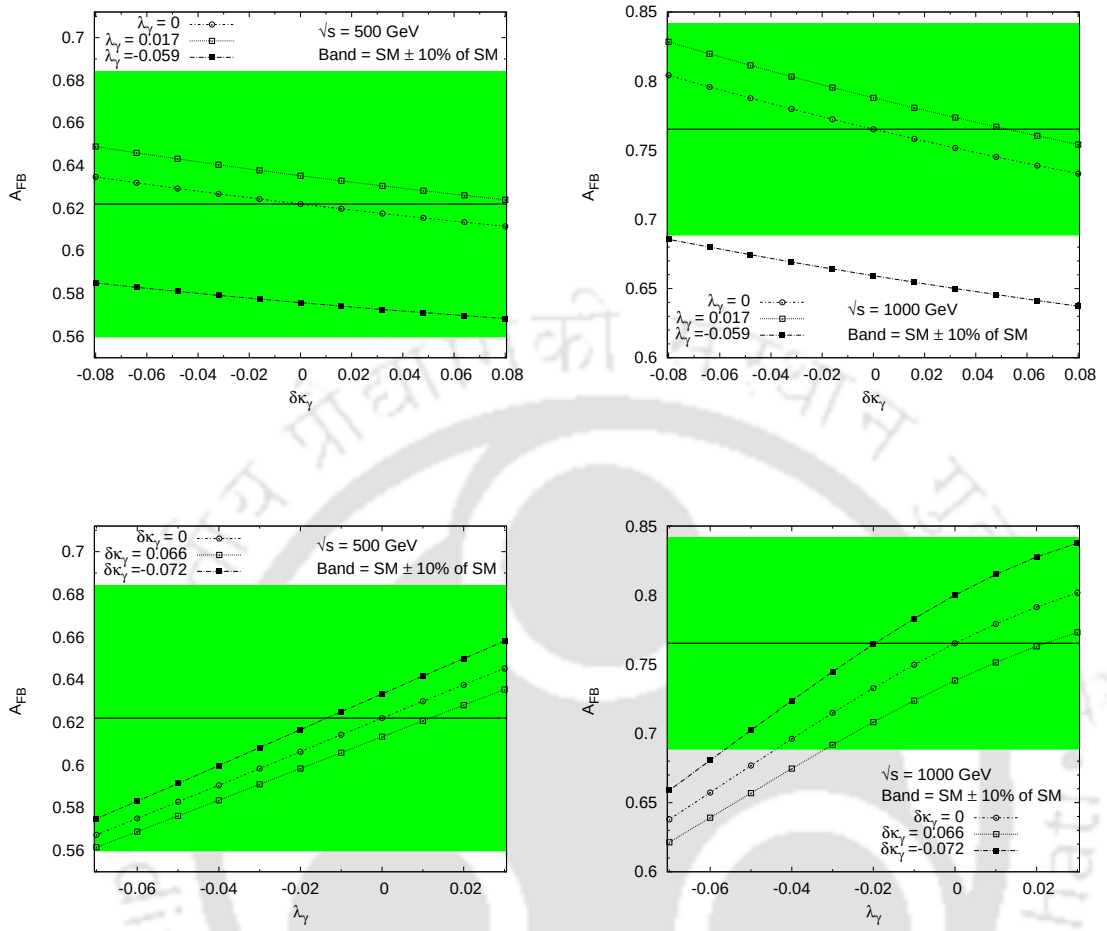

FIGURE 2.9: The forward-backward asymmetry against $\delta\kappa_\gamma$ (top row) and λ_γ (bottom row) at $\sqrt{s} = 500\ GeV$ (left) and $1000\ GeV$ (right). The green band corresponds to a $\pm 10\%$ deviation from the SM case.

We next consider the energy distribution of the muon. In Fig.2.10, the energy distribution against $x_\mu = \frac{E_\mu}{E_e}$, where E_e is the electron beam energy and E_μ is the energy of final muon, is presented, showing the effect of anomalous couplings for different combination of TGC parameters at $\sqrt{s}$ of 500 GeV and 1000 GeV. The first row presents the case integrating over the entire $\cos\theta_\mu$ region, while the second row considers only the backward region. Once again, we emphasis that it is only through a combination of different observables that one may be able to disentangle information regarding the $\delta\kappa_\gamma$ and λ_γ couplings. In the present case, for example, corresponding to $\delta\kappa_\gamma = -0.072$ and $\lambda_\gamma = -0.059$ at $\sqrt{s} =$ 500 GeV, the enhancement at low energy values is quite pronounced when only the backward hemisphere is considered, compared to the full angular region. A similar effect, but now diminishing, is seen in the case of $\delta\kappa_\gamma = 0$ and $\lambda_\gamma = +0.017$ at $\sqrt{s} = 1000$ GeV. In Table 2.4 we illustrate this effect quantitatively,

presenting deviations at specific x_μ values. As mentioned above, at 500 GeV collider the qualitatively different behavior of the case of $\delta\kappa_\gamma = -0.072$ and $\lambda_\gamma = -0.059$ is clearly demonstrated. These examples show that close scrutiny of the distributions could give additional handle in distinguishing the effects of different possible parameter combinations. A more detailed picture could be made available by exploiting the energy-angle double distribution. In Fig. 2.11 and 2.12 energy distributions at fixed angle, corresponding to center of mass energies of 500 GeV and 1000 GeV, respectively, are presented. Case with negative values of λ_γ shows diminishing effect in the forward region, which switches to enhancing effect in the backward region. Positive λ_γ shows the opposite effect. In Table 2.5 and 2.6 quantitative illustration of the above for specific x_μ and $\cos\theta_\mu$ values are presented. The large deviations seen in the case of 1000 GeV center of mass energy, at large angles promise possibility to probe the couplings to small values. At the same time, one must keep in mind the proper unitarization of the parameters, while deriving such limits. As our aim is to identify observables sensitive to the anomalous couplings, rather than deriving the quantitative estimate of the reach of the collider in their measurements, we do not dwell on these details. In fact, any attempt of quantitative estimate of this kind should also take into account other collider and detector effects in a proper fashion, which is somewhat premature at this stage.

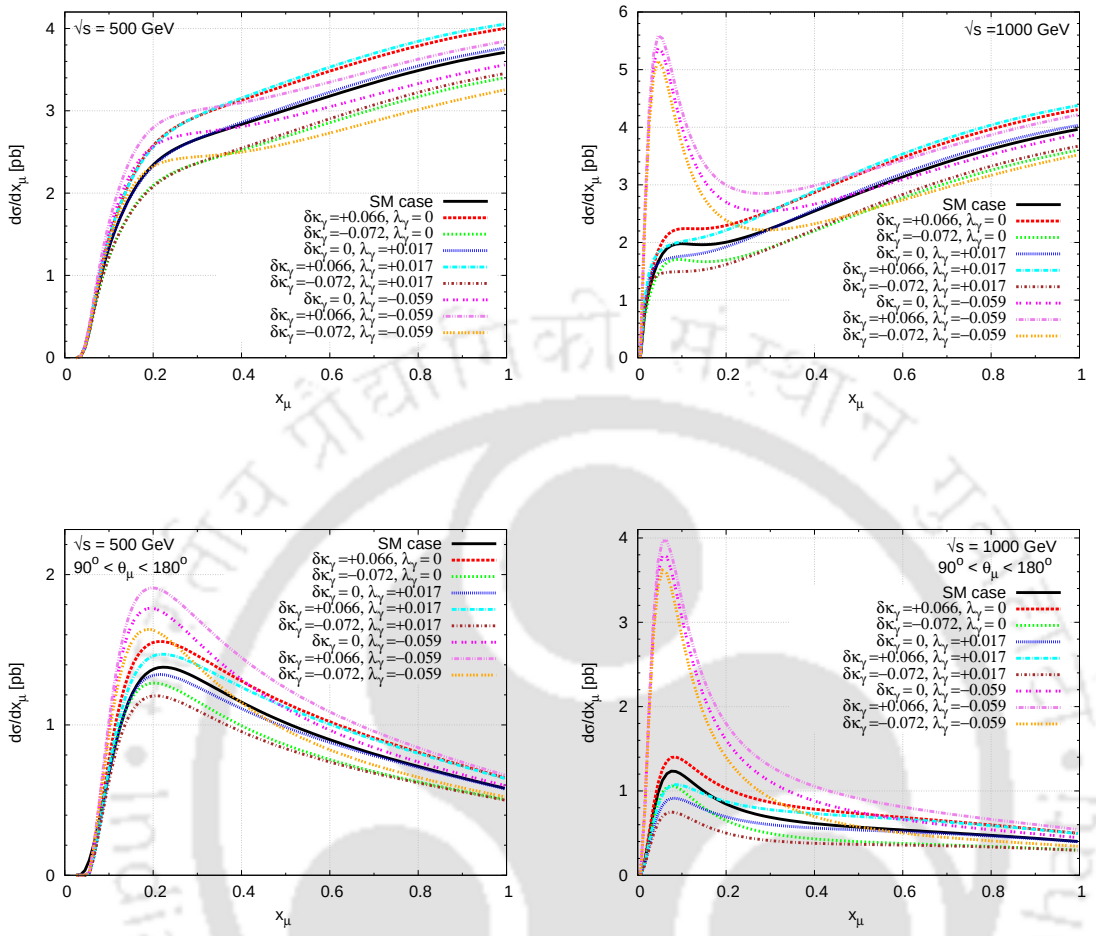

FIGURE 2.10: The energy distribution of the secondary muon for different combinations of $\delta\kappa_\gamma$ and λ_γ, compared with the SM case. The bottom row considers only the backward hemisphere. Center of mass energies considered are $\sqrt{s} = 500\ GeV$ (left) and $1000\ GeV$ (right).

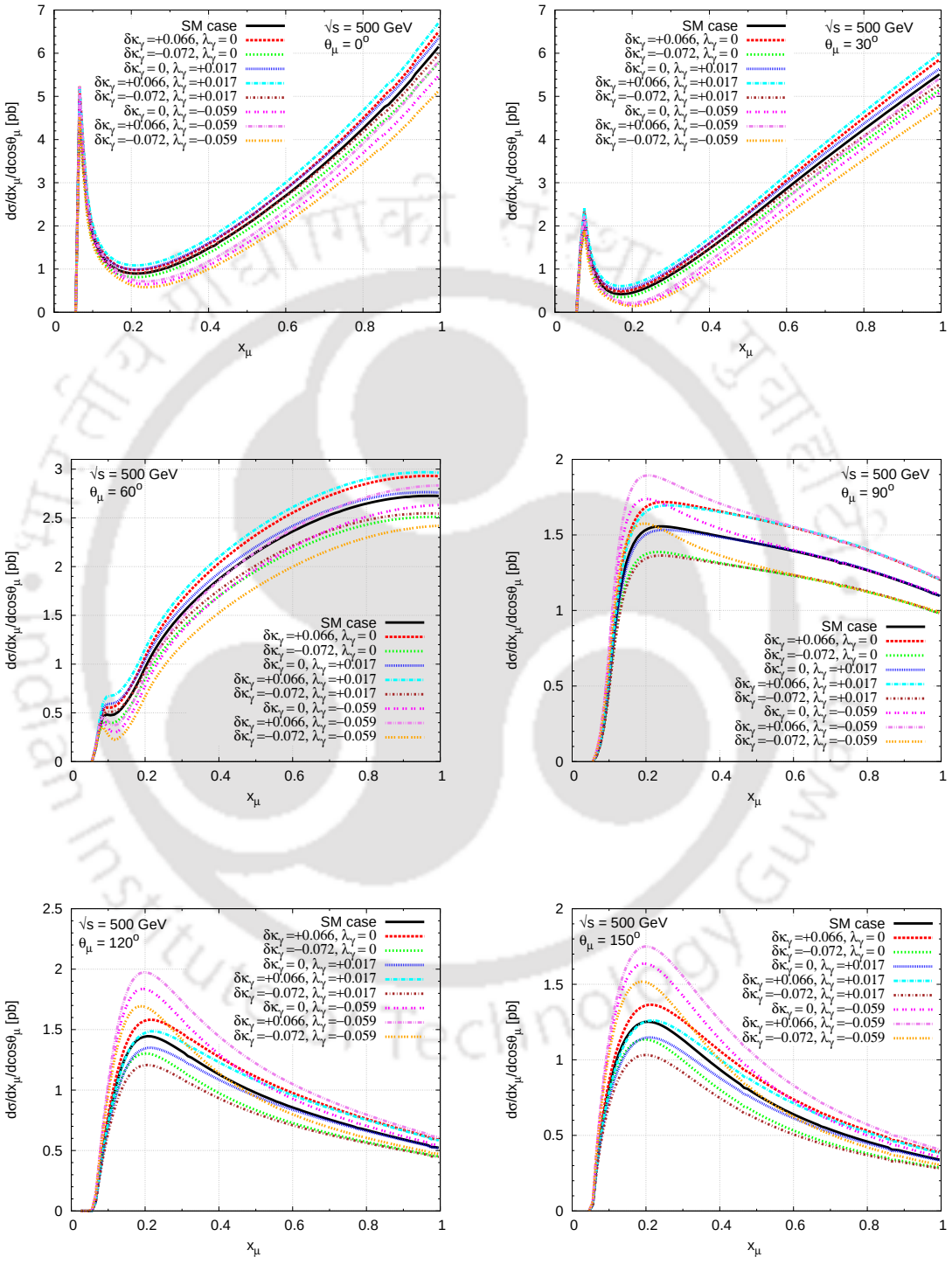

FIGURE 2.11: The energy distribution of the secondary muon for different combinations of $\delta\kappa_\gamma$ and λ_γ, considered at fixed muon angles (θ_μ) for $\sqrt{s} = 500\ GeV$.

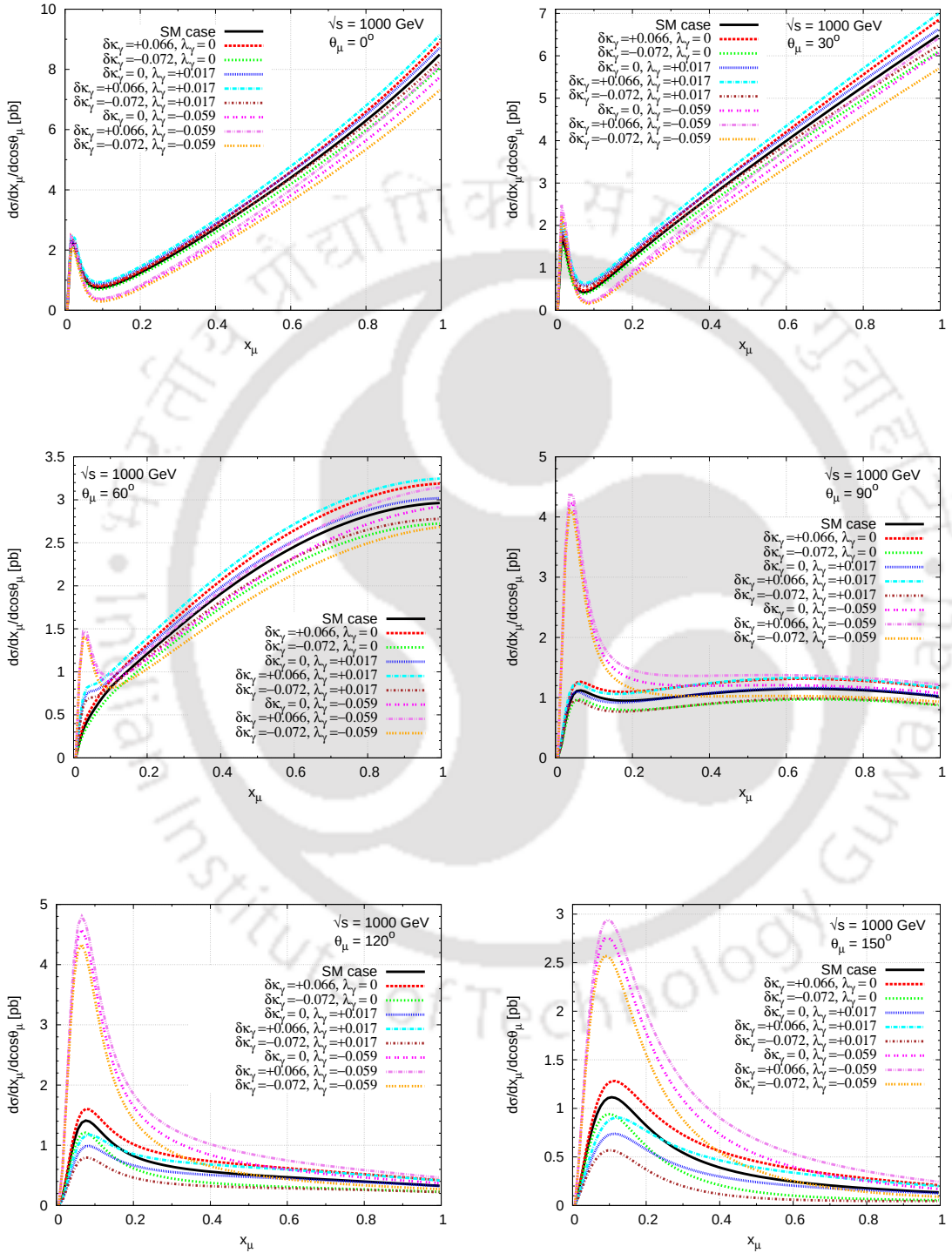

FIGURE 2.12: The energy distribution of the secondary muon for different combinations of $\delta\kappa_\gamma$ and λ_γ, considered at muon angles (θ_μ) for $\sqrt{s} = 1000\ GeV$.

$\delta\kappa_\gamma$	λ_γ	$\sqrt{s} = 500\ GeV$ $(0.2 \le x_\mu \le 0.25)$				$\sqrt{s} = 1000\ GeV$ $(0.03 \le x_\mu \le 0.08)$			
		Full angular region		$90^o \le \theta_\mu \le 180^o$		Full angular region		$90^o \le \theta_\mu \le 180^o$	
		N_{events}	Δ [%]	N_{events}	Δ [%]	N_{events}	Δ [%]	N_{events}	Δ [%]
SM	case	12200	0	7000	0	10000	0	6800	0
0.066	0	13600	11.5	7600	8.6	10500	5	7300	7.4
-0.072	0	11000	−10	6300	−10	8600	−14	5900	−13
0	0.017	12100	−1	6600	−6	8500	−15	4800	−29
0	-0.059	13300	9	8800	26	28000	180	22400	229
0.066	0.017	13600	12	7300	4	9900	1	5500	−19
0.066	-0.059	13700	12	9500	36	29500	195	23400	244
-0.072	0.017	10900	−11	5800	−17	7500	−25	4000	−41
-0.072	-0.059	12000	−2	12000	71	26600	166	21300	213

TABLE 2.4: The number of events within specified x_μ bins for different combinations of $\delta\kappa_\gamma$ and λ_γ at $\sqrt{s} = 500\ GeV$ and $1000\ GeV$, along with the corresponding percentage deviation (Δ) from the SM case. Two cases of (i) full angular region, and (ii) the backward hemisphere alone, are separately presented. An integrated luminosity of 100 fb^{-1} is considered.

$\sqrt{s} = 500\ GeV$		$\theta_\mu = 30^o$ $x_\mu = 0.95 - 1.0$		$\theta_\mu = 60^o$ $x_\mu = 0.95 - 1.0$		$\theta_\mu = 90^o$ $x_\mu = 0.056 - 0.106$		$\theta_\mu = 120^o$ $x_\mu = 0.056 - 0.106$		$\theta_\mu = 150^o$ $x_\mu = 0.056 - 0.106$	
$\delta\kappa_\gamma$	λ_γ	N_{events}	Δ [%]	N_{events}	Δ [%]	N_{events}	Δ [%]	N_{events}	Δ [%]	N_{events}	Δ [%]
SM Case		24500	0	13500	0	7750	0	7250	0	6200	0
0.066	0	26150	7	14550	8	8000	3	7900	9	6750	9
-0.072	0	23000	−6	12450	−8	6900	−11	6400	−12	5650	−9
0	0.017	25350	4	13750	2	7600	−2	6750	−7	5750	−7
0	-0.059	22250	−9	13000	−4	8700	12	9000	24	8250	33
0.066	0.017	26900	10	14750	9	8250	7	7400	2	6250	1
0.066	-0.059	24000	−2	14000	4	9400	21	9750	35	8750	41
-0.072	0.017	23500	−4	12650	−6	6750	−13	6000	−17	5250	−15
-0.072	-0.059	20900	−15	11900	−12	7850	1	8200	13	7500	21

TABLE 2.5: The number of events within specified x_μ bins, and for fixed θ_μ, for different combinations of $\delta\kappa_\gamma$ and λ_γ at $\sqrt{s} = 500\ GeV$, along with the corresponding percentage deviation (Δ) from the SM case. An integrated luminosity of 100 fb^{-1} is considered.

$\sqrt{s} = 1000\ GeV$		$\theta_\mu = 30^o$ $x_\mu = 0.95 - 1.0$		$\theta_\mu = 60^o$ $x_\mu = 0.95 - 1.0$		$\theta_\mu = 90^o$ $x_\mu = 0.056 - 0.106$		$\theta_\mu = 120^o$ $x_\mu = 0.056 - 0.106$		$\theta_\mu = 150^o$ $x_\mu = 0.056 - 0.106$	
$\delta\kappa_\gamma$	λ_γ	N_{events}	Δ [%]	N_{events}	Δ [%]	N_{events}	Δ [%]	N_{events}	Δ [%]	N_{events}	Δ [%]
SM case		31250	0	14750	0	5000	0	6100	0	6000	0
0.066	0	33000	6	15900	8	5750	15	7200	18	7000	17
-0.072	0	29250	−6	13600	−8	4250	−15	5400	−2	5000	−17
0	0.017	32000	2	15000	2	4750	−5	4730	−2	4000	−33
0	-0.059	29100	−7	14500	−2	8750	75	16000	162	14500	141
0.066	0.017	33950	9	16225	10	5400	8	5850	−4	4750	−21
0.066	-0.059	30850	−1	15600	6	4500	−9	17100	180	15500	158
-0.072	0.017	30000	−4	13850	−6	4000	−20	3500	−43	3000	−50
-0.072	-0.059	27350	−13	13300	−10	8000	60	14800	142	13400	123

TABLE 2.6: The number of events within specified x_μ bins, and for fixed θ_μ, for different combinations of $\delta\kappa_\gamma$ and λ_γ at $\sqrt{s} = 1000\ GeV$, along with the corresponding percentage deviation (Δ) from the SM case. An integrated luminosity of 100 fb^{-1} is considered.

The features discussed above can be made more visible also through the angular distribution considered at fixed muon energies. In Fig. 2.13 and 2.15, the angular distributions of the muon at $x_\mu = 0.1,\ 0.2,\ 0.5, 1$ are presented for center of mass energy of 500 GeV and 1000 GeV, respectively. The figures reiterate the conclusions drawn from the energy distributions considered at different angle, above. The case of $\lambda_\gamma = 0$, positive, and negative can be possibly distinguished by the fact that, (i) the $\lambda_\gamma < 0$ case enhances the cross-section for large angles, while reducing it for forward angles, (ii) the $\lambda_\gamma > 0$ has the opposite effect of reducing the cross-section for large angles, while increasing it for smaller angles, (iii) the $\lambda_\gamma = 0$ case shows a monotonous effect for all angles. The effect is seen to be more pronounced in the low energy region. Please note that $x_\mu = 0.2$ corresponds to $E_\mu = 50$ GeV for 500 GeV collider, and $E_\mu = 100$ GeV for 1000 GeV collider, and therefore are very much in the efficiently-detectable range of values.

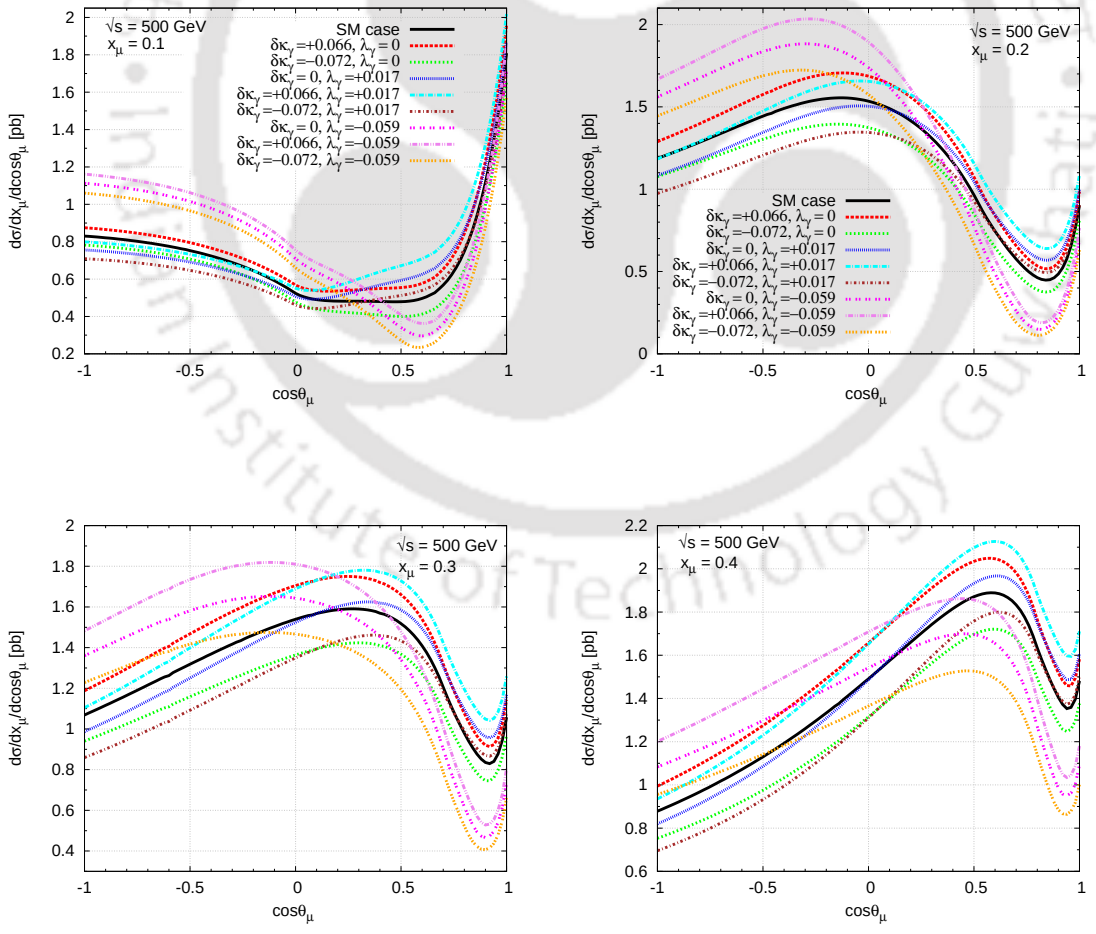

FIGURE 2.13: The energy-angle distribution of the secondary muon for different combinations of $\delta\kappa_\gamma$ and λ_γ, considered at fixed muon energy parameter (x_μ) at $\sqrt{s}$ of 500 GeV. The colour coding is the same in all plots.

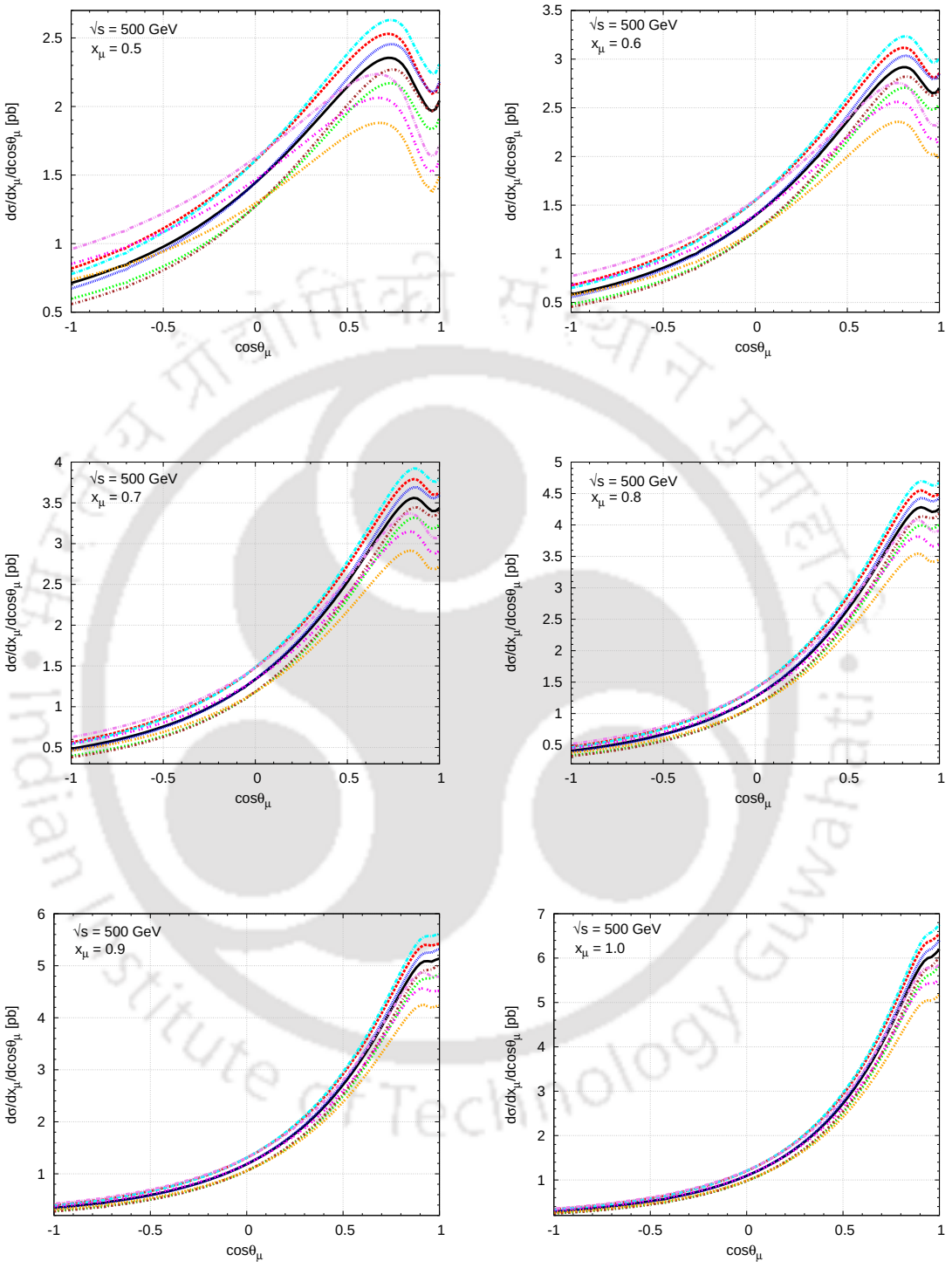

FIGURE 2.14: The energy-angle distribution of the secondary muon for different combinations of $\delta\kappa_\gamma$ and λ_γ, considered at fixed muon energy parameter (x_μ) at $\sqrt{s}$ of 500 GeV. The colour coding is the same as in Fig. 2.13.

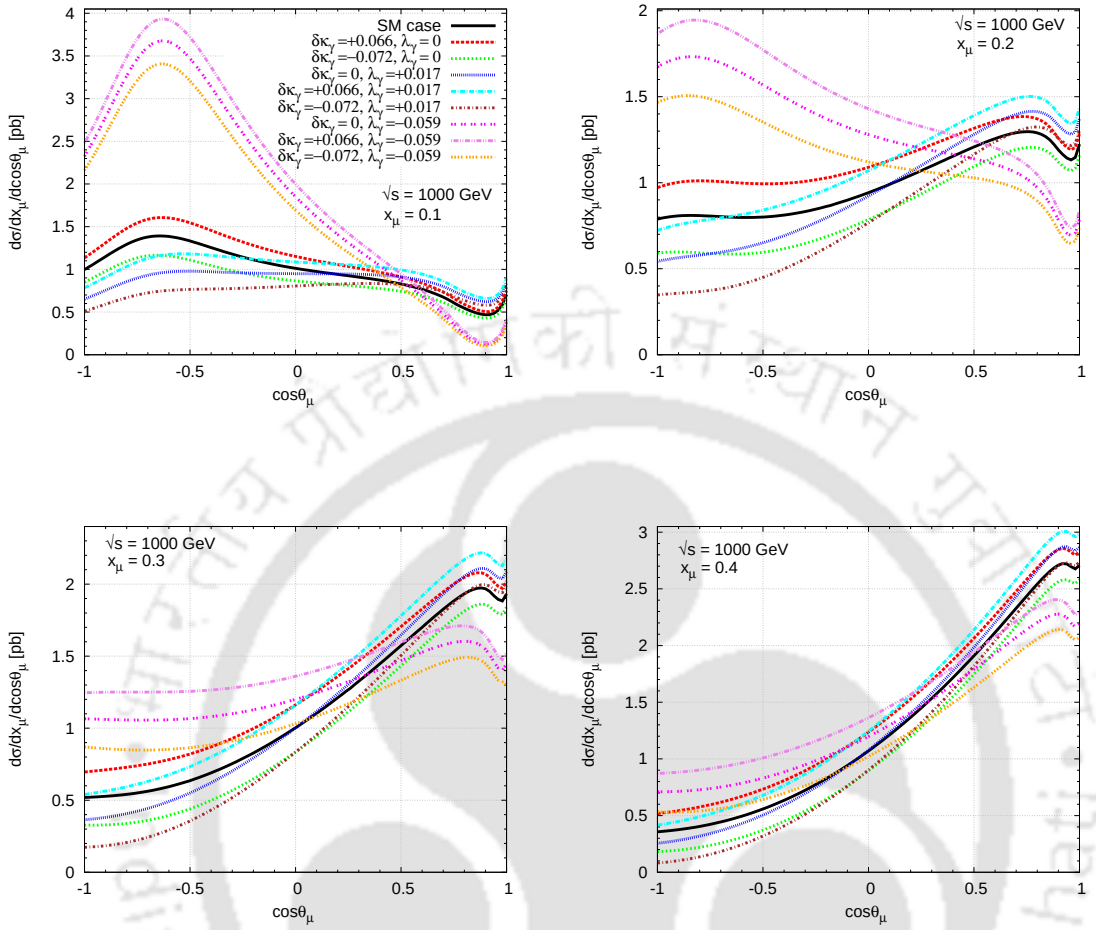

FIGURE 2.15: The energy-angle distribution of the secondary muon for different combinations of $\delta\kappa_\gamma$ and λ_γ, considered at fixed muon energy parameter (x_μ) at $\sqrt{s}$ of 1000 GeV. The colour coding is the same in all plots.

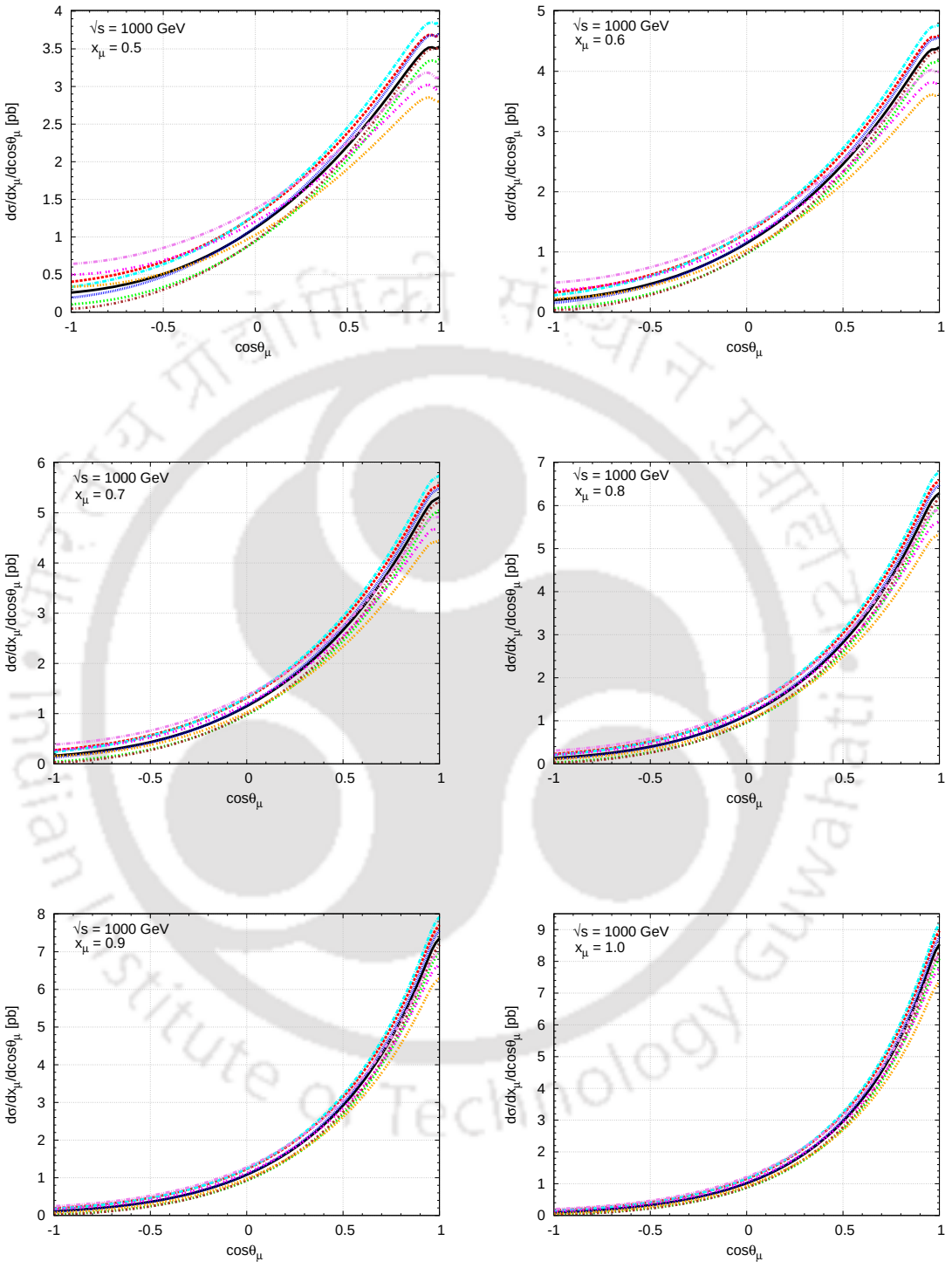

FIGURE 2.16: The energy-angle distribution of the secondary muon for different combinations of $\delta\kappa_\gamma$ and λ_γ, considered at fixed muon energy parameter (x_μ) at $\sqrt{s}$ of 1000 GeV. The colour coding is the same as in Fig. 2.15.

2.4 Summary and Conclusions

While considering the single W production in $e\gamma$ collisions, angular distribution of secondary muons in the lab frame is easily constructed, and is readily available in the literature, such is not the case of its energy distribution. Here we have presented a semi-analytical way to explore the secondary lepton energy-angle distributions in $e\gamma \to \nu W$ with $W \to l\bar{\nu}$. The advantage of such an observable in analyzing the SM case and probing possible new physics effects is demonstrated. Variables being defined in the lab frame, can be directly used to apply experimental cuts. With the W decaying into muons, this process has a spectacular final state of one single muon, and missing energy. The process is well suited to study the $WW\gamma$ coupling. It may be noted that the process has the advantage that, unlike other relevant process like the W pair production at e^+e^- collisions, it is devoid of effects from other anomalous couplings like WWZ. We have derived possible limits on the anomalous couplings $\delta\kappa_\gamma$ and λ_γ, which may be obtained from the cross-section measurement. It is seen that, assuming that $\lambda_\gamma = 0$, 3σ level of cross-section can probe $\delta\kappa_\gamma$ to the level of ± 0.004 for a small luminosity of 100 fb^{-1} at a center of mass energy of 500 GeV, which could be improved marginally at 1000 GeV collider. The presence of non-zero λ_γ changes this picture, and it is not possible to ascertain the case from cross-section measurements alone. The angular distributions along with forward-backward asymmetry improves the situation with better sensitivity. The real advantage of the energy-angle double distributions is utilized through considering the energy and angle distributions at specific values of the other parameter, which could be used in combination with other observable to distinguish different scenarios. Our analysis shows that the case of (i) $\lambda_\gamma = 0$, (ii) non-zero and positive λ_γ (iii) non-zero and negative λ_γ, can be distinguished by considering the angular distributions of the muons at fixed energies, as well as the energy distributions at fixed angles. On the other hand, the sign of $\delta\kappa_\gamma$ can be distinguished in the absence of λ_γ, whereas it is hard to do this if λ_γ is non-zero. Our illustrations are presented for a very moderate luminosity of 100 fb^{-1}, and using unpolarized beams. Being a purely weak interaction, left-handed polarization of the electrons will effectively increase the number of events, without affecting any of the conclusions qualitatively. While we have not attempted to present a quantitative estimate of the reach of ILC to probe the anomalous TGC, we hope that we have clearly demonstrated that the process considered, along with the methods described using energy-angle distributions can potentially

probe both $\delta\kappa_\gamma$ and λ_γ, and distinguish different possible scenarios. We are aware that the present considerations of the ILC do not favour a photon collider option as priority. At the same time, we hope that this study will help the case for this option at ILC, and expect it to be available eventually. Meanwhile, although more accurate estimates incorporating collider and detector effects are needed to make more quantitative conclusions, we hope our experimental colleagues and the community in general will find the study interesting and useful.

Note: Discussion on study of $WW\gamma$ vertex at LHC is provided in Appendix-A.3.

Chapter 3

Trilinear Higgs Self-Coupling

This chapter focuses on the effect of Higgs to gauge boson couplings in the extraction of trilinear Higgs self-couplings, through the process $e^-e^+ \to Zhh$ at the ILC. We carry out our analyses under the Higgs effective Lagrangian framework through a study of different observables including kinematic distributions.

3.1 Introduction

With the discovery of the new resonance of mass around 126 GeV at LHC [8, 9, 49–52], a new era is open in the investigations of elementary particle dynamics. The new particle is so far consistent in every way with the long expected Higgs boson of the Standard Model (SM). All the expected SM decays are observed at LHC. The spin and parity analysis favour a spin-zero, even-parity object [120, 121]. Thus, it is perhaps correct to state that the newly observed state is indeed a Higgs boson, establishing that the weakly interacting Higgs mechanism, if not entirely responsible, has a major role in the electroweak symmetry breaking (EWSB). While we wait for further statistics to establish more detailed identity of this excitement, it is worth revisiting the role of new physics in the Higgs sector in the light of the new measurements. It is well accepted that, even if all the properties of the new particle meets the expectations of the SM, there still remain several questions on the SM. One of the serious issues within the Higgs sector is the difficulty with quadratically diverging quantum corrections to the mass of the Higgs boson, or the so called hierarchy problem. This itself should convince us that the SM is at the best an effective theory, highly successful at the electroweak

scale. Among the plethora of suggestions to look beyond the SM, one could indeed narrow down to scenarios that can accommodate a light Higgs boson, very likely an elementary one, with properties very close to that of the SM Higgs boson. One may need to wait till LHC reveals further indications of new physics, if we are lucky, or perhaps even need to wait till the new generation lepton colliders, like the International Linear Collider (ILC) [34, 36, 122], start exploring the TeV scale physics. Being a discovery machine, LHC is capable of observing any direct production of new particle resonance at the energy scales explored, while the latter is more suitable to explore the new physics through detailed precision analysis, in the absence of any such direct observation of new physics.

Taking cue from the observations so far, one is somewhat compelled to consider a case with new physics somewhat decoupled from the electroweak physics, which in turn is dictated by the SM. In that case, the effect of new physics will be reflected in the various couplings through the quantum corrections they acquire. The best way to study such effects is through an effective Lagrangian, which encodes the new physics effects in higher dimensional operators with anomalous couplings. The study of Higgs sector through an effective Lagrangian goes back to Refs.[32, 46, 53, 84, 86, 123–129]. More recently, the Lagrangian including complete set of dimension-6 operators is studied by Refs. [33, 85, 88, 130]. For some of the recent references discussing the constraints on the anomalous couplings within different approaches, please see [89, 131–143]. Ref. [89] studied the H+V, where V= Z, W, associated production at LHC and TeVatron to discuss the bounds obtainable from the global fit to the presently available data, whereas Ref. [142] has discussed the constraint on the parameters coming from LHC results as well as other precision data from LEP, SLC and Tevatron. Experimental studies on the Higgs couplings at LHC are presented in, for example, Refs. [50, 144].

Higgs self couplings give direct information about the scalar potential, and therefore, very important to understand the nature of the EWSB. The process, $e^+e^- \to Zhh$ is one of the best suited to study the Higgs trilinear coupling [46, 102, 145–152]. At the same time, this process also depends on the Higgs-Gauge boson couplings, ZZh and $ZZhh$, which will affect the determination of the hhh coupling. Another process that could probe the hhh couplings is $e^+e^- \to \nu\bar{\nu}hh$ following the WW fusion [46, 149–151], which is also affected by the WWh and $WWhh$ couplings. In this chapter we will focus our attention on these processes in some detail within the framework of the effective Lagrangian. One goal of this study is

to investigate how significant is the effect of these Higgs-gauge boson couplings in the extraction of the hhh coupling .

The chapter is presented in the following way. In Section 3.2, the effective Lagrangian is presented with the currently available constraints on the parameters. In section 3.3, we briefly describe the method used for this study. In Section 3.4, the processes under consideration will be presented, with details. In Section 3.5 the results will be summarized.

3.2 General Setup

While the general case of Higgs Effective Lagrangian, along with experimental constrains is presented in details in Sec. 1.3.4, here we describe the parts relevant to the processes being considered. The effective Lagrangian with full set of dimension-6 operators involving the Higgs bosons is described in Refs. [32, 85, 89, 127, 128, 153]. In this chapter we shall restrict our discussion to the processes $e^+e^- \to Zhh$, and $e^+e^- \to \nu_e\bar{\nu}_e WW \to \nu_e\bar{\nu}_e hh$. Relevant to these processes, part of the Lagrangian is given by

$$\begin{aligned}\mathcal{L}_{\text{Higgs}}^{\text{anom}} \;=\; & \frac{\bar{c}_H}{2v^2}\partial^\mu\big(\Phi^\dagger\Phi\big)\partial_\mu\big(\Phi^\dagger\Phi\big) + \frac{\bar{c}_T}{2v^2}(\Phi^\dagger \overleftrightarrow{D}^\mu \Phi)(\Phi^\dagger \overleftrightarrow{D}_\mu \Phi) - \frac{\bar{c}_6}{v^2}\lambda\,\big(\Phi^\dagger\Phi\big)^3 \\ & + \frac{\bar{c}_\gamma}{m_W^2} g'^2\;\Phi^\dagger\Phi B_{\mu\nu}B^{\mu\nu} + \frac{\bar{c}_{HW}}{m_W^2} ig\;\big(D^\mu\Phi^\dagger\sigma_k D^\nu\Phi\big)W^k_{\mu\nu} \\ & + \frac{\bar{c}_{HB}}{m_W^2} ig'\;\big(D^\mu\Phi^\dagger D^\nu\Phi\big)B_{\mu\nu} + \frac{\bar{c}_W}{2m_W^2} ig\;\big(\Phi^\dagger\sigma_k \overleftrightarrow{D}^\mu\Phi\big)D^\nu W^k_{\mu\nu} \\ & + \frac{\bar{c}_B}{2m_W^2} ig'\;\big(\Phi^\dagger \overleftrightarrow{D}^\mu\Phi\big)\partial^\nu B_{\mu\nu}, \end{aligned} \tag{3.1}$$

where $\Phi^\dagger \overleftrightarrow{D}_\mu \Phi = \Phi^\dagger(D_\mu\Phi) - (D_\mu\Phi^\dagger)\Phi$, D_μ being the appropriate covariant derivative operator, and Φ, the usual Higgs doublet in the SM. Also, $W^k_{\mu\nu}$ and $B_{\mu\nu}$ are the field tensors corresponding to the $SU(2)_L$ and $U(1)_Y$ of the SM gauge groups, respectively, with gauge couplings g and g', in that order. σ_k are the Pauli matrices, and λ is the usual (SM) quartic coupling constant of the Higgs field. The

above Lagrangian, leads to the following in the unitary gauge and mass basis [87]

$$\begin{aligned}\mathcal{L}^{\rm anom}_{h,Z,W} = \quad & -v\lambda g^1_{hhh}h^3 + \frac{1}{2}g^2_{hhh}h\ \partial_\mu h\ \partial^\mu h - \frac{1}{4}g^1_{hZZ}Z_{\mu\nu}Z^{\mu\nu}h - g^2_{hZZ}Z_\nu\partial_\mu Z^{\mu\nu}h \\ & + \frac{1}{2}g^3_{hZZ}Z_\mu Z^\mu h - \frac{1}{2}g^1_{h\gamma Z}Z_{\mu\nu}F^{\mu\nu}h - g^2_{h\gamma Z}Z_\nu\partial_\mu F^{\mu\nu}h \\ & - \frac{1}{8}g^1_{hhZZ}Z_{\mu\nu}Z^{\mu\nu}h^2 - \frac{1}{2}g^2_{hhZZ}Z_\nu\partial_\mu Z^{\mu\nu}h^2 + \frac{1}{4}g^3_{hhZZ}Z_\mu Z^\mu h^2 \\ & - \frac{1}{2}g^1_{hWW}W^{\mu\nu}W^\dagger_{\mu\nu}h - \left[g^2_{hWW}W^\nu\partial^\mu W^\dagger_{\mu\nu}h + h.c.\right] + g\ m_W W^\dagger_\mu W^\mu h \\ & - \frac{1}{4}g^1_{hhWW}W^{\mu\nu}W^\dagger_{\mu\nu}h^2 - \frac{1}{2}\left[g^2_{hhWW}W^\nu\partial^\mu W^\dagger_{\mu\nu}h^2 + h.c.\right] + \frac{1}{4}g^2W^\dagger_\mu W^\mu h^2\end{aligned} \tag{3.2}$$

Various physical couplings present in the Lagrangian in Eq. 3.2 are given in terms of the parameters of the effective Lagrangian in Eq. 3.1 as

$$\begin{aligned}
& g^1_{hhh} = 1 + \frac{5}{2}\bar{c}_6, \qquad g^2_{hhh} = \frac{g}{m_W}\bar{c}_H \\
& g^1_{hZZ} = \frac{2g}{c_W^2 m_W}\left[\bar{c}_{HB}s_W^2 - 4\bar{c}_\gamma s_W^4 + c_W^2\bar{c}_{HW}\right] \\
& g^2_{hZZ} = \frac{g}{c_W^2 m_W}\left[(\bar{c}_{HW}+\bar{c}_W)c_W^2 + (\bar{c}_B+\bar{c}_{HB})s_W^2\right], \qquad g^3_{HZZ} = \frac{gm_Z}{c_W}\left[1-2\bar{c}_T\right] \\
& g^1_{h\gamma Z} = \frac{gs_W}{c_W m_W}\left[\bar{c}_{HW} - \bar{c}_{HB} + 8\bar{c}_\gamma s_W^2\right] \\
& g^2_{h\gamma Z} = \frac{gs_W}{c_W m_W}\left[\bar{c}_{HW} - \bar{c}_{HB} - \bar{c}_B + \bar{c}_W\right] \\
& g^1_{hhZZ} = \frac{g^2}{c_W^2 m_W^2}\left[\bar{c}_{HB}s_W^2 - 4\bar{c}_\gamma s_W^4 + \bar{c}_{HW}c_W^2\right] \\
& g^2_{hhZZ} = \frac{g^2}{2c_W^2 m_W^2}\left[(\bar{c}_{HW}+\bar{c}_W)c_W^2 + (\bar{c}_B+\bar{c}_{HB})s_W^2\right], \qquad g^3_{hhZZ} = \frac{g^2}{2c_W^2}\left[1-6\bar{c}_T\right] \\
& g^1_{hWW} = \frac{2g}{m_W}\bar{c}_{HW}, \qquad g^2_{hWW} = \frac{g}{2m_W}\left[\bar{c}_W + \bar{c}_{HW}\right] \\
& g^1_{hhWW} = \frac{g^2}{m_W^2}\bar{c}_{HW}, \qquad g^2_{hhWW} = \frac{g^2}{4m_W^2}\left[\bar{c}_W + \bar{c}_{HW}\right]
\end{aligned} \tag{3.3}$$

In total eight coefficients, namely, $\bar{c}_6$, $\bar{c}_H$, $\bar{c}_T$, $\bar{c}_\gamma$, $\bar{c}_B$, $\bar{c}_W$, $\bar{c}_{HB}$, $\bar{c}_{HW}$, govern the dynamics of Zhh and $\nu\bar{\nu}hh$ productions at ILC. Coming to the experimental constraints on these parameters, the first two, $\bar{c}_6$ and $\bar{c}_H$ influence only the Higgs self couplings, and therefore, practically, do not have any experimental constraints on them. Electroweak precision tests constrain $\bar{c}_T$, $\bar{c}_W$ and $\bar{c}_B$ as [88]

$$\begin{aligned}
& \bar{c}_T(m_Z) \in [-1.5, 2.2] \times 10^{-3}, \\
& (\bar{c}_W(m_Z) + \bar{c}_B(m_Z)) \in [-1.4, 1.9] \times 10^{-3}.
\end{aligned} \tag{3.4}$$

Note that $\bar{c}_W$ and $\bar{c}_B$ are not independently constrained, leaving possibility of having large values with cancellation between them as per the above constraint. $\bar{c}_W$ itself, along with $\bar{c}_{HW}$ and $\bar{c}_{HB}$ is constrained from LHC observations on associated production of Higgs along with W in Ref. [89]. Consideration of the Higgs associated production along with W, ATLAS and CMS along with D0 put a limit of $\bar{c}_W \in \left[-0.05, 0.04\right]$, when all other parameters are set to zero. A global fit using various information from ATLAS and CMS, including signal-strength information constrains the region in $\bar{c}_W - \bar{c}_{HW}$ plane, leading to a slightly more relaxed limit on $\bar{c}_W$, and a limit of about $\bar{c}_{HW} \in \left[-0.1, 0.06\right]$. The limit on $\bar{c}_{HB}$ estimated using a global fit in Ref. [89] is about $\bar{c}_{HB} \in [-0.05, 0.05]$ with a one parameter fit.

The purpose of this study is to understand how to exploit a precision machine like the ILC to investigate suitable processes so as to derive information regarding these couplings. In the next section we shall explain the processes of interest in the present case, and discuss the details to understand the influence of one or more of the couplings mentioned above.

3.3 Method

We use Mathematica[1]based package FeynRules[2] [154] to derive the Feynman rules related to Higgs effective Lagrangian using the publicly available free source for this model. These Feynman rules are incorporated into the event generator MadGraph [155–158] through the interface called UFO [159] generated for this model. The Fig. 3.1 shows the flow chart of computational method which we have followed in our analyses.

3.4 Discussion of the processes considered

It is generally expected that the ILC, with its clean environment, fixed center of mass energy, and additional features like availability of beam polarization, will be able to do the precision studies much more efficiently than what LHC could do. This is especially so in the case of Higgs self couplings which require very

[1]source: http://wolfram.com/mathematica/

[2]FeynRules is a Mathematica based program to derive Feynman rules from a Lagrangian.

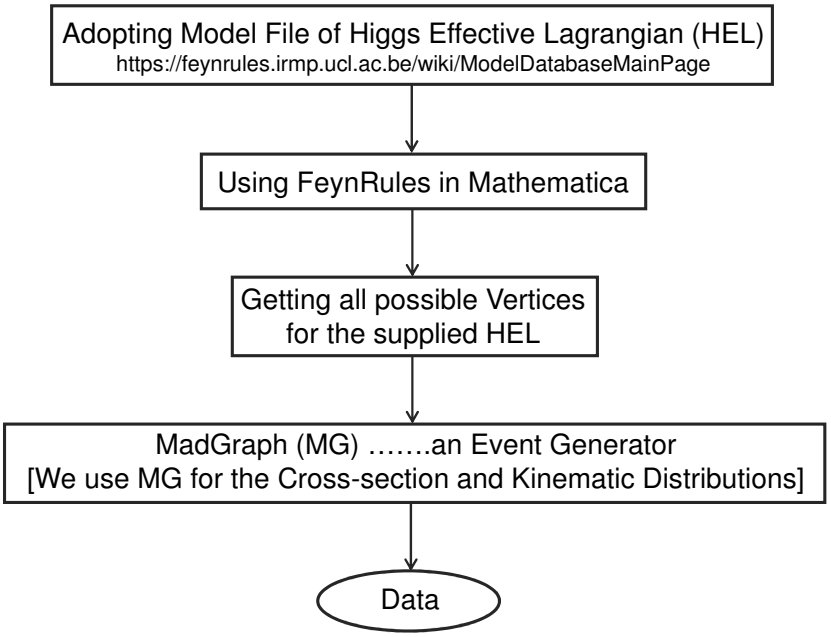

FIGURE 3.1: Flow chart of computational tools and method.

high energy and high luminosity version of LHC (LHC33 running at center of mass energy of 33 TeV). One of the best suited process to study the trilinear (self) coupling of the Higgs boson is $e^+e^- \to Zhh$, the phenomenological analysis of which is studied in detail within the context of the SM [146–148, 151]. The Feynman diagrams corresponding to this process in the SM are given in Fig. 3.2.

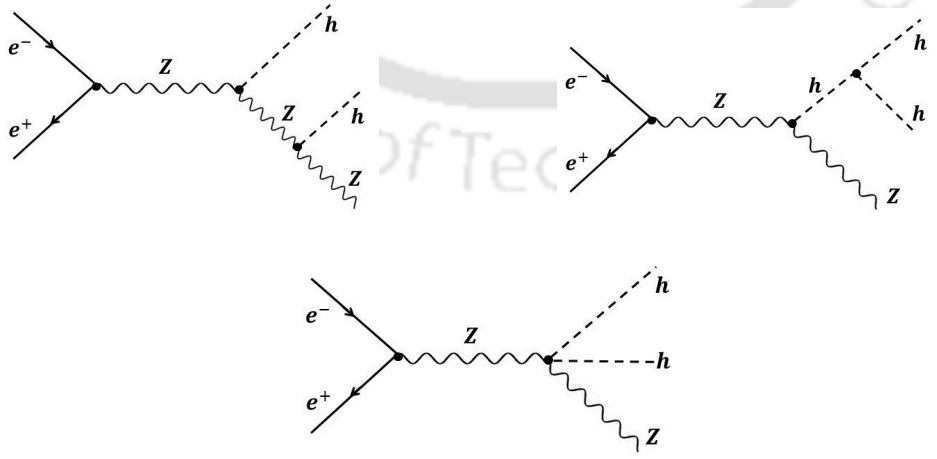

FIGURE 3.2: Feynman diagrams contributing to the process $e^-e^+ \to Zhh$ in Standard Model.

Another process that is relevant to the study of hhh coupling is $e^+e^- \to \nu_e\bar{\nu}_e hh$.

Note that the earlier process, $e^+e^- \to Zhh$, with the invisible decay of $Z \to \nu_e\bar{\nu}_e$ also leads to the same final state. However, this can be easily separated by considering the missing invariant mass. The rest of the process goes through the Feynman diagrams presented in Fig. 3.3.

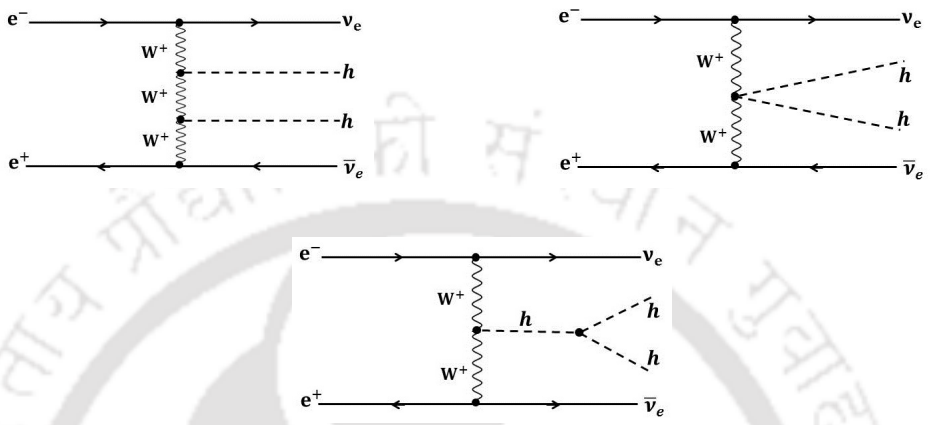

FIGURE 3.3: Feynman diagrams contributing to the process $e^-e^+ \to \nu_e\bar{\nu}_e hh$ in Standard Model, without considering $e^+e^- \to Zhh \to \nu_e\bar{\nu}_e hh$

Apart from the hhh coupling, these processes are influenced by gauge-Higgs couplings like ZZh, $ZZhh$, WWh and $WWhh$. Keeping in mind the above discussion of the effective couplings deviating from the SM due to the influence of the BSM at some higher energies, one must understand how such a scenario would affect the phenomenology, in order to draw any conclusion regarding these couplings. In the rest of this chapter we shall revisit these processes, with a specific purpose of understanding the correlation between the gauge-Higgs coupling and the trilinear Higgs couplings.

3.4.1 $e^+e^- \to Zhh$ Process

We shall first consider $e^+e^- \to Zhh$ process. In Fig.[3] D.1 (left) the cross-section is plotted against the center of mass energy for the SM case as well as for some selected $(\bar{c}_6, \bar{c}_H)$ points. The cross-section peaks around a center of mass energy of 600 GeV with a value of about 0.17 fb, which slides down to about 0.15 fb at 800 GeV. In order to avoid any complications arising from the threshold effects, we perform our analysis for an ILC running at a center of mass energy of 800 GeV, sufficiently away from the threshold value. This is one of the planned center of

[3]In all figures, for convenience we have removed "bar" from the symbols denoting the CP-conserving parameters.

mass energy of the proposed ILC. Fig. D.1 (right) shows the dependence of cross-section (σ) on $\bar{c}_W = -\bar{c}_B$ along with the 3σ limit at integrated luminosities of 100 fb^{-1} and 1000 fb^{-1}. Assuming all other couplings are absent, one can obtain a limit of $-0.009 \leq (\bar{c}_W = -\bar{c}_B) \leq +0.003$ with 100 fb^{-1} luminosity, which could be improved slightly to $-0.007 \leq (\bar{c}_W = -\bar{c}_B) \leq +0.002$ with 1000 fb^{-1}.

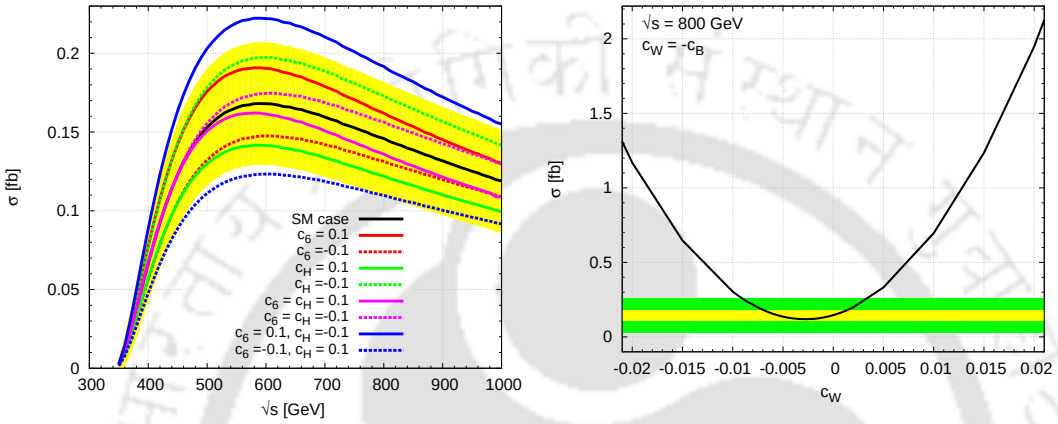

FIGURE 3.4: **Left**: Cross-section against $\sqrt{s}$ for the process $e^-e^+ \to Zhh$, for different values of the parameters $\bar{c}_6$ and $\bar{c}_H$, with all others kept to zero. **Right**: Cross-section against $\sqrt{s} = 800\ GeV$ against $\bar{c}_W$, keeping all other parameters zero. The green and yellow bands are correspond to 3σ deviation from the SM at integrated luminosities of 100 fb^{-1} and 1000 fb^{-1}, respectively.

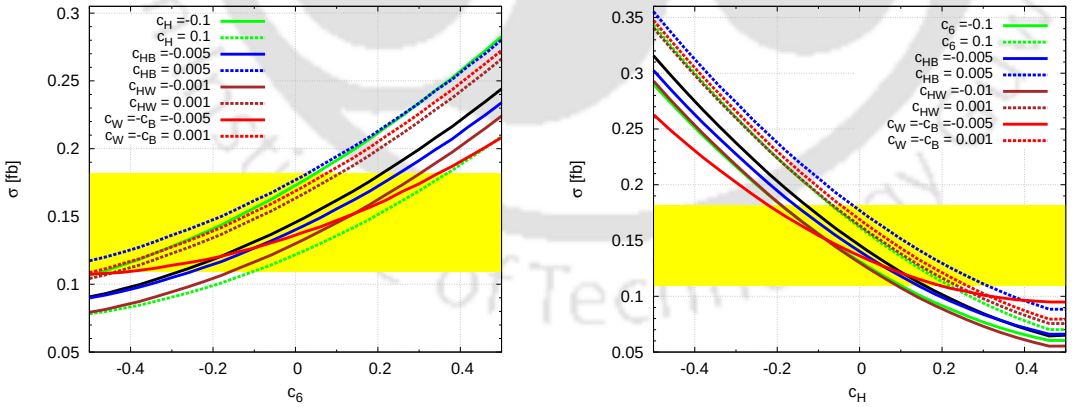

FIGURE 3.5: Cross-section of Zhh production against $\bar{c}_6$ (left) and $\bar{c}_H$ (right), when some of the other selected relevant parameters assume typical values is compared against the case when only $\bar{c}_6$ or $\bar{c}_H$ is present. The black solid line corresponds to the case when all parameters other than $\bar{c}_6$ (left) or $\bar{c}_H$ (right) vanish. The center of mass energy is assumed to be $\sqrt{s} = 800$ GeV. In each case, all other parameters are set to zero. The yellow band indicates the 3σ limit of the SM cross-section, with integrated luminosity of 1000 fb^{-1}.

We consider the influence of $\bar{c}_6$ on the cross-section in Fig. D.3 (left). We have compared the variation of cross-section with $\bar{c}_6$ keeping all other parameters to

the SM value, along with the cases when some of the relevant parameters having non-standard values. The 3σ region (yellow band) of the SM value of the cross-section, considering an integrated luminosity of 1000 fb^{-1}, is presented in these plots so as to make an estimate of the reach on the $\bar{c}_6$. The plots clearly indicate the correlation between the influence of different parameters on the cross-section. For example, assuming only $\bar{c}_6$ takes a non-zero value, the reach at 3σ level is approximately $-0.5 < \bar{c}_6 < 0.4$, as indicated by the black solid line. However, as indicated by the red solid line, if we assume a typical value of $\bar{c}_W = -\bar{c}_B = -0.005$, the lower limit is considerably relaxed, with some moderate change in the upper bound to 0.5. On the other hand, for the case with $\bar{c}_W = -\bar{c}_B = 0.001$, where the sign is reversed, the upper bound becomes more stringent, whereas the lower bound is more relaxed. A similar story can be read out for the cases with the presence of other parameters as well. The effect of all the parameters $\bar{c}_W$, $\bar{c}_{HW}$ and $\bar{c}_{HB}$, which contribute to the ZZh and $ZZhh$ couplings are found to be significant. Strong dependence of the sensitivity of $\bar{c}_6$ on the presence of $\bar{c}_H$ is somewhat expected, for both parameters contribute to the hhh coupling. In Fig. D.3 (right), similarly, we consider the variation of the cross-section with $\bar{c}_H$, again exploring the effect of different parameters on it. Here again, the dependence on all the parameters on the sensitivity of $\bar{c}_H$ on the cross-section is found to be significant for chosen typical values of the parameters.

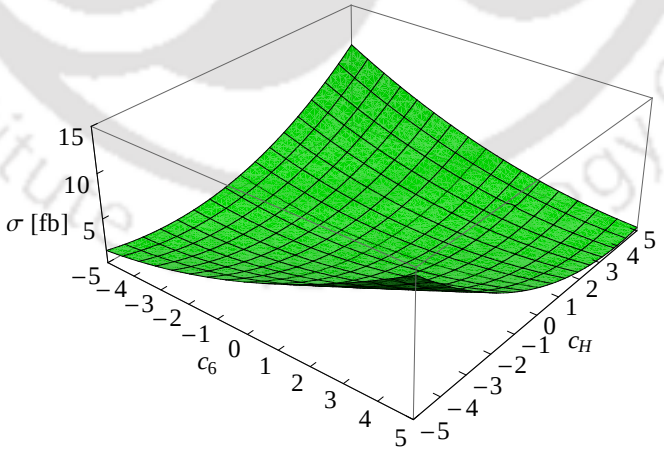

FIGURE 3.6: Cross-section of Zhh production plotted against $\bar{c}_6$ and $\bar{c}_H$ at $\sqrt{s} = 800$ GeV, with all other parameters set to zero.

In Fig. 3.6, the cross-section is plotted against $\bar{c}_6$ and $\bar{c}_H$. The correlation of the sensitivity between the two parameters is clear. The opposite sign combination seems to be more sensitive to the cross-section, and therefore more stringent

constraints could be drawn in this case compared to the same sign case.

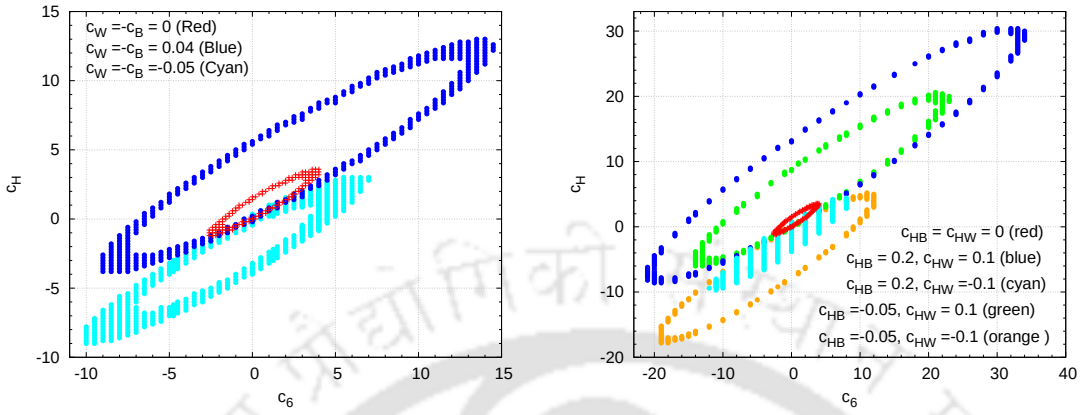

FIGURE 3.7: The shaded regions correspond to regions in the $\bar{c}_6$-$\bar{c}_H$ plane with the total cross-section is within the 3σ limit when $\bar{c}_6 = \bar{c}_H = 0$ in each case, for an integrated luminosity of 1000 fb^{-1} at a center of mass energy of 800 GeV. Values of the other anomalous couplings are as indicated in the figure, with all other couplings set to zero.

The reach of ILC on the trilinear Higgs coupling through the process being considered can be established by considering the 3σ limit of the cross-section at an integrated luminosity of 1000 fb^{-1} as presented in Fig. D.4, for the case of SM, and cases with non-vanishing anomalous ZZh and $ZZhh$ couplings. Please note that, when cross-section is considered as a function of $\bar{c}_6$ and $\bar{c}_H$, the result is a second order polynomial with these two parameters. With this, the 3σ limit of the cross-section leads to an elliptic equation correponding to the relation between these two parameters. This result in an elliptic band in the $\bar{c}_6 - \bar{c}_H$ plane respecting the 3σ limit of the cross-section. As is evident from the plots, these allowed bands of the parameters move in the parameter space, depending on the values of the other parameters, as illustrated by the cases of $\bar{c}_W = -\bar{c}_B$, $\bar{c}_{HW}$ and $\bar{c}_{HB}$. These results also illustrate how important the signs of different couplings are in a study of the sensitivity of the trilinear Higgs couplings. What we may learn from the above is that the limits drawn with assuming the absence of all other parameters may not depict the actual situation.

It is important to know the behaviour of the kinematic distributions, and how the anomalous parameters influence these, to derive any useful and reliable conclusions from the experimental results. This is so, even in cases where the fitting to obtain the reach of the parameters is done with the total number of events, as the reconstruction of events and the reduction of the background depend crucially on the kinematic distributions of the decay products. In the following we shall

present some illustrative cases of distributions at the production level, in order to understand the effect of different couplings on these. The changes in the kinematic distributions at the production level will also be carried over to the distributions of their decay products. Presently we would like to be content with the analysis at the production level, considering the limited scope of this work. As mentioned earlier we shall focus on an ILC running at a center of mass energy of 800 GeV for our study.

We first consider in Fig.D.5 (top row), the normalized angular distributions of the Z boson for the case of SM, as well as for different cases with anomalous couplings. The normalized distributions present the difference in the shape, which brings out the qualitative difference in a more visible manner. The figure on the left shows the case with $\bar{c}_W = -\bar{c}_B$ taking typical values, while the other parameters are set to zero, whereas the figure on the right considers $\bar{c}_{HW}$ and $\bar{c}_{HB}$ non-zero, while setting other parameters to zero. The case with only $\bar{c}_6$ and $\bar{c}_H$ taking non-zero values, when compared with the SM case shows a perceivable change in the distribution with more number of events piling in the small $\cos\theta_Z$ region. Such an experimental observations could therefore be considered as an indication of the anomalous hhh coupling. On the other hand, the presence of anomalous $\bar{c}_W$ and $\bar{c}_B$ couplings does not affect the distribution much. More importantly, in the presence of non-zero $\bar{c}_W$ and $\bar{c}_B$, the distribution remains close to the SM distribution, even with non-zero $\bar{c}_6$ and $\bar{c}_H$. Thus, a conclusion regarding the presence or otherwise of the hhh coupling drawn from the $\cos\theta_Z$ distribution will depend on the values of $\bar{c}_W$ and $\bar{c}_B$. The figure on the right tells a similar story for the case of $\bar{c}_{HW}$ and $\bar{c}_{HB}$ replacing $\bar{c}_W$. In Fig.D.5 (second row) and (third row), the P_T and energy distributions of the Z boson are plotted. Here too, we see that if only $\bar{c}_6$ and $\bar{c}_H$ are considered to be non-zero, events with high P_T and high energy Z bosons are preferred much more in comparison with the SM case. This conclusion is upset with the simultaneous presence of other parameters related to ZZh coupling. On the other hand, compared to the $\cos\theta_Z$ distribution, the difference with SM case is not completely washed out. For example the case of $\bar{c}_6 = -1,\ \bar{c}_H = +1$ has a slightly different distribution compared to the case of $\bar{c}_6 = +1,\ \bar{c}_H = -1$. Both of these cases have distinct features compare to the SM one. When $\bar{c}_{HB}$ and $\bar{c}_{HW}$ are present along with $\bar{c}_6$ and $\bar{c}_H$, the story is somewhat different. Here the distributions are sensitive to the signs of $\bar{c}_{HB}$ and $\bar{c}_{HW}$, but not the signs of $\bar{c}_6$ and $\bar{c}_H$. The energy distribution plotted in the last row of Fig. D.5 has features very similar to that of the $P_T(Z)$ distribution.

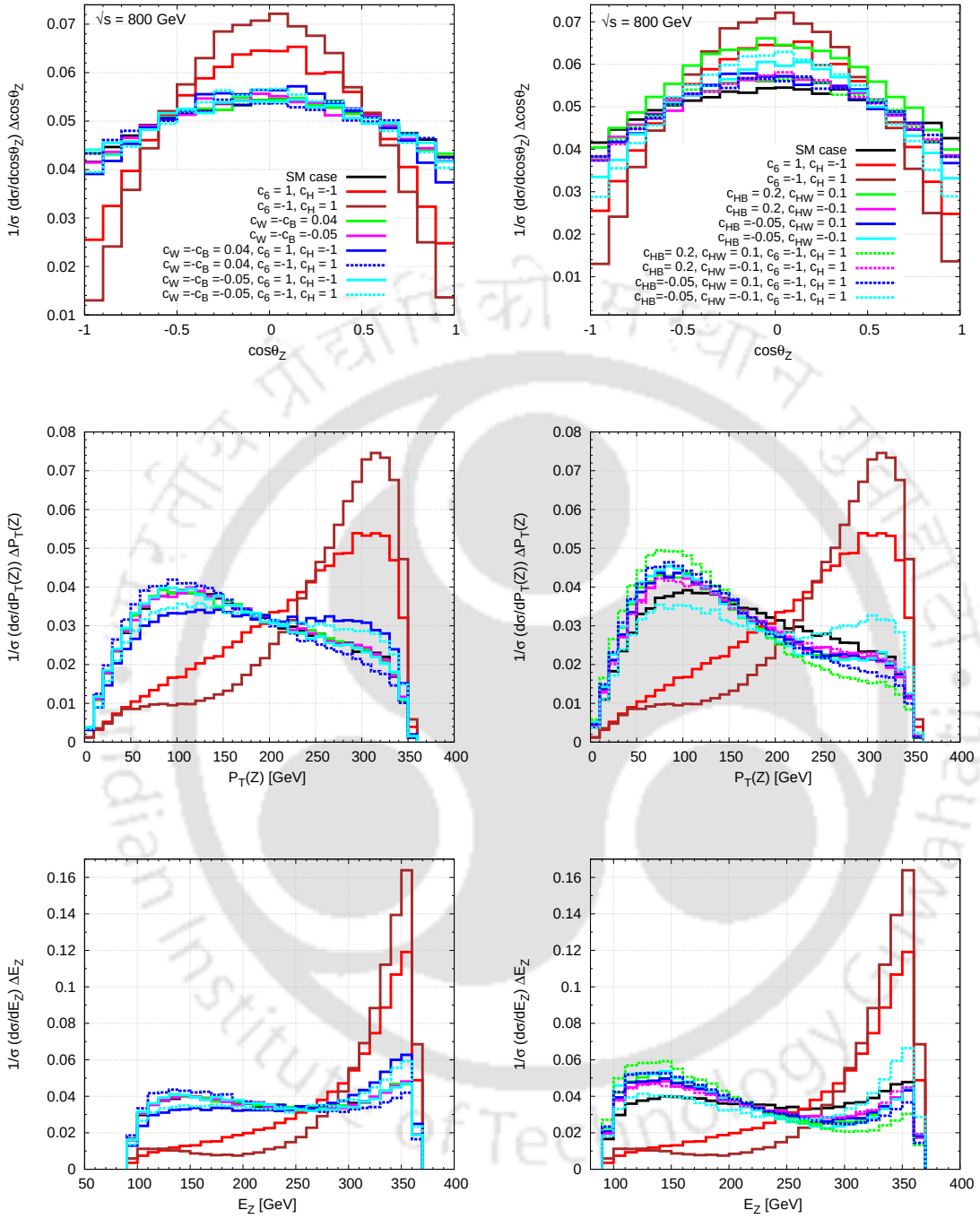

FIGURE 3.8: Distributions of the $\cos\theta_Z$, Transverse Momentum, and Energy of the Z boson for the anomalous coupling values as in the inset, illustrating how the presence of $\bar{c}_W$ (first column), and $\bar{c}_{HW}$ and $\bar{c}_{HB}$ (second column) affect the influence of $\bar{c}_6$ and $\bar{c}_H$. A center of mass energy of 800 GeV is assumed. Each column having same colour coding as in the plots at the top.

The distribution of the opening angle between the two Higgs bosons as well as their invariant mass distribution presented in Fig. 3.9 indicate the same feature captured in the various distributions of the Z bosons. While in all cases including

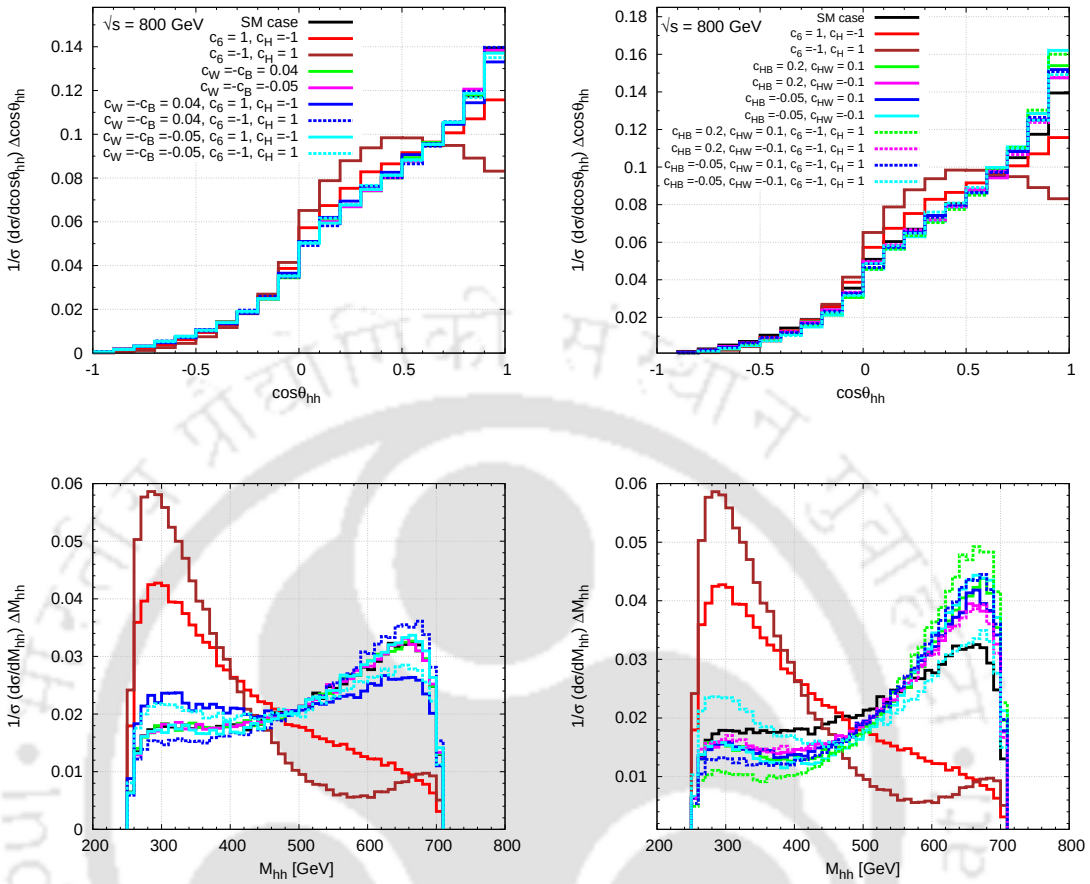

FIGURE 3.9: $\cos\theta_{hh}$ and the invariant mass of hh distributions for the anomalous coupling values as in the inset, illustrating how the presence of $\bar{c}_W$ (first column), and $\bar{c}_{HW}$ and $\bar{c}_{HB}$ (second column) affect the influence of $\bar{c}_6$ and $\bar{c}_H$. A center of mass energy of 800 GeV is assumed. Each column having same colour coding as in the plots at the top.

the SM case, most of the events are in the forward hemisphere, in the presence of non-vanishing $\bar{c}_6$ and $\bar{c}_H$, but with $\bar{c}_W = \bar{c}_{HW} = \bar{c}_{HB} = 0$, the events are more evenly distributed within the forward hemisphere, compared to the rest of the cases including the SM case. The hh invariant mass demonstrate an even more dramatic difference in the different cases mentioned above. Here again, while $\cos\theta_{hh}$ is indistinguishable from the SM when $\bar{c}_W$, $\bar{c}_{HW}$, $\bar{c}_{HB}$ are present along with $\bar{c}_6$ and $\bar{c}_H$, the invariant mass distribution has a different story to tell. These, similar to the E_Z and $P_T(Z)$ cases, different scenarios have distinct features.

The conclusions that we draw from the above considerations is that single parameter considerations to understand the effect of hhh coupling will not be realistic, if other relevant gauge-Higgs couplings receive anomalous contributions. Our preliminary investigation clearly indicates that the correlations can be rather strong,

for all the relevant parameters, and one need to consider a careful analysis to obtain realistic limits on the parameters. A combination of different kinematic distributions has the potential to distinguish different scenarios from each other.

3.4.2 $e^+e^- \to \nu_e\bar{\nu}_e hh$ process

We shall now turn our attention to the second process involving hhh couplings, as well as Higgs-gauge boson couplings. We consider the Higgs pair production with missing energy through the process $e^+e^- \to \nu_e\bar{\nu}_e hh$. The previous process, $e^+e^- \to Zhh$, with $Z \to \nu_e\bar{\nu}_e$ has the same final state. But, this can be easily separated from the rest of the contributions due, in the SM, to the channels presented in the Feynman diagrams given in Fig. 3.3, through, for example considering the missing invariant mass. The cross-section for the process is plotted against the center of mass energy for the case of polarized as well as unpolarized beams in Fig. 3.10. The advantage of very high energy collider is evident here. We shall consider a center of mass energy of 2 TeV, for which the cross-section is close to 0.4 fb in case of unpolarized beams, and slightly more than 1 fb for e^- beam of -80% polarization and e^+ beam with $+60\%$ polarization. This study will complement the study of the Zhh production in the sense that the physical couplings involved are hhh along with WWh and $WWhh$ instead of the ones involving the neutral gauge bosons. Although in the language of the effective Lagrangian, the couplings involved are similar to the ones in the previous process, their involvement in the current process is expected to be different.

As in the earlier case, the sensitivity of $\bar{c}_6$ and $\bar{c}_H$ on the total cross-section at the center of mass energy of 2 TeV is presented in Figs. 3.11, when all other parameters are set to zero, as well as in the presence of some of the relevant parameters. We have included the 3σ band of the SM cross-section assuming 1000 fb^{-1} luminosity. Clearly, the correlation is perceivable, and the conclusions are similar to the case of Zhh production, that the sensitivity of hhh coupling on the process considered strongly depend on the values of other parameters relevant to WWh and $WWhh$ couplings.

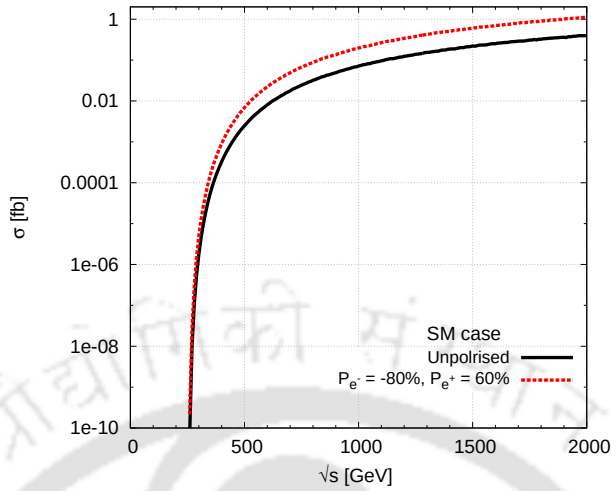

FIGURE 3.10: Total cross-section of $e^-e^+ \to \nu_e\bar{\nu}_e hh$ in the case of unpolarized and polarized beams, as indicated.

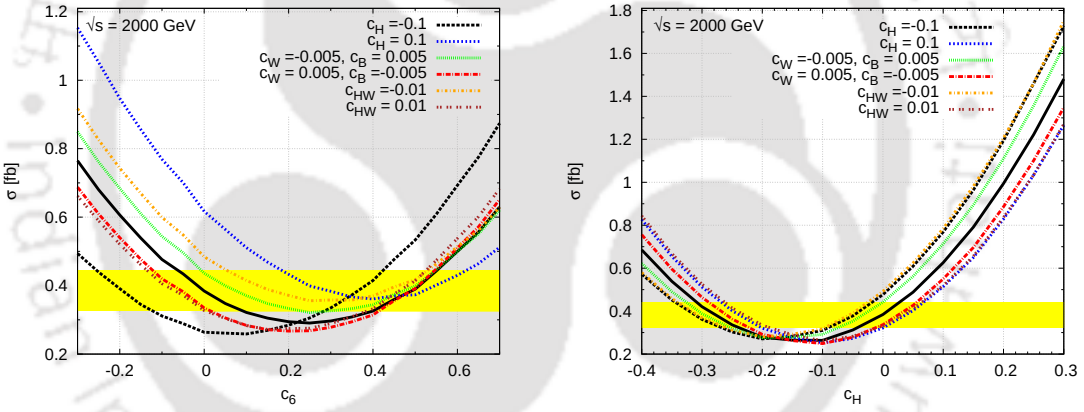

FIGURE 3.11: Cross-section of $\nu_e\bar{\nu}_e hh$ production against $\bar{c}_6$ (left) and $\bar{c}_H$ (right), when some of the other selected relevant parameters assume typical values is compared against the case when only $\bar{c}_6$ or $\bar{c}_H$ is present. The black solid lines corresponds to the case when all parameters other than $\bar{c}_6$ (left) or $\bar{c}_H$ (right) vanish. The center of mass energy is assumed to be $\sqrt{s} = 2$ TeV. In each case, all other parameters are set to zero. The yellow band indicates the 3σ limit of the SM cross-section.

Moving on to the kinematic distributions, we shall present the distributions of the opening angle between the two Higgs bosons in Fig.3.12 (first row). The effect of $\bar{c}_6$, and $\bar{c}_H$ keeping other parameters zero are presented in first column, whereas the second column presents the effect of $\bar{c}_W$ and $\bar{c}_{HW}$ along with $\bar{c}_6$ and $\bar{c}_H$ as indicated. In both figures, the SM case is presented for comparison. The dependence of the Higgs-gauge boson couplings on the sensitivity of hhh coupling is clear from the plots. The hh invariant mass as well as the missing invariant mass distributions also indicate a similar dependence, as presented in Fig.3.12 (second

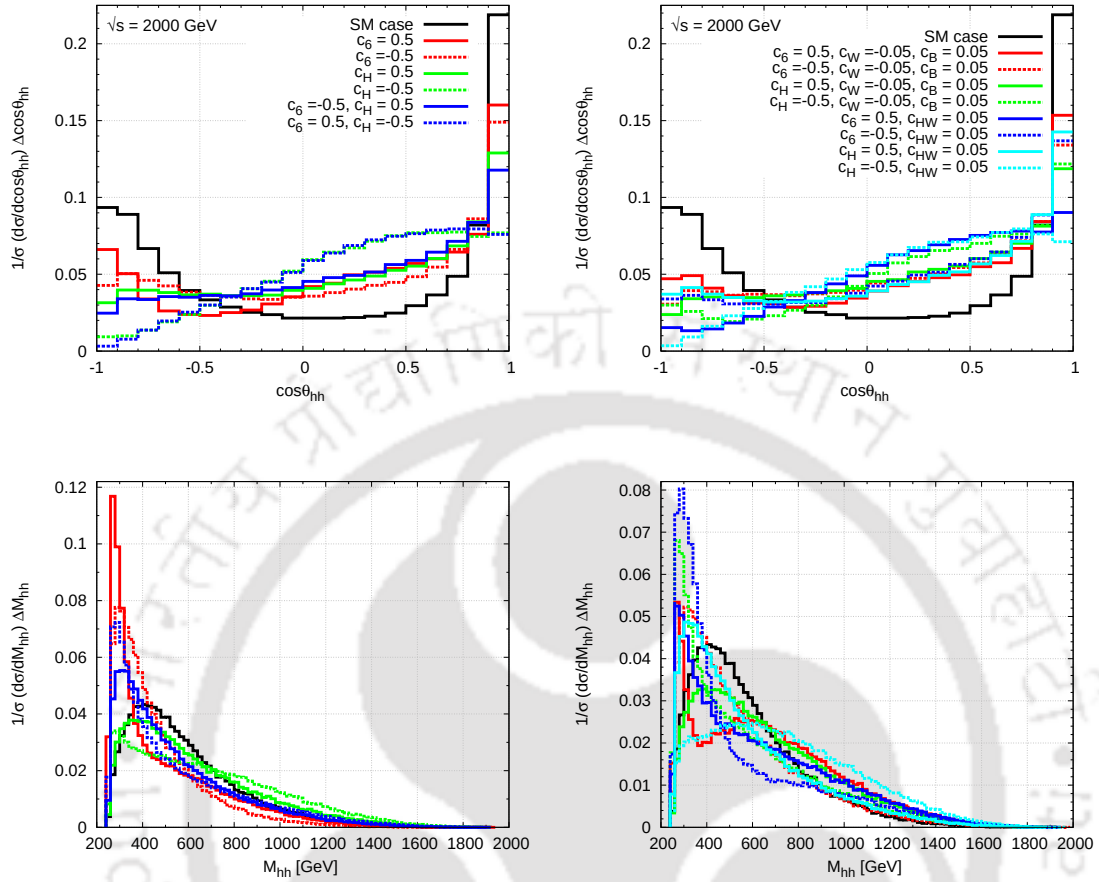

FIGURE 3.12: Kinematic distributions with the anomalous coupling values as in the inset, First column showing the presence of $\bar{c}_6$ and $\bar{c}_H$ whereas second column illustrating how the presence $\bar{c}_{HW}$ affect the influence of $\bar{c}_6$ and $\bar{c}_H$. A center of mass energy of 2000 GeV is assumed. Each column having same colour coding as in the plots at the top.

row) and Fig. 3.13 (first row) respectively. On the other hand, the missing transverse energy distribution given in Fig. 3.13 (second row) does not show much influence of the Higgs-gauge boson couplings on the sensitivity of $\bar{c}_6$ and $\bar{c}_H$. Here again, comparison of different distributions should be able to distinguish different scenarios.

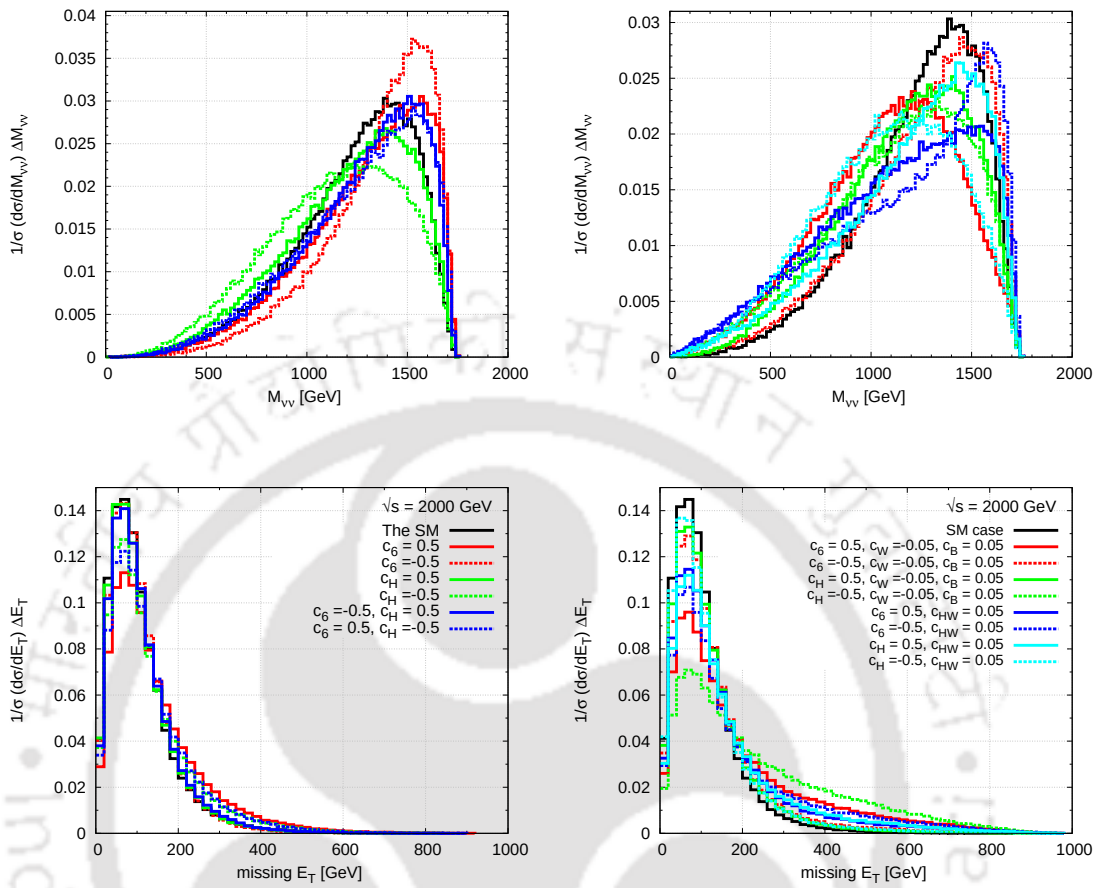

FIGURE 3.13: Kinematic distributions with the anomalous coupling values as in the inset, First column showing the presence of $\bar{c}_6$ and $\bar{c}_H$ whereas second column illustrating how the presence $\bar{c}_{HW}$ affect the influence of $\bar{c}_6$ and $\bar{c}_H$. A center of mass energy of 2000 GeV is assumed. Each column having same colour coding as in the plots at the bottom.

3.5 Summary and Conclusions

Precise knowledge of the trilinear Higgs self-coupling, which is typically probed directly through processes involving Higgs pair production, play a vital role in reconstructing the Higgs potential. Typically, such processes also involve other couplings from the Higgs sector, like the Higgs-gauge boson couplings. We consider the Zhh and $\nu\bar{\nu}hh$ productions at ILC to understand the influence of the ZZh and $ZZhh$ couplings, in $e^-e^+ \to Zhh$, and WWh and $WWhh$ couplings, in $e^-e^+ \to \nu_e\bar{\nu}_e hh$, on the sensitivity of hhh coupling on this process. Single and two parameter limits on the $\bar{c}_6$ and $\bar{c}_H$ couplings, which are related to the hhh couplings, are considered in the case of an ILC with $\sqrt{s} = 800$ GeV and integrated luminosity of 1000 fb^{-1}, to see how the other parameters, $\bar{c}_W$, $\bar{c}_{HW}$ and c_{HB} influence the limits. It is seen that these latter parameters have significant influence

of the reach of $\bar{c}_6$ and $\bar{c}_H$, indicating that prior, and somewhat precise knowledge of the Higgs-gauge boson coupling is necessary to draw any conclusion on the influence of trilinear couplings on the process considered. The kinematic distributions also indicate a strong influence of Higgs-gauge boson couplings, showing that, in the presence of very moderate Higgs-gauge boson couplings, it is difficult to extract reliable information regarding $\bar{c}_6$ and $\bar{c}_H$. A similar story is unfolded by considerations of $e^+e^- \to \nu_e\bar{\nu}_e hh$, where the influence of WWh and $WWhh$ on the sensitivity of the trilinear Higgs self-coupling is explored. Concluding, one may need to rely on knowledge of the Higgs-gauge boson couplings from elsewhere, or consider clever combinations of observables to distinguish different scenarios, and thus to extract meaningful information regarding the trilinear Higgs couplings.

Note: As per suggestion from one of referees, results for the Zhh production at center of mass energy of 500 GeV can be seen in Appendix-D.

Chapter 4

Higgs to Gauge Boson Couplings

This chapter focuses on the effect of CP-violating Higgs-gauge boson couplings and how the effect of these couplings are influenced by the presence of CP-conserving Higgs-gauge boson couplings. We consider the process $e^-e^+ \to W^-W^+h$ at the ILC, where we carry out our analyses considering a Higgs effective Lagrangian framework.

4.1 Introduction

As described in detail in Chapter 3, in the light of the discovery and measurements at LHC, an effective Lagrangian approach is suitable to study the details of the Higgs and gauge boson couplings. Our study of the hhh couplings through $e^+e^- \to Zhh$ found that a precise knowledge of the WWh and ZZh couplings is necessary to derive information regarding the trilinear couplings. Here we shall discuss the process, $e^+e^- \to W^-W^+h$, which is well suited to study the Higgs to gauge boson couplings [46, 102, 145–152]. At the same time, this process also depends on the trilinear Gauge boson couplings like $WW\gamma$, which can contaminate the effects of Higgs to gauge boson couplings. In this report we will focus our attention on this process in some detail within the framework of the effective Lagrangian. One goal of this study is to investigate CP violation in Higgs sector through Higgs to gauge bosons couplings, and to understand the significance of other couplings in their measurement.

The chapter is presented in the following way. In Section 4.2, the effective Lagrangian is presented, with experimental constraints on the parameters. In section 4.3, we will describe the schematic of computational methods. In Section 4.4, the process under consideration will be presented, with details. In Section 4.5 the results will be summarized.

4.2 General Setup

Refs. [32, 85, 89, 127, 128, 153] present the most general effective Lagrangian with dimension-6 operators involving the Higgs bosons. Part of this Lagrangian relevant to the process $e^+e^- \to W^-W^+h$ considered in this report is given by

$$\begin{aligned}
\mathcal{L}_{\text{Higgs}}^{\text{CPC}} &= \frac{\bar{c}_H}{2v^2}\partial^\mu\big(\Phi^\dagger\Phi\big)\partial_\mu\big(\Phi^\dagger\Phi\big) + \frac{\bar{c}_T}{2v^2}(\Phi^\dagger \overleftrightarrow{D}^\mu \Phi)(\Phi^\dagger \overleftrightarrow{D}_\mu \Phi) \\
&\quad -\frac{\bar{c}_6}{v^2}\lambda\,\big(\Phi^\dagger\Phi\big)^3 + \frac{\bar{c}_\gamma}{m_W^2}g'^2\;\Phi^\dagger\Phi B_{\mu\nu}B^{\mu\nu} \\
&\quad +\frac{\bar{c}_{HW}}{m_W^2}ig\;\big(D^\mu\Phi^\dagger\sigma_k D^\nu\Phi\big)W^k_{\mu\nu} + \frac{\bar{c}_{HB}}{m_W^2}ig'\;\big(D^\mu\Phi^\dagger D^\nu\Phi\big)B_{\mu\nu} \\
&\quad +\frac{\bar{c}_W}{2m_W^2}ig\;\big(\Phi^\dagger\sigma_k \overleftrightarrow{D}^\mu\Phi\big)D^\nu W^k_{\mu\nu} + \frac{\bar{c}_B}{2m_W^2}ig'\;\big(\Phi^\dagger \overleftrightarrow{D}^\mu\Phi\big)\partial^\nu B_{\mu\nu}, \\
\mathcal{L}^{\text{CPV}} &= \frac{ig\tilde{c}_{HW}}{2m_W^2}D^\mu\Phi^\dagger\sigma_k D^\nu\Phi\tilde{W}^k_{\mu\nu} + \frac{ig'\tilde{c}_{HB}}{m_W^2}D^\mu\Phi^\dagger D^\nu\Phi\tilde{B}_{\mu\nu} \\
&\quad +\frac{g'^2\tilde{c}_\gamma}{m_W^2}\Phi^\dagger\Phi B_{\mu\nu}\tilde{B}_{\mu\nu} + \frac{g^3\tilde{c}_{3W}}{m_W^2}\epsilon_{ijk}W^i_{\mu\nu}W^{\nu j}_{\rho}\tilde{W}^{\rho\mu k}
\end{aligned} \tag{4.1}$$

where the dual field strength tensor are defined as $\tilde{B}_{\mu\nu} = \frac{1}{2}\epsilon_{\mu\nu\rho\sigma}B^{\rho\sigma}$, $\tilde{W}^k_{\mu\nu} = \frac{1}{2}\epsilon_{\mu\nu\rho\sigma}W^{k\rho\sigma}$ and $\Phi^\dagger \overleftrightarrow{D}_\mu \Phi = \Phi^\dagger(D_\mu\Phi) - (D_\mu\Phi^\dagger)\Phi$, D^μ being the appropriate covariant derivative operator, and Φ, the usual Higgs doublet in the SM. Also, $W^k_{\mu\nu}$ and $B_{\mu\nu}$ are the field tensors corresponding to the $SU(2)_L$ and $U(1)_Y$ of the SM gauge groups, respectively, with gauge couplings g and g', in that order. σ_k are the Pauli matrices, and λ is the usual (SM) quartic coupling constant of the Higgs field. The above Lagrangian, leads to the following CP-conserving ($\mathcal{L}_{hV}^{\text{CPC}}$), and

CP-violating ($\mathcal{L}_{hV}^{\rm CPV}$) parts in the mass basis [87].

$$\begin{aligned}
\mathcal{L}_{hV}^{\rm CPC} &= -\frac{1}{4}g^1_{hzz}Z_{\mu\nu}Z^{\mu\nu}h - g^2_{hzz}Z_\nu\partial_\mu Z^{\mu\nu}h + \frac{1}{2}g^3_{hzz}Z_\mu Z^\mu h - \frac{1}{2}g^1_{h\gamma z}Z_{\mu\nu}F^{\mu\nu}h \\
&\quad -g^2_{h\gamma z}Z_\nu\partial_\mu F^{\mu\nu}h - \frac{1}{8}g^1_{hhzz}Z_{\mu\nu}Z^{\mu\nu}h^2 - \frac{1}{2}g^2_{hhzz}Z_\nu\partial_\mu Z^{\mu\nu}h^2 \\
&\quad +\frac{1}{4}g^3_{hhzz}Z_\mu Z^\mu h^2 - \frac{1}{2}g^1_{hww}W^{\mu\nu}W^\dagger_{\mu\nu}h \\
&\quad -\left[g^2_{hww}W^\nu\partial^\mu W^\dagger_{\mu\nu}h + h.c.\right] + g\ m_W W^\dagger_\mu W^\mu h - \frac{1}{4}g^1_{hhww}W^{\mu\nu}W^\dagger_{\mu\nu}h^2 \\
&\quad -\frac{1}{2}\left[g^2_{hhww}W^\nu\partial^\mu W^\dagger_{\mu\nu}h^2 + h.c.\right] + \frac{1}{4}g^2W^\dagger_\mu W^\mu h^2 \qquad (4.2)
\end{aligned}$$

$$\begin{aligned}
\mathcal{L}_{3V} &= \left[ig^1_{\gamma ww}W^\dagger_{\mu\nu}A^\mu W^\nu + h.c.\right] + ig^2_{\gamma ww}F_{\mu\nu}W^\mu W^{\nu\dagger} \\
&\quad +\left[ig^1_{zww}W^\dagger_{\mu\nu}Z^\mu W^\nu + h.c.\right] + ig^2_{zww}Z_{\mu\nu}W^\mu W^{\nu\dagger} \qquad (4.3)
\end{aligned}$$

$$\begin{aligned}
\mathcal{L}_{hV}^{\rm CPV} &= -\frac{1}{4}\tilde{g}_{h\gamma\gamma}F_{\mu\nu}\tilde{F}^{\mu\nu}h - \frac{1}{4}\tilde{g}_{hzz}Z_{\mu\nu}\tilde{Z}^{\mu\nu}h - \frac{1}{2}\tilde{g}_{h\gamma z}Z_{\mu\nu}\tilde{F}^{\mu\nu}h \\
&\quad -\frac{1}{2}\tilde{g}_{hww}W^{\mu\nu}\tilde{W}^\dagger_{\mu\nu}h - \frac{1}{8}\tilde{g}_{hh\gamma\gamma}F_{\mu\nu}\tilde{F}^{\mu\nu}h^2 - \frac{1}{8}\tilde{g}_{hhzz}Z_{\mu\nu}\tilde{Z}^{\mu\nu}h^2 \\
&\quad -\frac{1}{4}\tilde{g}_{hh\gamma z}Z_{\mu\nu}\tilde{F}^{\mu\nu}h^2 - \frac{1}{4}\tilde{g}_{hhww}W^{\mu\nu}\tilde{W}^\dagger_{\mu\nu}h^2 + i\tilde{g}^1_{hzww}\tilde{Z}^{\mu\nu}W_\mu W^\dagger_\nu h \\
&\quad -\left[i\tilde{g}^2_{hzww}\tilde{W}^{\mu\nu}Z_\mu W^\dagger_\nu h + h.c.\right] \qquad (4.4)
\end{aligned}$$

The physical couplings relevant to the process, $e^+e^- \to WWh$, and associated with the Lagrangian in Eq. 4.2 - 4.4 expressed in terms of the effective couplings presented in Eq. 4.1 are listed in Table 4.1. In total there are nine parameters which are relevant to the process considered, viz, $\bar{c}_T, \bar{c}_\gamma, \bar{c}_B, \bar{c}_W, \bar{c}_{HB}, \bar{c}_{HW}, \tilde{c}_{HW}, \tilde{c}_{HB}, \tilde{c}_\gamma$. Out of these, six parameters are related to CP-conserving couplings and the rest three of them are connected with CP-violating couplings. Electroweak precision data put the following constraints [88], on the couplings.

$$\bar{c}_T(m_Z) \in [-1.5, 2.2] \times 10^{-3} \quad \text{and} \quad (\bar{c}_W(m_Z) + \bar{c}_B(m_Z)) \in [-1.4, 1.9] \times 10^{-3} \qquad (4.5)$$

This means, we can safely ignore the effect of $\bar{c}_T$ in our analysis. On the other hand, $\bar{c}_W$ and $\bar{c}_B$ are not independently constrained, leaving possibility of having large values with cancellation between them as per the above constraint. $\bar{c}_W$ itself, along with $\bar{c}_{HW}$ and $\bar{c}_{HB}$ is constrained from LHC observations on associated production of Higgs along with W in Ref. [89]. Consideration of the Higgs associated production along with W, ATLAS and CMS along with D0 put a limit of

CP-conserving couplings

$$g^1_{hzz} = \frac{2g}{c_W^2 m_W}\left[\bar{c}_{HB} s_W^2 - 4\bar{c}_\gamma s_W^4 + c_W^2 \bar{c}_{HW}\right]$$

$$g^2_{hzz} = \frac{g}{c_W^2 m_W}\left[(\bar{c}_{HW} + \bar{c}_W)c_W^2 + (\bar{c}_B + \bar{c}_{HB})s_W^2\right]$$

$$g^3_{hzz} = \frac{g m_Z}{c_W}\left[1 - 2\bar{c}_T\right]$$

$$g^1_{hz\gamma} = \frac{g s_W}{c_W m_W}\left[\bar{c}_{HW} - \bar{c}_{HB} + 8\bar{c}_\gamma s_W^2\right]$$

$$g^2_{hz\gamma} = \frac{g s_W}{c_W m_W}\left[\bar{c}_{HW} - \bar{c}_{HB} - \bar{c}_B + \bar{c}_W\right]$$

$$g^1_{hww} = \frac{2g}{m_W}\bar{c}_{HW},$$

$$g^2_{hww} = \frac{g}{2m_W}\left[\bar{c}_W + \bar{c}_{HW}\right]$$

$$g^1_{\gamma ww} = e\left[1 - 2\bar{c}_W\right],$$

$$g^2_{\gamma ww} = e\left[1 - 2\bar{c}_W - \bar{c}_{HB} - \bar{c}_{HW}\right]$$

$$g^1_{zww} = \frac{g}{c_W}\left[c_W^2 - \bar{c}_{HW} + (2s_W^2 - 3)\bar{c}_W\right]$$

$$g^2_{zww} = \frac{g}{c_W}\left[c_W^2(1 - \bar{c}_{HW}) - s_W^2 \bar{c}_{HB} + (2s_W^2 - 3)\bar{c}_W\right]$$

CP-violating couplings

$$\tilde{g}_{h\gamma\gamma} = -\frac{8\ g\ \tilde{c}_\gamma\ s_W^2}{m_W},$$

$$\tilde{g}_{hz\gamma} = \frac{g\ s_W}{c_W m_W}\left[\tilde{c}_{HW} - \tilde{c}_{HB} + 8\tilde{c}_\gamma s_W^2\right]$$

$$\tilde{g}_{hzz} = \frac{2\ g}{c_W^2 m_W}\left[\tilde{c}_{HW} s_W^2 - 4\tilde{c}_\gamma s_W^4 + c_W^2 \tilde{c}_{HW}\right]$$

$$\tilde{g}_{hww} = \frac{2\ g}{m_W}\tilde{c}_{HW}$$

$$\tilde{g}^1_{hzww} = \frac{g^2}{c_W m_W}\left[\tilde{c}_{HW}(2 - s_W^2) + \tilde{c}_{HB} s_W^2\right]$$

$$\tilde{g}^2_{hzww} = \frac{2g^2}{m_W} c_W \tilde{c}_{HW}$$

TABLE 4.1: Physical couplings in Eq. 4.2-4.4 are given in terms of the effective couplings in Eq. 4.1.

$\bar{c}_W \in \big[-0.03, 0.01\big]$, when all other parameters are set to zero. A global fit using various information from ATLAS and CMS, including signal-strength information constrains the region in $\bar{c}_W - \bar{c}_{HW}$ plane, leading to a slightly more relaxed limit on $\bar{c}_W$, and a limit of about $\bar{c}_{HW} \in \big[-0.1, 0.06\big]$. The limit on $\bar{c}_{HB}$ estimated using a global fit in Ref. [89] is about $\bar{c}_{HB} \in [-0.05, 0.05]$ with a one parameter fit. The CP-violating couplings are largely unconstrained so far.

In the next section we shall explain the process of interest in the present case, and discuss the details to understand the influence of the couplings mentioned above.

4.3 Method

We use Mathematica[1] based package FeynRules[2] [154] to derive the Feynman rules related to Higgs effective Lagrangian using the publicly available free source for this model. These Feynman rules are incorporated into the event generator MadGraph [155–158] through the interface called UFO [159] generated for this model. The Fig. 4.1 shows the flow chart of computational method which we have followed in our analyses.

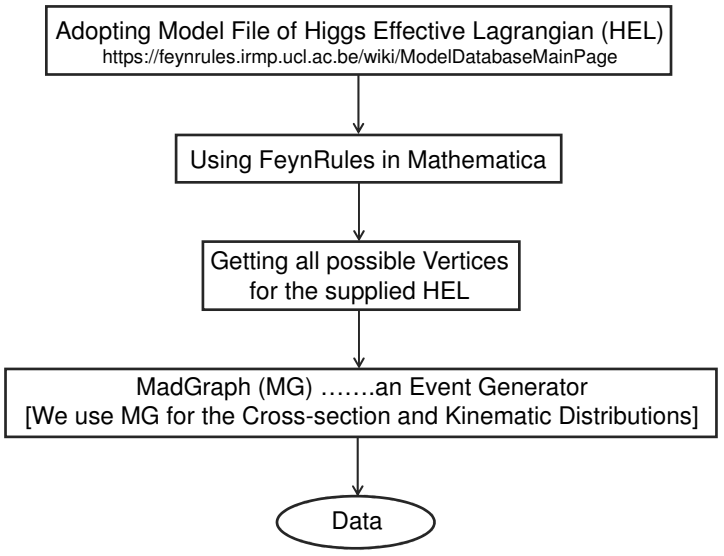

FIGURE 4.1: Flow chart of computational tools and method.

[1]source: http://wolfram.com/mathematica/
[2]FeynRules is a Mathematica based program to derive Feynman rules from a Lagrangian.

4.4 Results and Discussion

The Feynman diagrams corresponding to the process $e^-e^+ \to W^-W^+h$ in the SM are given in Fig. 4.2. This process is influenced by Higgs to charged gauge bosons as well as neutral gauge bosons couplings like WWh, ZZh, $WW\gamma$ and WWZ, apart from the fermionic couplings, which are taken to be the standard couplings in our study. The effective Lagrangian in Eq. 4.1, apart from allowing

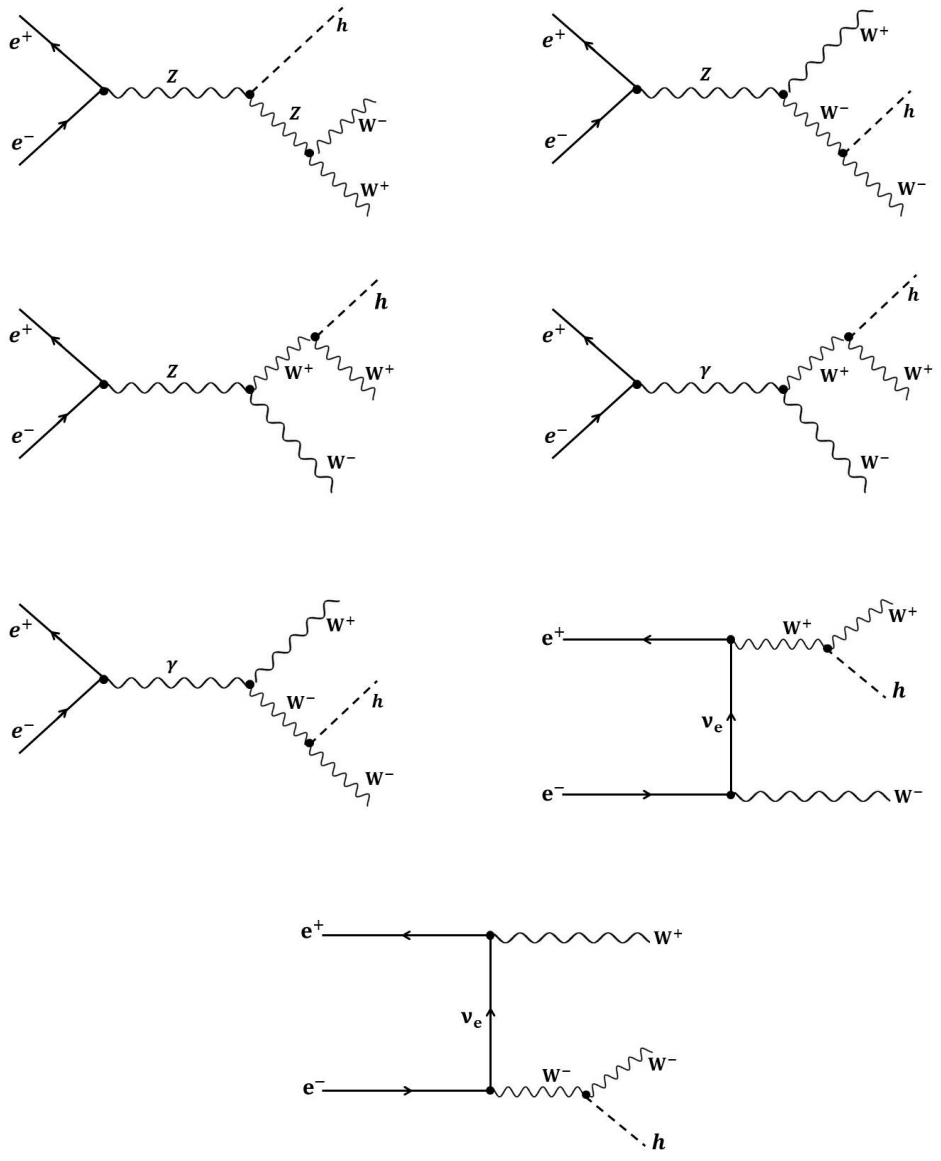

FIGURE 4.2: Feynman diagrams contributing to the process $e^-e^+ \to W^-W^+h$ in the SM.

the existing Higgs and gauge boson couplings to be non-standard, introduces new

couplings which are absent in the SM at tree level. In a specific model such effects appear at higher orders with new particle present in the loops. When the masses of such particles are taken to be large, the effect of such quantum correction can be considered in terms of changed couplings. Such effective couplings arising in the present analysis are presented in Table 4.1. Our numerical analyses are carried out using MadGraph, with the Effective Lagrangian implemented through Feynrules [87].

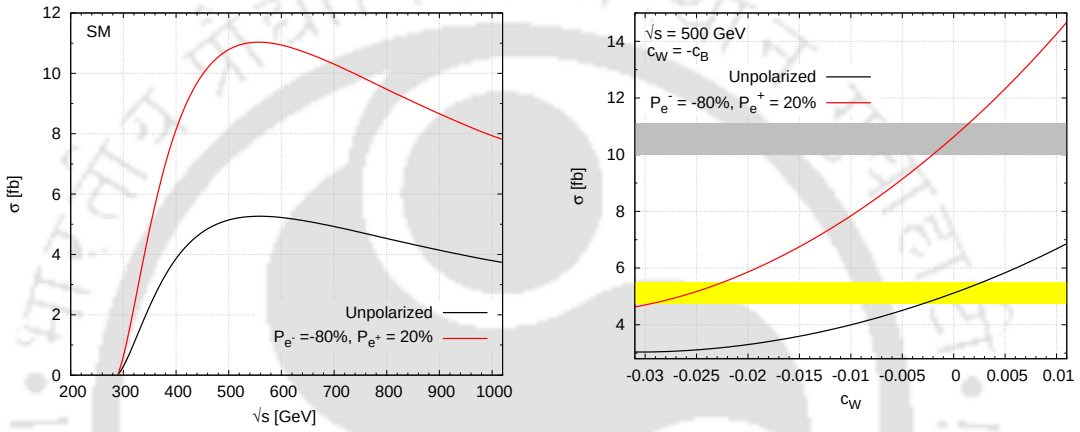

FIGURE 4.3: **Left**: The total cross-section against $\sqrt{s}$ in the SM. **Right**: The total cross-section against anomalous coupling parameter ($\bar{c}_W$) at $\sqrt{s} = 500\ GeV$, where yellow and grey bands correspond to 3σ deviations at an integrated luminosity of 300 fb^{-1}, form the SM with unpolarized and polarized beams, respectively.

As the first observable, we consider the cross-section. Fig.4.3 (left) presents the total cross-section against center-of-mass energy for the WWh production. The cross-section peaks around center-of-mass energy of 500 GeV, and therefore, our further detailed analysis will be done for a collider of this energy. As expected, the polarization hugely improves the situation. The case of typical polarization combination expected at ILC, 80% left polarized electron beam and 20% right polarized positron beam, is considered [122]. Although the quoted expectation in case of positron beam polarization is more than 20%, we have considered a very conservative approach here. In Fig.4.3 (right) the cross-section against anomalous coupling parameter ($\bar{c}_W$) at fixed center-of-mass energy of 500 GeV is considered along with the role of polarized beams. In order to be consistent with the experimental constraint (Eq. 4.5), we choose $\bar{c}_B = -\bar{c}_W$ throughout our analysis [3]. Notice that the cross-section is enhanced rapidly, even for the very

[3]In all figures, for convenience we have removed "bar" from the symbols denoting the CP-conserving parameters.

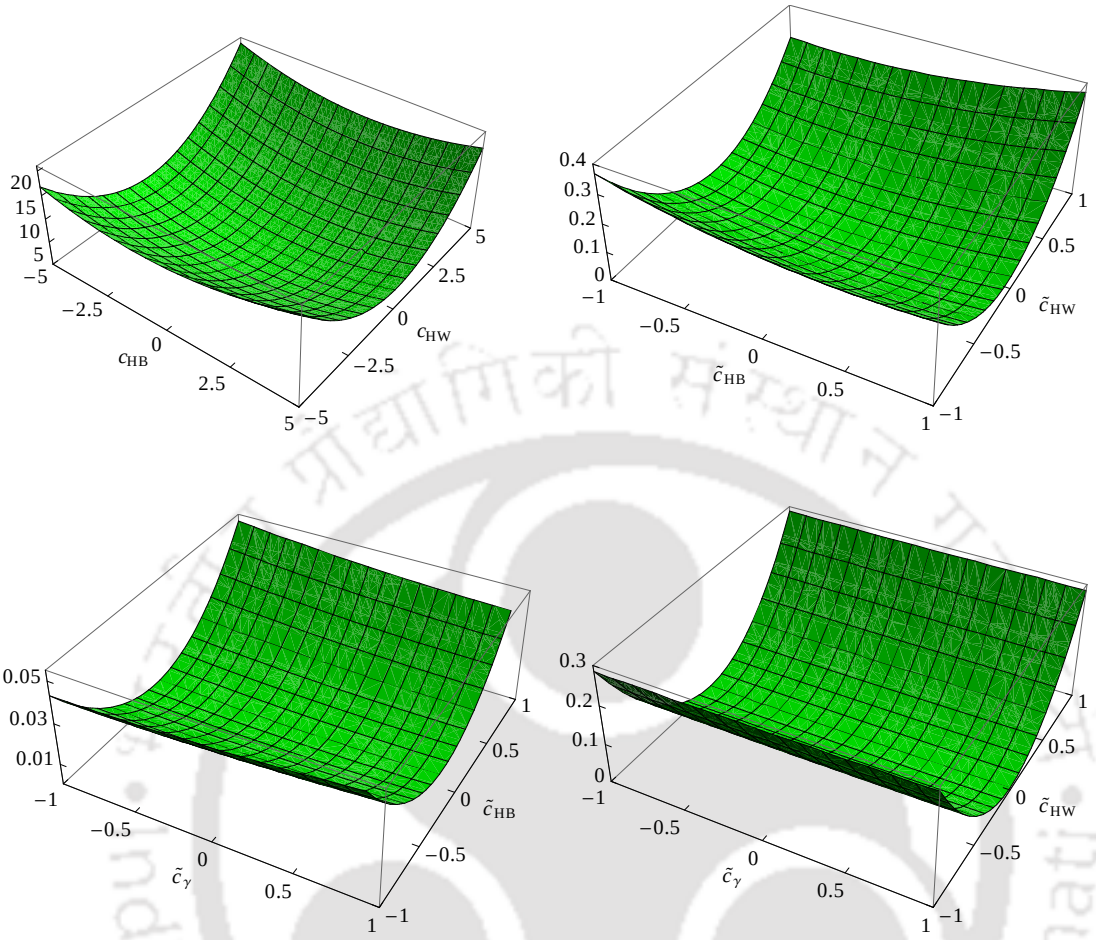

FIGURE 4.4: **Left**: Showing the cross-section against CP-conserving couplings parameters $\bar{c}_{HB}$ and $\bar{c}_{HW}$ (top left), against CP-violating couplings parameters $\tilde{c}_{HB}$ and $\tilde{c}_{HW}$ (top right), $\tilde{c}_\gamma$ and $\tilde{c}_{HB}$ (bottom left) and $\tilde{c}_\gamma$ and $\tilde{c}_{HW}$ (bottom right). The center of mass energy is assumed to be $\sqrt{s} = 500$ GeV. In each case, all other parameters are set to zero, where "σ $[pb]$" is taken along z-axis.

small values of $\bar{c}_W$, showing the high sensitivity of the cross-section on this parameter. Assuming that no other couplings affect the process, single parameter reach corresponding to 3σ limit with 300 fb^{-1} integrated luminosity is obtained as $-0.003 \leq (\bar{c}_W = -\bar{c}_B) \leq +0.003$ in the case of unpolarized beam, which is improved to $-0.002 \leq (\bar{c}_W = -\bar{c}_B) \leq +0.002$ with 80% left polarized electron beam and 20% right polarized positron beam. Fig. 4.4 presents the surface plots taking two-parameter combinations to study the correlation. We see again that $\tilde{c}_\gamma$ has insignificant effects, while other combinations have perceivable correlations.

Coming to the CP-violating couplings $\tilde{c}_{HW}$, $\tilde{c}_{HB}$ and $\tilde{c}_A$, the single parameter reach of ILC at 500 GeV with 300 fb^{-1} at 3σ level could be obtained from Fig. 4.5, 4.7 and 4.9, respectively. The effects of other couplings in deriving these limits are also indicated in these figures. Clearly, precise knowledge of the CP-conserving

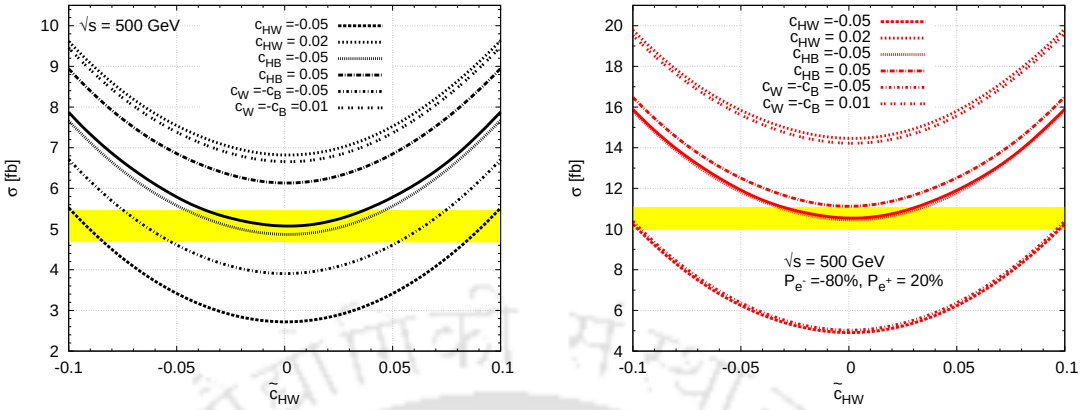

FIGURE 4.5: Cross section against $\tilde{c}_{HW}$ in the presence of selected CP-conserving (left) and CP-violating (right) couplings. The black solid line corresponds to the case when only $\tilde{c}_{HW}$ is present. The center of mass energy is assumed to be $\sqrt{s} = 500$ GeV. In each case, all other parameters are set to zero. The yellow band indicates the 3σ limit of the SM cross-section , with an integrated luminosity of 300 fb^{-1}.

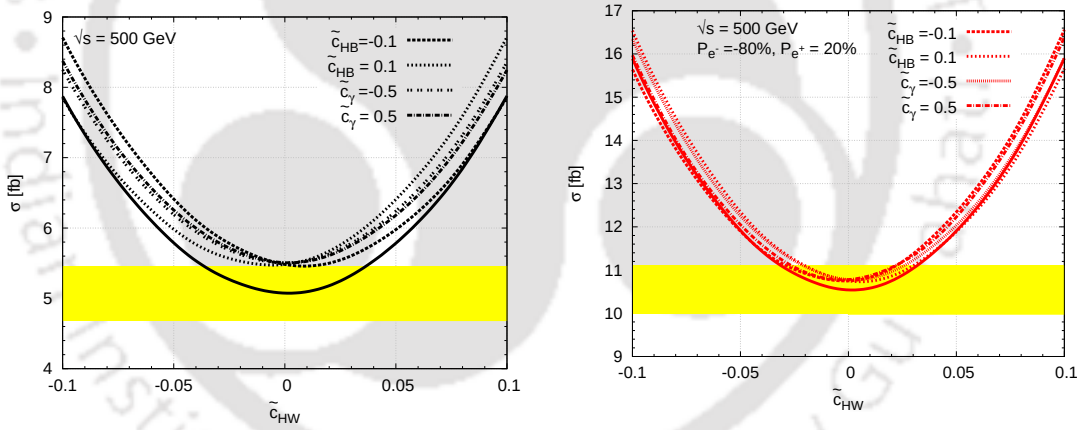

FIGURE 4.6: Cross section against $\tilde{c}_{HW}$ in the presence of selected CP-conserving (left) and CP-violating (right) couplings. The black solid line corresponds to the case when only $\tilde{c}_{HW}$ is present. The center of mass energy is assumed to be $\sqrt{s} = 500$ GeV. In each case, all other parameters are set to zero. The yellow band indicates the 3σ limit of the SM cross-section , with an integrated luminosity of 300 fb^{-1}.

parameters $\bar{c}_W$, $\bar{c}_{HW}$ and $\bar{c}_{HB}$ are required to obtain reasonably robust estimate of the CP-violating parameters. Among the CP-violating couplings, $\tilde{c}_{HW}$ affects the cross-section most significantly, and the limits derivable on the other parameters are sensitive to their presence. The effect of the $\tilde{c}_\gamma$ is much smaller than the other couplings in finding the sensitivity of $\tilde{c}_{HW}$, and therefore not presented.

The correlation between the $\bar{c}_{HW}$ and $\bar{c}_{HB}$ are presented in Fig. 4.11, where the yellow and grey bands band show the present limits derived from the LHC results

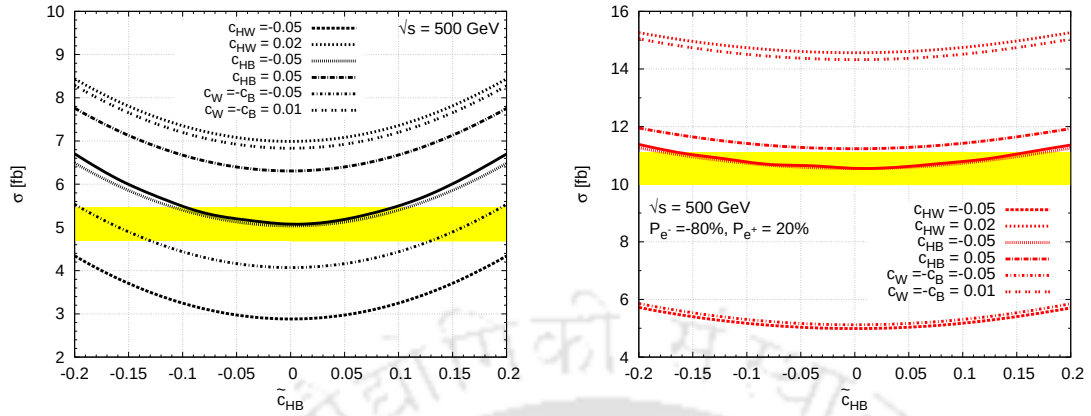

FIGURE 4.7: Cross section against $\tilde{c}_{HB}$ in the presence of selected CP-conserving (left) and CP-violating (right) couplings. The black solid line corresponds to the case when only $\tilde{c}_{HB}$ is present. The center of mass energy is assumed to be $\sqrt{s} = 500$ GeV. In each case, all other parameters are set to zero. The yellow band indicates the 3σ limit of the SM cross-section , with an integrated luminosity of 300 fb^{-1}.

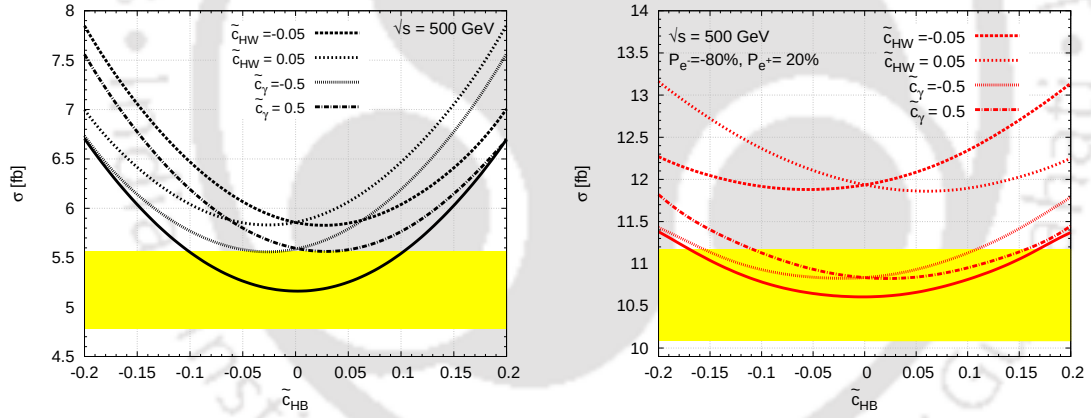

FIGURE 4.8: Cross section against $\tilde{c}_{HB}$ in the presence of selected CP-conserving (left) and CP-violating (right) couplings. The black solid line corresponds to the case when only $\tilde{c}_{HB}$ is present. The center of mass energy is assumed to be $\sqrt{s} = 500$ GeV. In each case, all other parameters are set to zero. The yellow band indicates the 3σ limit of the SM cross-section , with an integrated luminosity of 300 fb^{-1}.

on associated production of Higgs boson with the W boson [89]. In the absence of any other parameter, the allowed region in the $\bar{c}_{HW} - \bar{c}_{HB}$ plane is restricted to a narrow band (red). This band is not much affected by the presence of $\bar{c}_W$, if it is positive (green band). On the other hand, if $\bar{c}_W$ is negative, within the present bounds, it can significantly affect the allowed region (blue band) in the $\bar{c}_{HW} - \bar{c}_{HB}$ plane. The presence of CP-violating parameters are found to be insignificant here.

It is essential to know the behaviour of various kinematic distributions, and how the

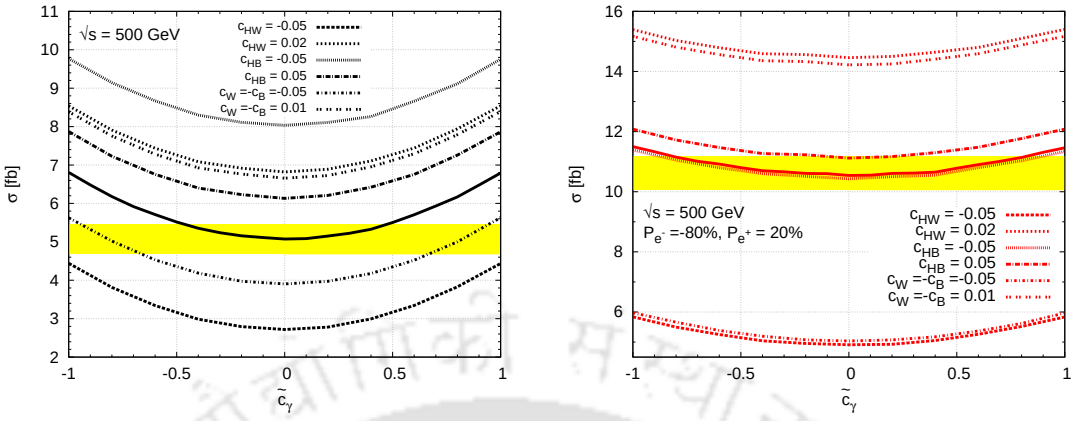

FIGURE 4.9: Cross section against $\tilde{c}_\gamma$ in the presence of selected CP-conserving (left) and CP-violating (right) couplings. The black solid line corresponds to the case when only $\tilde{c}_\gamma$ is present. The center of mass energy is assumed to be $\sqrt{s} = 500$ GeV. In each case, all other parameters are set to zero. The yellow band indicates the 3σ limit of the SM cross-section , with an integrated luminosity of 300 fb^{-1}.

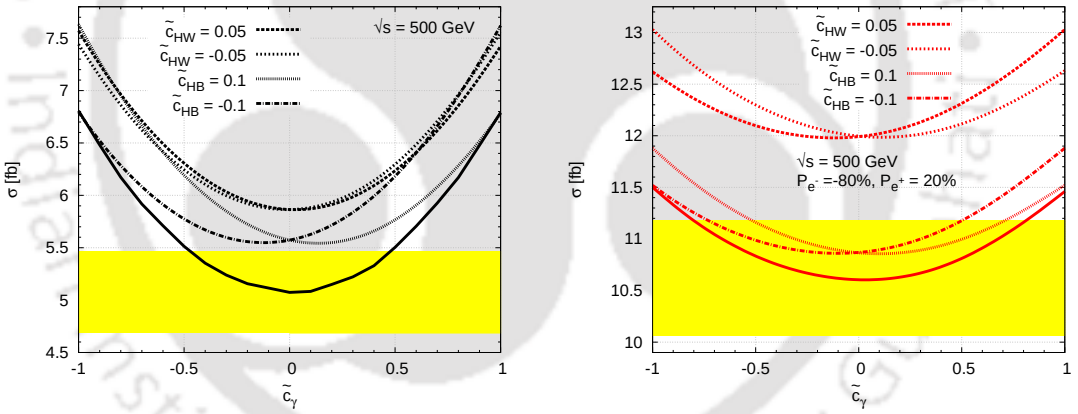

FIGURE 4.10: Cross section against $\tilde{c}_\gamma$ in the presence of selected CP-conserving (left) and CP-violating (right) couplings. The black solid line corresponds to the case when only $\tilde{c}_\gamma$ is present. The center of mass energy is assumed to be $\sqrt{s} = 500$ GeV. In each case, all other parameters are set to zero. The yellow band indicates the 3σ limit of the SM cross-section , with an integrated luminosity of 300 fb^{-1}.

anomalous coupling parameters influence these, in order to derive any useful and reliable information from the experimental results. This is so, even in cases where the fitting to obtain the reach of the parameters is done with the total number of events, as the reconstruction of events and the reduction of the background depend crucially on the kinematic distributions of the decay products. In the following we shall present some illustrative cases of distributions at the production level, to understand the effect of different couplings on these. We shall also see how

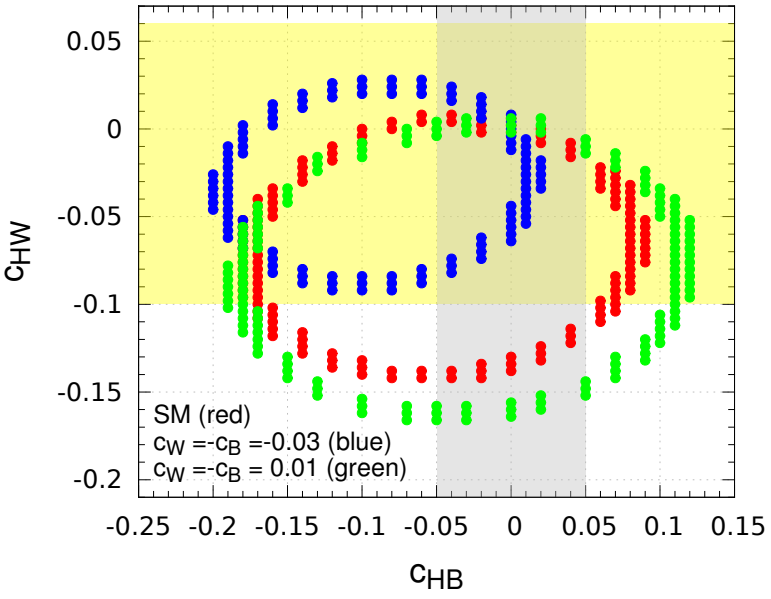

FIGURE 4.11: The ellipses correspond to regions in the $\bar{c}_{HB} - \bar{c}_{HW}$ plane with the total cross-section is within the 3σ limit of SM cross-section (red), and cros sections with $\bar{c}_W = -0.03$ (blue) and $\bar{c}_W = +0.01$ (green). An integrated luminosity of 300 fb^{-1} is considered, and the center of mass energy is taken as 500 GeV. The yellow and grey bands correspond to the present limits of $\bar{c}_{HW}$ and $\bar{c}_{HB}$, respectively.

these distributions can be effectively used to distinguish specific scenarios. The changes in the kinematic distributions at the production level will also be carried over to the distributions of their decay products. Presently we would like to be content with the analysis at the production level, considering the limited scope of this work. As mentioned earlier we shall focus on an ILC running at a center of mass energy of 500 GeV for our study.

We first consider in Fig.4.12, the normalized angular distributions of the Higgs boson for the SM case, as well as different cases with anomalous couplings (both CP-conserving and violating) as indicated in the figure, while all other parameters are set to zero. The normalized distributions provide clear information on the shape of the distribution, bringing out the qualitative difference between different cases considered. Advantage of beam polarization is evident (figure on the right) when compared to the corresponding unpolarized case (figure on the left). Presence of $\tilde{c}_{HW}$ alone (red solid) changes the distribution so that the cross-section has an enhancement in the central region with a corresponding reduction in the axial region, when compared to the SM case (black solid). This effect is nullified when considered together with non-zero values of $\bar{c}_W$ (cyan solid). Similarly, negative

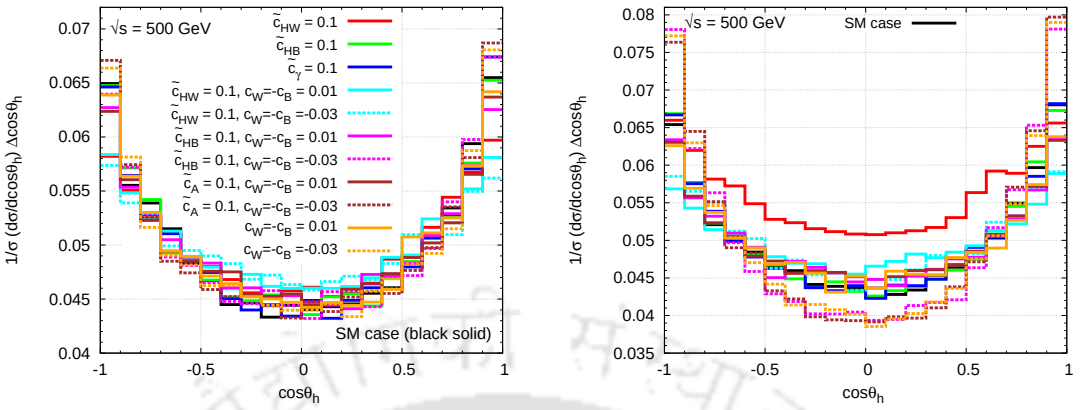

FIGURE 4.12: Distribution of the $\cos\theta_h$ for different anomalous couplings, with unpolarized (left) and polarized with $P_{e^-} = -80\%$, $P_{e^+} = +20\%$ (right) beams. A center of mass energy of 500 GeV is assumed. Color coding in the right figure is the same as that in the left figure.

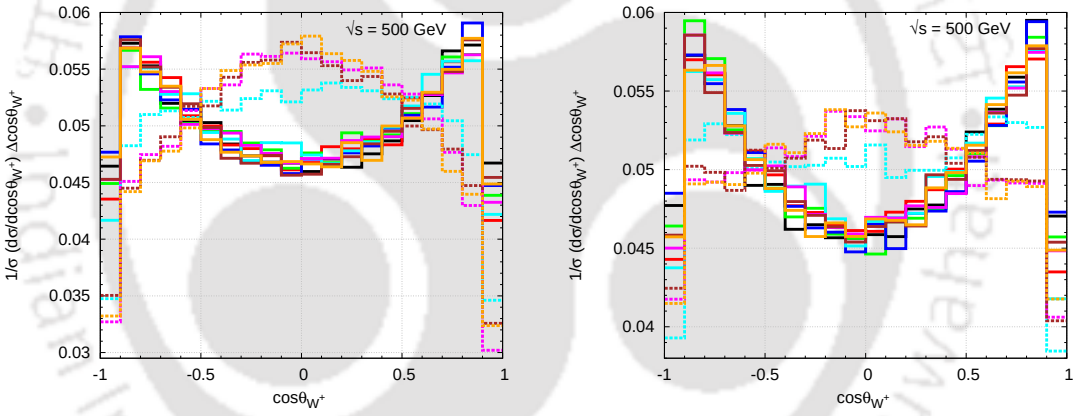

FIGURE 4.13: Distribution of the $\cos\theta_{W^+}$ for different anomalous couplings, with unpolarized (left) and polarized with $P_{e^-} = -80\%$, $P_{e^+} = +20\%$ (right) beams. A center of mass energy of 500 GeV is assumed. The colour coding is the same as in Fig. 4.12.

value of c_W in the absence of other couplings shows (light brown dashed) deviation in the distribution compared to the SM case, which is nullified by the presence of $\tilde{c}_{HW}$ (cyan dashed). The effect of $\tilde{c}_{HB}$ and $\tilde{c}_{\gamma}$ are not significant with or without the presence of other parameters.

Fig.4.13 presents the normalized angular distributions of the W^+. The negative value of $\bar{c}_W$ changes the nature of the distribution drastically (dashed light brown) compared to the SM case (black solid). Other coupling combinations do not have significant effect, except again for $\tilde{c}_{HW}$. Fig.4.14 shows the normalized $\cos\theta_{W^+h}$ distribution, where θ_{W^+h} is the angle between W^+ and h. Here $\tilde{c}_{HW}$ has significant effect, which is not affected by the presence of $\bar{c}_W$. On the other hand, the

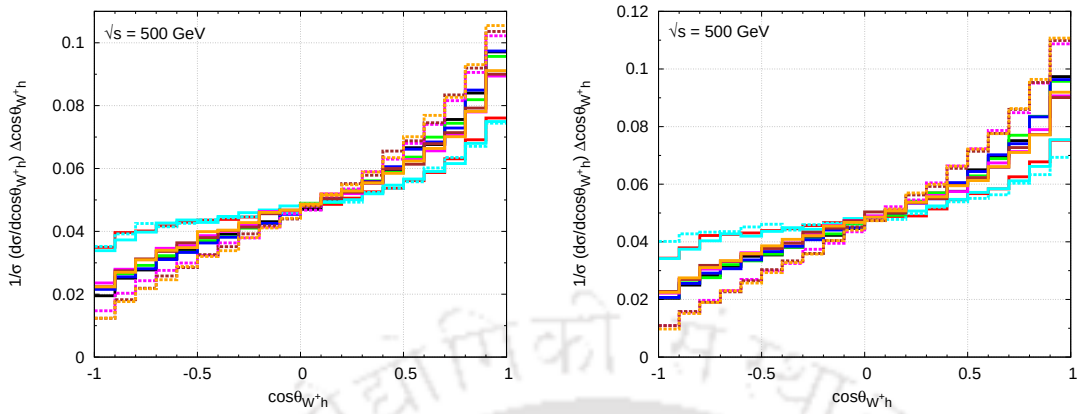

FIGURE 4.14: Distribution of the $\cos\theta_{W^+h}$ for different anomalous couplings, with unpolarized (left) and polarized with $P_{e^-} = -80\%$, $P_{e^+} = +20\%$ (right) beams. A center of mass energy of 500 GeV is assumed. The colour coding is the same as in Fig. 4.12.

presence of negative $\bar{c}_W$ alone has the opposite effect. As in the other two angular distributions, $\tilde{c}_{HB}$ and $\tilde{c}_\gamma$ have insignificant effect. Considering these three angular distributions together might allow us to distinguish different scenarios. For example, if $\tilde{c}_{HW}$ alone is present, we may expect significant effect in $\cos\theta_h$ and $\cos\theta_{W^+h}$ distributions, whereas $\cos\theta_{W^+}$ distribution remains more or less unaffected. Along with $\tilde{c}_{HW}$, if $\bar{c}_W$ was present (either positive or negative), the effect in $\cos\theta_h$ is nullified, whereas the effect would remain in $\cos\theta_{W^+h}$. The change in $\cos\theta_{W^+}$, as shown in Fig. 4.13 (left) indicates the presence of negative value of $\bar{c}_W$ with or without the presence of other couplings. Table 4.2 summarizes the cases that could be distinguished from these observations.

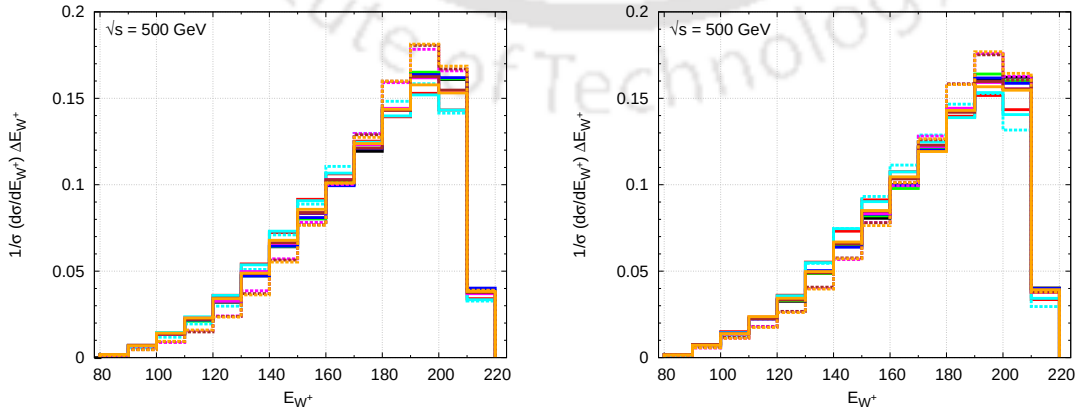

FIGURE 4.15: The energy distribution of W-boson for different anomalous couplings, with unpolarized (left) and polarized with $P_{e^-} = -80\%$, $P_{e^+} = +20\%$ (right) beams. A center of mass energy of 500 GeV is assumed. The colour coding is the same as in Fig. 4.12.

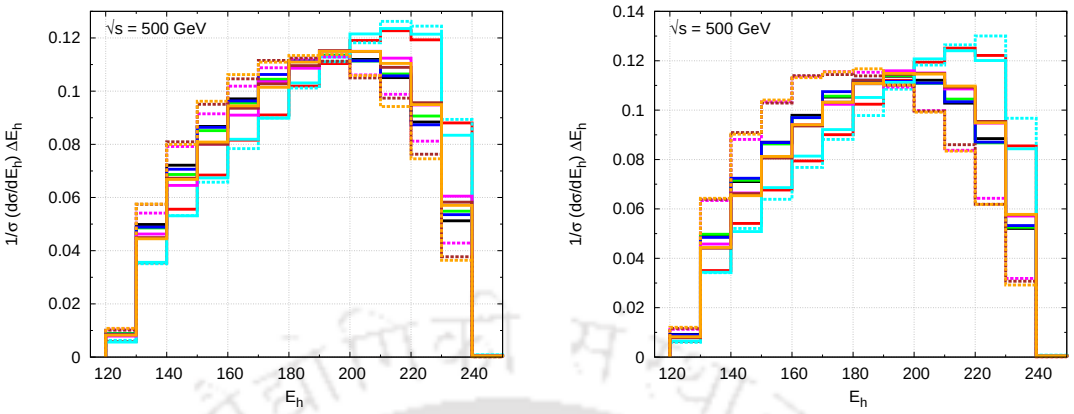

FIGURE 4.16: The energy distribution of the Higgs boson for different anomalous couplings, with unpolarized (left) and polarized with $P_{e^-} = -80\%$, $P_{e^+} = +20\%$ (right) beams. A center of mass energy of 500 GeV is assumed. The colour coding is the same as in Fig. 4.12.

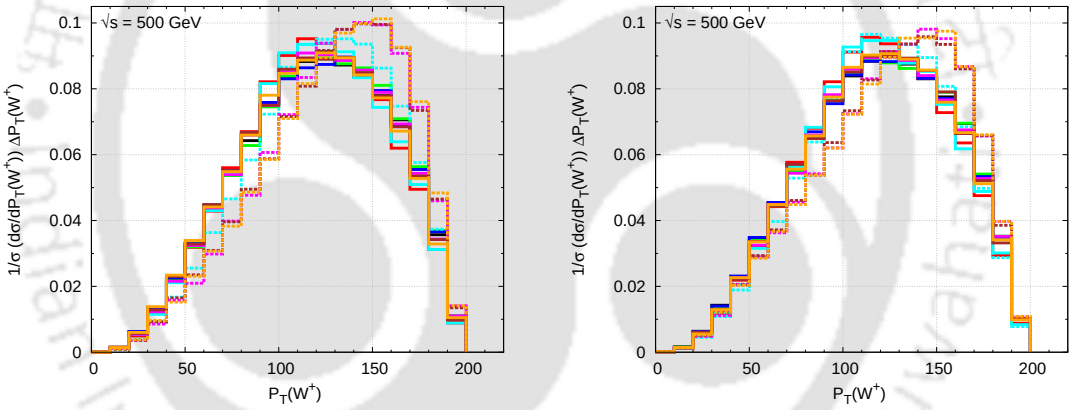

FIGURE 4.17: The transverse momentum distribution of W-boson for different anomalous couplings, with unpolarized (left) and polarized with $P_{e^-} = -80\%$, $P_{e^+} = +20\%$ (right) beams. A center of mass energy of 500 GeV is assumed. The colour coding is the same as in Fig. 4.12.

We also note that apart from the case of $\cos\theta_h$, the beam polarization does not change the qualitative picture. At the same time, the picture is clearer in the case of polarized beams compared to the case of unpolarized beams. Fig.4.14 suggests that the Forward-Backward asymmetry is a quantitative estimator of the presence of anomalous couplings. The percentage of deviation from the SM case for the cases of considered set of parameters at fixed center-of-mass energy of 500 *GeV* without and with polarized beams are given in Table 4.3, where the asymmetry is defined as

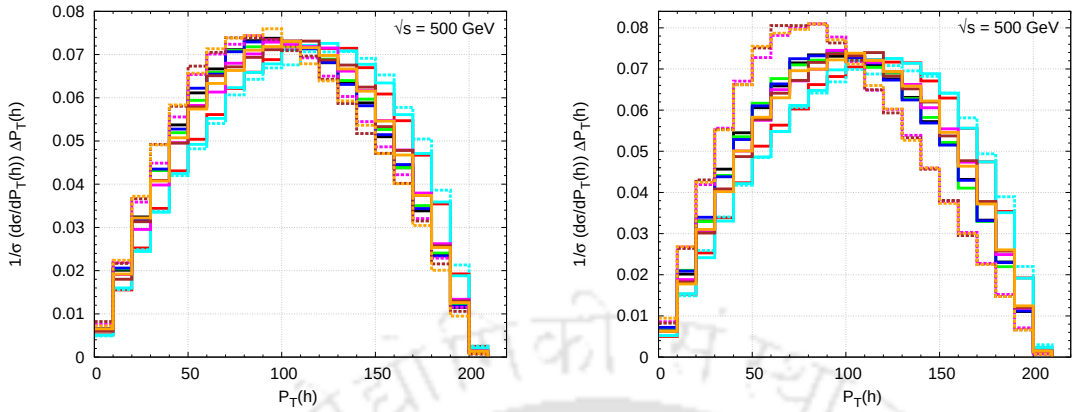

FIGURE 4.18: The transverse momentum distribution of the Higgs boson for different anomalous couplings, with unpolarized (left) and polarized with $P_{e^-} = -80\%$, $P_{e^+} = +20\%$ (right) beams. A center of mass energy of 500 GeV is assumed. The colour coding is the same as in Fig. 4.12.

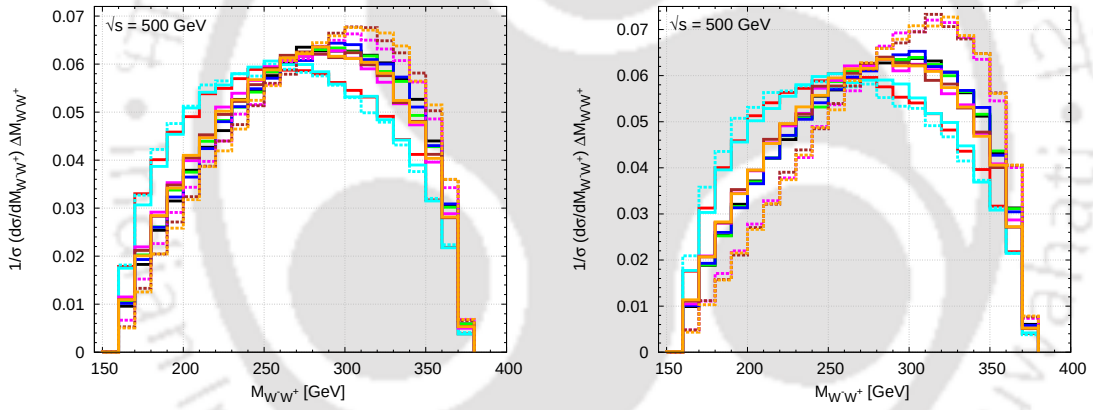

FIGURE 4.19: The invariant mass distribution of W^-W^+ for different anomalous couplings, with unpolarized (left) and polarized with $P_{e^-} = -80\%$, $P_{e^+} = +20\%$ (right) beams. A center of mass energy of 500 GeV is assumed. The colour coding is the same as in Fig. 4.12.

$$A_{FB} = \frac{\left[\int_{-1}^{0} \frac{d\sigma}{d\cos\theta} d\cos\theta - \int_{0}^{1} \frac{d\sigma}{d\cos\theta} d\cos\theta\right]}{\left[\int_{-1}^{0} \frac{d\sigma}{d\cos\theta} d\cos\theta + \int_{0}^{1} \frac{d\sigma}{d\cos\theta} d\cos\theta\right]} \tag{4.6}$$

$$\Delta A_{FB}(\%) = \frac{\left|A_{FB}^{Ano.} - A_{FB}^{SM}\right|}{A_{FB}^{SM}} \times 100. \tag{4.7}$$

Finally, we consider the normalized invariant mass distributions of W^-W^+ and W^+h. The Fig.4.19 presents the sensitivity of invariant mass distribution to the anomalous couplings parameters for the same set of parameters as in the inset of

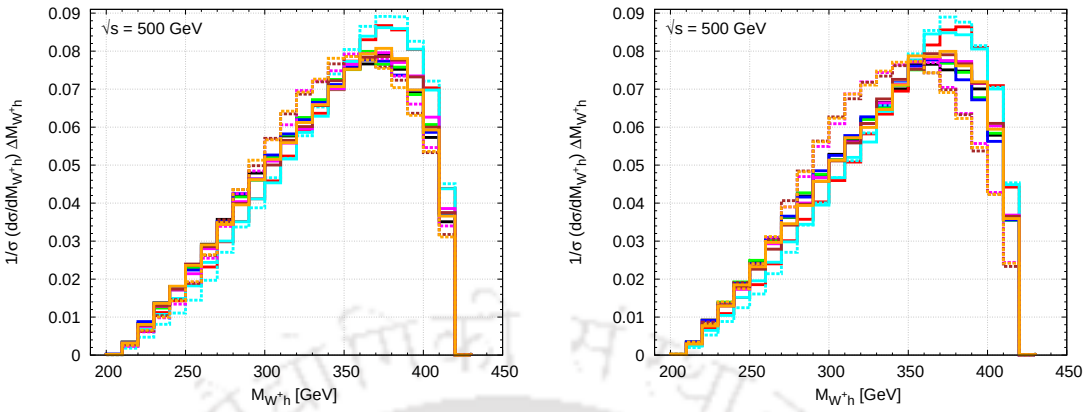

FIGURE 4.20: The invariant mass distribution of Wh for different anomalous couplings, with unpolarized (left) and polarized with $P_{e^-} = -80\%$, $P_{e^+} = +20\%$ (right) beams. A center of mass energy of 500 GeV is assumed. The colour coding is the same as in Fig. 4.12.

Couplings	$\cos\theta_h$	$\cos\theta_{W^+}$	$\cos\theta_{W^+h}$
$\tilde{c}_{HW}$ alone	yes	no	yes
$\bar{c}_W$ (positive) alone	no	no	no
$\bar{c}_W$ (negative) alone	yes	yes	yes
$\tilde{c}_{HW}$ and $\bar{c}_W$ (positive)	no	no	yes
$\tilde{c}_{HW}$ and $\bar{c}_W$ (negative)	no	yes	yes

TABLE 4.2: Presence (yes) or absence (no) of deviations that could be expected in case of different scenarios with combinations of $\bar{c}_W$ and $\tilde{c}_{HW}$ realized from Fig. 4.12 - 4.14.

$\tilde{c}_{HW}$	$\bar{c}_W = -\bar{c}_B$	$\Delta A_{FB}(\cos\theta_{W^+h})\%$	
		Unpolarized Beams	$P_{e^-} = -80\%$, $P_{e^+} = 20\%$
0.1	0	50	54
0.1	0.01	52	51
0.1	-0.03	52	64
0	0.01	13	14
0	-0.03	31	42
SM case; $A_{FB} =$		0.31	0.32

TABLE 4.3: Observed Forward-Backward asymmetry and its deviation from the SM in the angular distribution at center of mass energy of 500 GeV.

Fig.4.12. The combinations of the parameters affected are similar to the case of $\cos\theta_{W^+h}$. This can thus provides an additional tool to distinguish these scenarios. Again, the use of polarized beams marginally improve the situation.

4.5 Summary and Conclusions

In this work the process $e^-e^+ \to W^-W^+h$, which is associated with the Higgs to gauge bosons couplings namely WWh, $WW\gamma$ and ZZh, is considered. The reach of an ILC at $\sqrt{s} = 500\ GeV$ with an integrated luminosity of 300 fb^{-1} in probing different relevant parameters of the corresponding effective Lagrangian are presented. The influence of the presence of other couplings in the probe of each of the couplings are studied. In general it is observed that the CP-violating coupling $\tilde{c}_\gamma$ has very small effect on almost all of the observables considered while the other two CP-violating couplings $\tilde{c}_{HW}$ and $\tilde{c}_{HB}$ can have significant effects. Study of the $\bar{c}_{HW} - \bar{c}_{HB}$ plane shows that the allowed region can be narrowed to a very small band. While this band is unaffected by the presence of $\bar{c}_W > 0$, the effect is significant if $\bar{c}_W < 0$. Considering the angular distributions of the Higgs boson $(\cos\theta_h)$, the W^+ boson $(\cos\theta_{W^+})$ and the distributions of the angle between W^+ and h, $(\cos\theta_{W^+h})$ has proved to provide a handle in distinguishing the presence of different combinations of $\bar{c}_W$ and $\tilde{c}_{HW}$. All other parameters have indistinguishable effect on these distributions. The invariant mass distributions of WW pair as well as W^+h pair are also sensitive to some combinations of the above parameters. A quantitative estimate of the Forward-Backward asymmetry corresponding to the angle between W^+ and h show that large deviations of up to 50% is possible for moderate values of the couplings. In all cases, suitably chosen beam polarization is found to be advantageous, as illustrated with an 80% left polarized electron beam and 20% right polarized positron beam. The study has shown that WWh production at ILC is useful in detecting the anomalous couplings in Higgs-gauge boson interactions. Detailed analysis involving standard kinematic distributions could be used to distinguish different scenarios involving the couplings. While the numerical study need to be improved with more realistic collider and detector information, as well as study of the background processes, we hope to have conveyed the importance of the process in determining and disentangling the effects of anomalous Higgs-gauge boson couplings.

Chapter 5

Summary and Conclusions

The discovery of Higgs boson by the LHC in 2012, and associated measurements of its decay properties, has established the Higgs mechanism as the method of Electroweak Symmetry Breaking (EWSB). It is also clear that all indications point to the fact that the properties of this Higgs boson is very similar to that the Standard Model (SM) of particle physics proposes. At the same time, no direct or indirect hint to new physics effects are indicated by the LHC measurements so far. On the other hand, many well established reasons, like the presence of dark matter in the universe, tiny masses of the neutrinos, baryon asymmetry, and the well known hierarchy problem in the Higgs sector of the SM, strongly suggest that the SM is far from a complete theory of elementary particles. Effects beyond the SM are expected to arise at TeV energy scales. This difficult position of the present juncture of the particle physics also makes it an extremely interesting era. That is, while we expect new physics around the corner, the effects are expected to be small and indirect at the electroweak scale. Detailed precision study of different sectors through the study of interaction couplings, and correlations of various effects, are necessary to bring out such small effects. On the one hand, precise measurements through clever designs are necessary to measure such effects experimentally, while on the other hand, thorough and detailed theoretical study is necessary to support such measurements. Indirect effects of new physics is best analyzed with the help of effective field theory, where physics beyond the SM are encoded in the effective couplings between the SM particles. On the experimental front, the LHC is making fabulous breakthroughs as an explorer of new energy frontiers. In a quick time, it discovered the Higgs boson, establishing the quick computational and analysis power of the experimental collaboration. At the same

time, being a hadronic machine, it has its own limitations in precision studies. For example, it will require a very high energy and high luminosity version of LHC to probe the trilinear self couplings of the Higgs bosons. On the other hand, the proposed International Linear Collider (ILC) is a machine meant to perform detailed precision measurements. Its clean environment, and control over the initial state makes the machine suitable to probe even the rare processes. Taking this philosophy, this thesis focuses its study on the EWSB sector to probe the new physics effects through detailed study of the Higgs boson self couplings, Higgs boson and gauge boson couplings, as well as the trilinear gauge boson couplings (TGC) at the ILC. We consider an effective Lagrangian framework for our study, and investigate the effective anomalous couplings through the study of

1. Anomalous trilinear gauge boson coupling ($WW\gamma$) in the $e^-\gamma$ collisions.

2. The Higgs self couplings in the processes:
   (i) $e^-e^+ \to Zhh$,
   (ii) $e^-e^+ \to \nu_e\bar{\nu}_e hh$.

3. Higgs to gauge boson couplings through the process: $e^-e^+ \to W^-W^+h$.

In the first chapter we have provided a brief introduction of the standard model of particle physics along with its main drawbacks. Describing the standard mechanism of electroweak symmetry breaking we have briefly discussed how the elementary particles acquire their masses through the Higgs mechanism. This chapter also describes the theoretical background of the work considered, as enlisted above. We have presented a clear picture of the present status of the related work available in the literature, and provided the experimental status of the scenarios being considered.

In order to understand the electroweak sector precisely, we have carried out an investigation of anomalous $WW\gamma$ coupling in the $e^-\gamma$ collisions, for typical ILC machine considered at $\sqrt{s} = 500 - 1000\ GeV$. Unlike the well studied W pair production process, the process under consideration is not contaminated by other couplings like WWZ. Two parameters $\delta\kappa_\gamma$ and λ_γ, which are associated with the anomalous $WW\gamma$ coupling are constrained by the LEP, Tevatron and LHC experiments. Through the angular and energy spectrum of the secondary lepton (muon), we have established that the process is capable of probing the anomalous couplings much beyond the present limits. Not only that, study of cleverly chosen

combinations of different observables could be employed to disentangle the effects of these couplings, and even to probe their signs. To summarize some details, it is seen that, assuming that $\lambda_\gamma = 0$, 3σ level of cross section can probe $\delta\kappa_\gamma$ to the level of ± 0.004 for a small luminosity of 100 fb^{-1} at a center of mass energy of 500 GeV, which could be improved marginally at 1000 GeV collider. The presence of non-zero λ_γ changes this picture, and it is not possible to ascertain the case from cross section measurements alone. The angular distributions along with forward-backward asymmetry improves the situation with better sensitivity. In our analysis, it has been shown that the case of (i) $\lambda_\gamma = 0$, (ii) non-zero and positive λ_γ (iii) non-zero and negative λ_γ, can be distinguished by considering the angular distributions of the muons at fixed energies, as well as the energy distributions at fixed angles. On the other hand, the sign of $\delta\kappa_\gamma$ can be distinguished in the absence of λ_γ, whereas it is hard to do this if λ_γ is non-zero. Our illustrations are presented for a very moderate luminosity of 100 fb^{-1}, and using unpolarized beams. Being a purely weak interaction, left-handed polarization of the electrons will effectively increase the number of events, without affecting any of the conclusions qualitatively. While we have not attempted to present a quantitative estimate of the reach of ILC to probe the anomalous TGC, we hope that we have clearly demonstrated that the process considered, along with the methods described using energy-angle distributions can potentially probe both $\delta\kappa_\gamma$ and λ_γ to much better precision than other potential processes, and distinguish different possible scenarios.

In the third chapter of the thesis, we have probed the effective Higgs couplings involving the trilinear Higgs self coupling (hhh) through $e^+e^- \to Zhh$ process at an ILC running at a center of mass energy of 800 GeV, and $e^+e^- \to \nu_e\bar{\nu}_e hh$ at a very high energy ILC (perhaps the CLIC option). It is recognized that these are two of the best processes to study this coupling. Note that the first process is affected by other possible new physics effects arising through the ZZh and $ZZhh$, while the second process is also influenced by WWh and $WWhh$ anomalous couplings, apart from hhh coupling. It is shown that the detailed kinematic distributions could be utilized to disentangle the effects of these couplings. In the effective Lagrangian framework these couplings can be understood as arising from the effective operators describing the Lagrangian, and therefore can be written in terms of the corresponding coefficients. While our investigation has not taken into account the details of detector effects and background analysis, this preliminary study is partly aimed at understanding the effect of other anomalous

couplings relevant to this process. Single and two parameter reach of ILC with integrated luminosity of 1000 fb^{-1} on the effective couplings, $\bar{c}_6$ and $\bar{c}_H$, which are directly connected to the hhh couplings, are obtained. The main influence of the ZZh and $ZZhh$ couplings arise through the parameters $\bar{c}_W$, $\bar{c}_{HW}$ and $\bar{c}_{HB}$. It is seen that these latter parameters have significant influence on the reach of $\bar{c}_6$ and $\bar{c}_H$, indicating that prior, and somewhat precise knowledge of the Higgs-gauge boson couplings is necessary to draw any conclusion on the influence of trilinear couplings on the process considered. The kinematic distributions also indicate a strong influence of Higgs-gauge boson couplings, showing that, in the presence of very moderate Higgs-gauge boson couplings, it is difficult to extract reliable information regarding $\bar{c}_6$ and $\bar{c}_H$ without fixing the Higgs-gauge boson couplings somewhat precisely. A similar story is unfolded by considerations of $e^+e^- \to \nu_e\bar{\nu}_e hh$, where the influence of WWh and $WWhh$ on the sensitivity of the trilinear Higgs self-coupling is explored. Here again, the main influence come from the presence of $\bar{c}_W$, $\bar{c}_{HW}$ and $\bar{c}_{HB}$. To summarize, one need to rely on a priori knowledge of the Higgs-gauge boson couplings from elsewhere, or consider clever combination of observables to distinguish different scenarios and to extract meaningful information on the trilinear Higgs couplings.

In the fourth chapter, we have considered the study of Higgs to gauge boson couplings through the process $e^-e^+ \to W^-W^+h$, which is influenced by WWh, $WW\gamma$ and ZZh couplings. The reach of an ILC at $\sqrt{s} = 500\ GeV$ with an integrated luminosity of 300 fb^{-1} in probing different relevant parameters of the corresponding effective Lagrangian is presented. The influence of the presence of other couplings in the probe of each of the couplings is studied. In general it is observed that the CP-violating parameter $\tilde{c}_\gamma$ has very small effect on almost all of the observables considered, while $\tilde{c}_{HW}$ and $\tilde{c}_{HB}$ have significant effect. In the CP-conserving couplings, study of the $\bar{c}_{HW} - \bar{c}_{HB}$ plane shows that the allowed region can be narrowed to a very small band using the process considered. While this band is unaffected by the presence of $\bar{c}_W > 0$, the effect is significant if $\bar{c}_W < 0$. Considering the angular distributions of the Higgs boson ($\cos\theta_h$), the W^+ boson ($\cos\theta_{W^+}$) and the distributions of the angle between W^+ and h ($\cos\theta_{W^+h}$) proved to provide a handle in distinguishing the presence of different combinations of $\bar{c}_W$ and $\tilde{c}_{HW}$. All other parameters have insignificant effect on these distributions. The invariant mass distributions of WW pair as well as W^+h pair are also sensitive to some combinations of the above parameters. A quantitative estimate of the Forward-Backward asymmetry corresponding to the angle between W^+ and h

showed that large deviations of up to 50% is possible for moderate values of the couplings. In all cases, suitably chosen beam polarization is found to be advantageous, as illustrated with an 80% left polarized electron beam and 20% right polarized positron beam. The study has shown that WWh production at ILC is a suitable process in detecting the anomalous couplings in Higgs-gauge boson interactions. Detailed analysis involving standard kinematic distributions could be used to distinguish different scenarios involving the couplings. While the numerical study need to be improved with more realistic collider and detector information, as well as study of the background processes, the study conveys the importance of the process in determining and disentangling the effects of anomalous Higgs-gauge boson couplings.

In summary, in this thesis we have considered one of the important topics of the present day particle physics, namely the study of Higgs boson couplings. Detailed knowledge of the properties of the Higgs boson, including the nature and strength of its couplings with gauge bosons as well as its self-couplings is very important to establish an accurate picture of the EWSB. The thesis endeavors to understand the new physics effects modeled through an effective Lagrangian in the processes considered. The study is carried out in the context of ILC, which is suitable for precise measurements of these couplings. We have probed the trilinear Higgs self-couplings, Higgs boson couplings with gauge bosons, as well as the trilinear gauge boson couplings through suitably chosen processes. The study could extract information on the relevance of the related parameters appearing in the effective Lagrangian, so as to focus on the significant ones, neglecting those which has relatively negligible effect on the processes considered. Our numerical analyses provide estimate of the reach of ILC in probing these significant parameters. The study has also considered the interdependence of the couplings, and wherever possible discussed methods to distinguish the effects of these couplings. In conclusion, we believe our study has established the importance to understand the interdependence of different couplings while extracting the limits on anomalous couplings, and also the need of combinations of different processes and observables in fixing these parameters. We hope, the study, while preliminary in terms of its numerical predictions, has provided with qualitative understanding of some of the interdependences, and usefulness of certain observables in extracting information on some of the very important couplings related to the EWSB.

Appendix A

Energy Distribution Function of Photon Beam at ILC

A.1 Photon Energy Distribution Function

The colliding photons in a realistic electron-photon collider does not have a fixed energy, rather the beam will have distribution of photons with energy varying over an allowed range (which depends on the initial electron and laser photon energies among other things). In such colliders, the cross section and other observables should, therefore, be properly folded with a luminosity distribution function to get the measurable quantities, as is done in Eq. 2.19.

At ILC high energy, high luminosity photon beam is obtained by Compton backscattering of low energy, high intensity laser beam off high energy electron beam. Ideal Compton backscattered photon spectrum is given by [38]

$$\begin{aligned} f_{\gamma/e}(x) &= \frac{1}{D(\xi)}\left[1-x+\frac{1}{1-x}-4\,\frac{x}{\xi(1-x)}+4\,\frac{x^2}{\xi^2(1-x)^2}\right] \\ D(\xi) &= \left(1-\frac{4}{\xi}-\frac{8}{\xi^2}\right)\,\ln(1+\xi)+\frac{1}{2}+\frac{8}{\xi}-\frac{1}{2(1+\xi)^2}, \end{aligned} \tag{A.1}$$

where $x = \frac{\omega}{E_e}$, with E_e the energy of the initial electron and ω the energy of the scattered photon. x thus gives the fraction of the electron energy carried by the scattered photon. Dependence of the distributions on the initial laser photon energy (ω_0) comes through $\xi \approx \frac{4E_e\omega_0}{m_e^2}$, where m_e is the electron mass. The maximum value of x is $x_{max} = \frac{\xi}{1+\xi}$. It is, but not possible to increase ω_0

and E_e to any value to get larger x_{max}. It is found that for ξ beyond $\sim$ 4.8, conversion efficiency drops down drastically due to e^+e^- pair production between the laser photons and the backscattered photons, setting an absolute upper limit on $x \approx 0.83$. This value essentially means that with an electron beam of energy $E_e = 250$ GeV, we can effectively go up to $\omega_0 \approx 1.26$ eV. In a realistic collider, one need to also worry about the non-linear effects making the actual photon spectrum deviating from the ideal case in Eq. A.1. For more details on photon collider one may refer to, for example, Refs. [38, 39, 122, 122, 160] and references therein.

A.2 Photon Beam Polarization

It is true in general, the Compton-backscattered photon is polarized. The polarization depends upon the initial electron and laser beam polarization. But in the high energy region, it is noted that $P_\gamma = -P_e$ [38, 39, 160]. This could be used to the advantage of the physics studies being considered. In our analysis, we have not gone into these details. We have assumed unpolarized initial electron and laser beams, which produces an unpolarized high energy photon beam (to a very good approximation). For more details on photon collider one may refer to Ref. [38, 39, 122, 160].

A.3 $WW\gamma$ study at the LHC using Equivalent Photon Approximation (EPA)

The $WW\gamma$ vertex studied through photon induced processes like $pp \to \gamma\gamma X \to WWX$ at LHC [161] using EPA [162]. It is expected that $\delta\kappa_\gamma$ and λ_γ could be proved to the limit, $-0..013 < \delta\kappa_\gamma < 0.012$ and $-0.011\lambda_\gamma < 0.010$.

Appendix B

FORM Program to Compute the LIA of $e^-\gamma \to \nu_e W^-$

We present the FORM [117] program, which we have used to simplify the Lorentz Invariant Amplitude (LIA) of the process $e^-\gamma \to \nu_e W^- \to \nu_e \bar{\nu}_\mu \mu^-$.

```
*I: LORENTZ INVARIANT AMPLITUDE FOR THE PROCESS e-gam-->nuw-->ln
*   Satendra Kumar and Dr. P. Poulose@07-08-2014
      Vectors p, q, pp, qp, qpp, ppp, ke, kg, kn,
                knb, qp, km,w,xp,yp,zp;
      Symbols s, dkg, rs, t, u, wmass, emass, mumass,
                  xlambda, dkappa,
                  a, b, c, ctnb, stnb, stnb,
                  spnb, cpnb, st, ct,
                  Ew, Enb, Em, I, lg, tau, x;
      Indices rho, rhop, sig, sigp, beta, betap,
                alpha, alphap, lambda, lambdap;
*
      L M1sq =
*     interaction through electron propagator
      g_(1,km)*g_(1,sig)*g7_(1)/2
      *g_(1,knb)*g_(1,sigp)*
*
      g_(2,kn)*g_(2,rho)*g7_(2)/2
      *g_(2,p,alpha)*g_(2,ke)*g_(2,alphap)
```

```
        *g_(2,p)*g_(2,rhop)*
*
        (-1)*d_(alpha,alphap) * d_(rho,sig)*d_(rhop,sigp);

        L M2sq =
*       interaction through w boson propagator
        g_(1,km,sig)*g7_(1)/2*g_(1,knb)*g_(1,sigp)*
*
        g_(2,kn,beta)*g7_(2)/2*g_(2,ke)*g_(2,betap)*
*
        (-1)*d_(alpha,alphap)*d_(sig,lambda)*
*
        d_(sigp,lambdap)*
*
        d_(rho,beta)*
*
        d_(rhop,betap)*
*
        (d_(lambda,rho)*2*qp(alpha)+d_(alpha,rho)*2
        *kg(lambda)-d_(alpha,lambda)*(kg(rho)+qp(rho))
       +(dkg+lg)*(kg(lambda)*d_(alpha,rho)
        -kg(rho)*d_(alpha,lambda))-
        lg/wmass^2*(kg(rho)+qp(rho))*(qp(alpha)
        *kg(lambda)-(kg.qp)*d_(alpha,lambda)))
        *(d_(lambdap,rhop)*2*qp(alphap)
        +d_(alphap,rhop)*2*kg(lambdap)-
        d_(alphap,lambdap)*(kg(rhop)
        +qp(rhop))+(dkg+lg)*(kg(lambdap)
        *d_(alphap,rhop)-kg(rhop)*d_(alphap,lambdap))-
        lg/wmass^2*(kg(rhop)+qp(rhop))*(qp(alphap)
        *kg(lambdap)-(kg.qp)*d_(alphap,lambdap)));

        L M1M2C =
*       interacting term
        g_(1,km)*g_(1,sig)*g7_(1)/2*g_(1,knb)*g_(1,sigp)*
*
```

```
        g_(2,kn,rho)*g7_(2)/2*g_(2,p)
        *g_(2,alpha)*g_(2,ke)*g_(2,betap)*
*
        (-1)*d_(alpha,alphap)*d_(rho,sig)*
*
        d_(lambdap,sigp)*
*
        d_(rhop,betap)*
*
        (d_(lambdap,rhop)*2*qp(alphap)
        +d_(alphap,rhop)*2*kg(lambdap)-
        d_(alphap,lambdap)*(kg(rhop)
        +qp(rhop))+(dkg+lg)*(kg(lambdap)
        *d_(alphap,rhop)-kg(rhop)*d_(alphap,lambdap))
        -lg/wmass^2*(kg(rhop)+qp(rhop))*(qp(alphap)
        *kg(lambdap)-(kg.qp)*d_(alphap,lambdap)));

        L M2M1C =
*       interacting term
        g_(1,km)*g_(1,sig)*g7_(1)/2*g_(1,knb)*g_(1,sigp)*
*
        g_(2,kn,beta)*g7_(2)/2*g_(2,ke)
        *g_(2,alphap)*g_(2,p)*g_(2,rhop)*
*
        (-1)*d_(alpha,alphap)*d_(rhop,sigp)*
*
        d_(lambda,sig)*
*
        d_(rho,beta)*
*
        (d_(lambda,rho)*2*qp(alpha)+d_(alpha,rho)*2*kg(lambda)
        -d_(alpha,lambda) *(kg(rho)+qp(rho))+(dkg+lg)*(kg(lambda)
        *d_(alpha,rho)-kg(rho)*d_(alpha,lambda))-
        lg/wmass^2*(kg(rho)+qp(rho))*(qp(alpha)
        *kg(lambda)-(kg.qp)*d_(alpha,lambda)));
```

```
        L Msq1 = M1sq/rs^6/x;
        L Msq2 = M2sq/rs^6/x;
        L Mint = (M1M2C + M2M1C)/rs^6/x;
*
        Trace4, 1;
        Trace4, 2;
        Contract 0;
        id q = p-kn;
        id p = ke+kg;
        id qp = kg-pp;
        id pp = kn-ke;
        id kn = ke+kg-km-knb;
        id e_?(w?,xp?,yp?,zp?)= I*(
        w(0)*xp(1)*yp(2)*zp(3) - w(0)*xp(1)*yp(3)*zp(2)
       -w(0)*xp(2)*yp(1)*zp(3) + w(0)*xp(2)*yp(3)*zp(1)
       -w(0)*xp(3)*yp(2)*zp(1) + w(0)*xp(3)*yp(1)*zp(2)
       -w(1)*xp(0)*yp(2)*zp(3) + w(1)*xp(0)*yp(3)*zp(2)
       +w(1)*xp(2)*yp(0)*zp(3) - w(1)*xp(2)*yp(3)*zp(0)
       +w(1)*xp(3)*yp(2)*zp(0) - w(1)*xp(3)*yp(0)*zp(2)
       -w(2)*xp(1)*yp(0)*zp(3) + w(2)*xp(1)*yp(3)*zp(0)
       +w(2)*xp(0)*yp(1)*zp(3) - w(2)*xp(0)*yp(3)*zp(1)
       +w(2)*xp(3)*yp(0)*zp(1) - w(2)*xp(3)*yp(1)*zp(0)
       -w(3)*xp(1)*yp(2)*zp(0) + w(3)*xp(1)*yp(0)*zp(2)
       +w(3)*xp(2)*yp(1)*zp(0) - w(3)*xp(2)*yp(0)*zp(1)
       +w(3)*xp(0)*yp(2)*zp(1) - w(3)*xp(0)*yp(1)*zp(2));
        id xp?.yp?=xp(0)*yp(0) - xp(1)*yp(1)-xp(2)*yp(2)-xp(3)*yp(3);
        id ke(0)=rs/2;
        id ke(1)=rs/2*st;
        id ke(2)=0;
        id ke(3)=rs/2*ct;
        id kg(0)= rs/2;
        id kg(1)=rs/2*st;
        id kg(2)=0;
        id kg(3)=-rs/2*ct;
        id knb(0)=Enb;
        id knb(1)=Enb*stnb*cpnb;
```

```
id knb(2)=Enb*stnb*spnb;
id knb(3)=Enb*ctnb;
id km(0)=Em;
id km(1)=0;
id km(2)=0;
id km(3)=Em;
id stnb*stnb = 1-ctnb^2;
id st^2 = 1-ct^2;
id spnb^2 =1-cpnb^2;
id ctnb = 1-(wmass*wmass/2/Em/Enb);
id Enb = (s-2*rs*Em+wmass*wmass)/2/rs;
id Em= rs*x/2;
id Em^(-1)= 2/rs/x;
id u = wmass^2-t-s;
id s = rs*rs;
id I = 0;
id wmass^2= rs*rs*tau;
id wmass^2*wmass^(-2)=1;
id wmass^(-2)= 1/(rs*rs*tau);
id lg = xlambda;
id dkg = dkappa;
bracket dkappa, xlambda;
Print Msq1,Msq2,Mint;
```

Appendix C

EWSB with Dimension-Six Operators

We have explained the standard mechanism of electroweak symmetry breaking (EWSB) in the Introduction (1.1). Here we discuss the EWSB with dimension-six operators. The position of the electroweak minimum changes w.r.t. the SM prediction due to the additional terms originating from the dimension-six operators $\sim |H|^6$. To find the new minimum we consider the potential as given in Ref. [163]

$$V_{SM+6} = \mu^2|H|^2 + \lambda|H|^4 + \frac{c_6}{\Lambda^2}\lambda|H|^6, \tag{C.1}$$

which contains an additional interaction term, where the energy scale $\Lambda >> v$. Now imposing the condition for minimization $\frac{\partial V}{\partial |H|^2} = 0$, left with

$$(|H|^2)_{\pm} = \frac{\Lambda^2}{3c_6}\left(-1 \pm \sqrt{1 - \frac{3\mu^2 c_6}{\Lambda^2\lambda}}\right) \tag{C.2}$$

In order to consider the SM vacuum, choose the + solution, and obtained :

$$\frac{v^2}{2} \equiv (|H|)^2_+ = \frac{\Lambda^2}{3c_6}\left(-1 \pm \sqrt{1 - \frac{3\mu^2 c_6}{\Lambda^2\lambda}}\right) \tag{C.3}$$

After simplifying, one can get expression for μ^2:

$$\mu^2 = -\lambda v^2\left(1 + \frac{3c_6 v^2}{4\Lambda^2}\right) \tag{C.4}$$

Now ignoring the Goldstone modes, one can expand the Higgs field $|H|$ in terms of the physical scalar Higgs boson about this minimum , $H \sim \left(0, \frac{(v+h)}{\sqrt{2}}\right)$. Next start by examining the terms arising from the SM Lagrangian and the dimension-six operators that contribute to the kinetic term as

$$\mathcal{L}_{kinetic} = (D_\mu H)^\dagger (D^\mu H) + \frac{\bar{c}_H}{2\Lambda^2}(\partial^2 |H|^2)^2, \tag{C.5}$$

where D_μ is the covariant derivative that includes all the interaction terms of the Higgs field with the gauge bosons. After expansion of this, we left with

$$\mathcal{L}_{kinetic} = \frac{1}{2}\Big(1 + \frac{c_H v^2}{\Lambda^2}\Big)\partial_\mu h \partial^\mu h + \frac{c_H v}{\Lambda^2} h \partial h \partial^\mu h + \frac{c_H}{2\Lambda^2} h \partial h \partial^\mu h + ..., \tag{C.6}$$

while the gauge boson interactions being ignored. To canonically normalize the Higgs boson kinetic term and to remove derivative interactions, considering the following non-linear transformation:

$$h = \Big(1 + \frac{a_0' v^2}{\Lambda^2} h'\Big) + \frac{a_1' v}{\Lambda^2} h'^2 + \frac{a_2'}{\Lambda^2} h'^3. \tag{C.7}$$

Now plugging this equation into Eq. (C.6) and find the values of the constants a_i' that cancel all the terms except $\frac{1}{2}\partial_\mu h \partial^\mu h$,

$$a_0' = -\frac{1}{2} c_H, \qquad a_1' = -\frac{1}{2} c_H, \qquad a_2' = -\frac{1}{6} c_H, \tag{C.8}$$

and get the following form,

$$h = \Big(1 - \frac{c_H v^2}{2\Lambda^2} h'\Big) - \frac{c_H v}{2\Lambda^2} h'^2 - \frac{c_H}{6\Lambda^2} h'^3. \tag{C.9}$$

Note that this shift should be performed everywhere in the Lagrangian, and arises changes in as well as new interactions. Now, first perform the shift in the terms contributing to the Higgs boson scalar mass. The relevant terms,

$$\mathcal{L}_{m_h} = -\frac{\mu^2}{2} h^2 - \frac{3\lambda v^2}{2} h^2 - \frac{15 c_6 \lambda v^4}{8\Lambda^2} h^2. \tag{C.10}$$

where the last term comes from the $|H|^6$ interaction. Now substitute the μ^2 using Eq. (C.4) and perform the shift of Eq. (C.9) and keeping terms up to h^2 and $\mathcal{O}(\Lambda^{-2})$:

$$\mathcal{L}_{m_h} = -\lambda v^2 \Big(1 - \frac{c_H v^2}{\Lambda^2} + \frac{3 c_6 \lambda v^4}{2\Lambda^2}\Big) h'^2, \tag{C.11}$$

from this, one can get easily the Higgs mass term as,

$$m_h^2 = 2\lambda v^2\Big(1 - \frac{c_H v^2}{\Lambda^2} + \frac{3c_6\lambda v^4}{2\Lambda^2}\Big). \tag{C.12}$$

Now one can see the relevant terms are the same as those that appear in the potential of Eq. (C.1), when deriving the expression for the trilinear coupling after expanding about the minimum and canonically normalizing via Eq. (C.9),

$$\mathcal{L}_{self} = -V_{SM+6} = -\mu^2|H|^2 - \lambda|H|^4 - \frac{c_6}{\Lambda^2}\lambda|H|^6. \tag{C.13}$$

Moreover, expanding this about the electroweak minimum, we left with

$$\mathcal{L}_{self} = -\mu^2\frac{(v+h)^2}{2} - \lambda\frac{(v+h)^4}{4} - \frac{c_6}{\Lambda^2}\lambda\frac{(v+h)^6}{8}. \tag{C.14}$$

After omitting terms with $h^n,\ n > 4$, and constant terms we arrive at

$$\begin{aligned}\mathcal{L}_{self} &= -\frac{\mu^2}{2}(2hv + h^2) - \frac{\lambda}{4}(4hv^3 + 6h^2v^2 + 4h^3v + h^4)\\ &\quad -\frac{c_6\lambda}{8\Lambda^2}(6v^5h + 6v^5h + 15v^4h^2 + 20v^3h^3 + 15v^2h^4).\end{aligned} \tag{C.15}$$

It is convenient to calculate the $h^2,\ h^3$ and h^4 terms as a function of h' up to h'^4:

$$\begin{aligned}h^2 &= h'^2\Big[1 - \frac{c_H v^2}{\Lambda^2} - \frac{c_H v}{\Lambda^2}h' - \frac{c_H}{3\Lambda^2}h'^2\Big] + \mathcal{O}(h'^5),\\ h^3 &= h'^3\Big[1 - \frac{3c_H v^2}{2\Lambda^2} - \frac{3c_H v}{2\Lambda^2}h'\Big] + \mathcal{O}(h'^5),\\ h^4 &= h'^4\Big[1 - \frac{2c_H v^2}{\Lambda^2}\Big] + \mathcal{O}(h'^5)\end{aligned} \tag{C.16}$$

All these terms can be substituted into Eq. (C.15), we get the terms up to $\mathcal{O}(h'^4)$

$$\mathcal{L}_{self} = -\lambda\Big[v + \frac{5c_6v^3}{2\Lambda^2} - \frac{5c_Hv^3}{2\Lambda^2}\Big]h'^3 - \frac{\lambda}{4}\Big[1 + \frac{15c_6v^2}{2\Lambda^2} - \frac{28c_Hv^2}{3\Lambda^2}\Big]h'^4 \tag{C.17}$$

from here we can see how the parameters c_6 and c_H associated with Higgs self-couplings, affected the standard Higgs potential. Definitely, we will left with the standard Higgs potential if c_6 and c_H found to be zero from future experiments. Rest part of this mechanism (say: Yukawa terms, Higgs-gauge bosons interaction terms etc.) can be seen in Ref. [163].

Appendix D

Results for $e^-e^+ \to Zhh$ at the center-of-mass energy of 500 GeV

In chapter-3, we have presented results for the same process at the center-of-mass energy of 800 GeV. Here we present the phenomenological analysis of considered process in detail within the context of the SM at the center-of-mass energy of 500 GeV, which is one of typical values at the ILC. In Fig.D.1 (left), the cross-section is plotted against the center-of-mass energy for the SM case as well as for some selected $(\bar{c}_6, \bar{c}_H)$ values. The green and the yellow bands correspond to the 3σ limit with an integrated luminosity of 100 fb^{-1} and 1000 fb^{-1}, respectively,

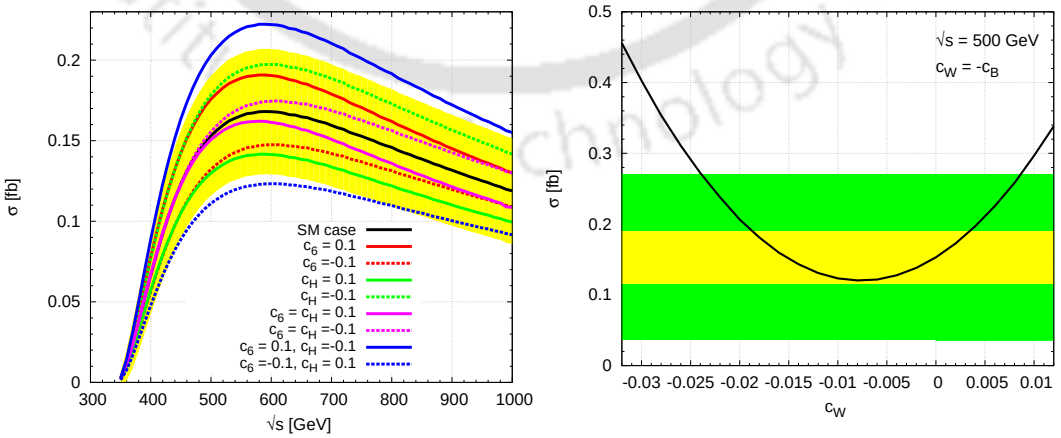

FIGURE D.1: **Left**: The total cross-section against $\sqrt{s}$ for the process $e^-e^+ \to Zhh$, for different values of the parameters $\bar{c}_6$ and $\bar{c}_H$, with all others kept to zero. **Right**: The total cross-section against anomalous coupling parameter $(\bar{c}_W)$, where the green and yellow bands correspond to 3σ deviations from the SM with integrated luminosities of 100 fb^{-1} and 1000 fb^{-1} respectively.

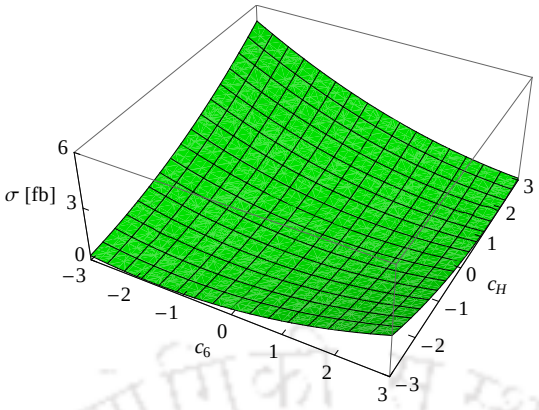

FIGURE D.2: Cross section of Zhh production plotted against $\bar{c}_6$ and $\bar{c}_H$ at $\sqrt{s} = 500$ GeV, with all other parameters set to zero.

assuming only statistical uncertainty. The cross-section peaks around a center-of-mass energy of 600 GeV with a value of about 0.17 fb, which slides down to about 0.15 fb at 500 GeV. We perform our analysis for an ILC running at a center-of-mass energy of 500 GeV, which is one of the planned center-of-mass energy of the proposed ILC. Fig. D.1 (right) shows the dependence of cross-section (σ) on $\bar{c}_W = -\bar{c}_B$ along with the 3σ limit at integrated luminosities of 100 fb^{-1} and 1000 fb^{-1}. Assuming all other couplings are absent, one can obtain a limit of $-0.024 \leq (\bar{c}_W = -\bar{c}_B) \leq +0.0085$ with 100 fb^{-1} luminosity, which could be improved slightly to $-0.019 \leq (\bar{c}_W = -\bar{c}_B) \leq +0.003$ with 1000 fb^{-1}. Although, compared to the present bounds, these limits are about an order of magnitude better in the case of lower limit, and somewhat better than that in the case of upper limit, we do not anticipate to probe the reach of this coupling through this process. On the other hand, expecting that $\bar{c}_W$ is measured, through other processes like WW pair production beforehand, the cross-section measurement for the process being considered here could indicate the influence of other anomalous couplings involved. Below we shall explore the interconnection of these couplings on the cross-section, and try to understand how some specific scenarios could be disentangled. One may note that the cross-section is small compared to many other typical electroweak processes, and one will need to be patient to reach a very high luminosity of a few 1000 fb^{-1} to make any meaningful study. This would be the case with any process involving trilinear Higgs couplings, and therefore, the process under scrutiny is not at any particular disadvantage because of this.

We consider the influence of $\bar{c}_6$ on the cross-section in Fig. D.3 (left). We have compared the variation of cross-section with $\bar{c}_6$ keeping all other parameters to the SM value (black curve), along with the cases when the above mentioned relevant

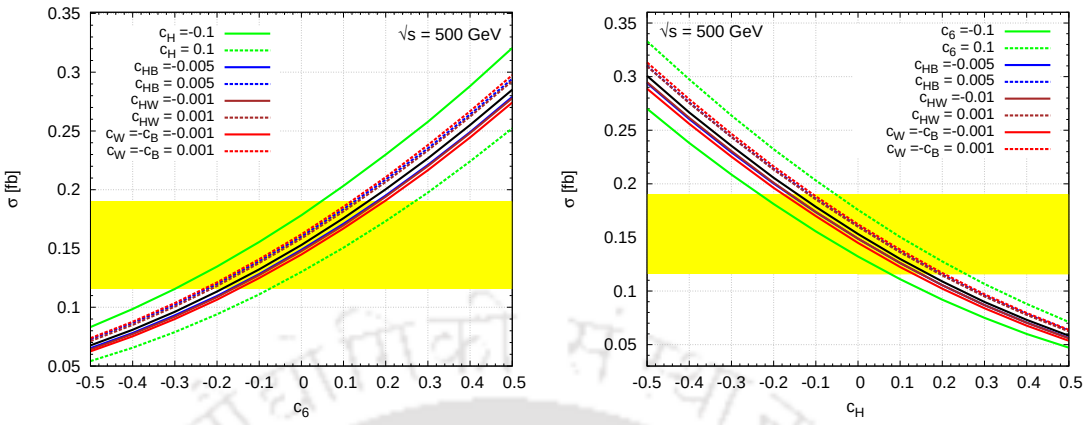

FIGURE D.3: Cross section of Zhh production against $\bar{c}_6$ (left) and $\bar{c}_H$ (right), when some of the other selected relevant parameters assume typical values is compared against the case when only $\bar{c}_6$ or $\bar{c}_H$ is present (black solid curve). The center-of-mass energy is assumed to be $\sqrt{s} = 500$ GeV. In each case, all other parameters are set to zero. The yellow band indicates the 3σ limit of the SM cross-section, with an integrated luminosity of 1000 fb^{-1}.

parameters having non-standard values (colored curves). The yellow band denotes 3σ region of the SM value of the cross-section, considering an integrated luminosity of 1000 fb^{-1}. Fig. D.3 (right) presents a similar picture for the case of $\bar{c}_H$. The values of the couplings $\bar{c}_W$, $\bar{c}_{HW}$ and $\bar{c}_{HB}$ are chosen, assuming that they are available at permill level from other observations like production of WW and Zh at ILC, where $WWZ(\gamma)$ and ZZh couplings are expected to be measured quite accurately. Clearly, $\bar{c}_W$ is the most sensitive, and $\bar{c}_{HW}$ influence almost at the same level, whereas $\bar{c}_{HB}$ is about 5 times smaller. The influence of these couplings on the derivable bounds is tabulated in Table D.1. These limits indicate that, in order to get better than 30-20% accuracy in the measurement of $\bar{c}_{6,H}$, the couplings $\bar{c}_W$ and $\bar{c}_{HW}$ need to be measured better than permill level. Coming to the influence of $\bar{c}_6$ and $\bar{c}_H$ on each other, in Fig. 3.6, the cross-section is plotted against these couplings. The correlation of the sensitivity between the two parameters is clear. The opposite sign combination seems to be more sensitive to the cross-section, and therefore more stringent constraints could be drawn in this case compared to the same sign case. Considering the two parameters $\bar{c}_6$ and $\bar{c}_H$ relevant to the trilinear Higgs coupling, the reach of ILC through the Zhh production cross-section at 3σ level with an integrated luminosity of 1000 fb^{-1} is presented in Fig. D.4, for the case of SM, and cases with non-vanishing anomalous ZZh and $ZZhh$ couplings (through the couplings, $\bar{c}_W$, $\bar{c}_{HW}$ and $\bar{c}_{HB}$). Note that, when cross-section is considered as a function of $\bar{c}_6$ and $\bar{c}_H$, the result is a second

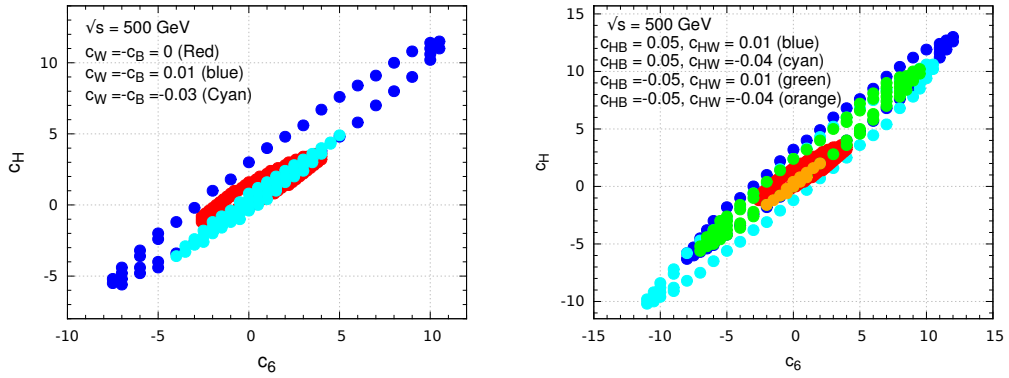

FIGURE D.4: The shaded regions correspond to regions in the $\bar{c}_6$-$\bar{c}_H$ plane with the total cross-section is within the 3σ limit when $\bar{c}_6 = \bar{c}_H = 0$ in each case, for an integrated luminosity of 1000 fb^{-1} at a center-of-mass energy of 500 GeV. Values of the other anomalous couplings are as indicated in the figure, with all other couplings set to zero.

order polynomial of these two parameters. With this, the 3σ limit of the cross-section leads to an elliptic equation corresponding to the relation between these two parameters. This result in an elliptic band in the $\bar{c}_6 - \bar{c}_H$ plane respecting the 3σ limit of the cross-section. As is evident from the plots, these allowed bands of the parameters move in the parameter space, depending on the values of the other parameters. For illustration, we have chosen the maximum allowed values of these parameters in this analysis. From the right side plot, evidently, the influence is more for the positive values of $\bar{c}_W$. This is unlike the case of single parameter consideration, where the influence was more symmetric. At the same time, for positive values of $\bar{c}_{HW}$, the influence of $\bar{c}_{HB}$ seems to be somewhat negligible, whereas, for the negative values of $\bar{c}_{HW}$ and $\bar{c}_{HB}$, the sensitivity is

Other Couplings	$\bar{c}_6$	$\bar{c}_H$
SM	[-0.19, +0.16]	[-0.14, +0.16]
$\bar{c}_H$ or $\bar{c}_6 = -0.1$	[-0.30, +0.04]	[-0.22, +0.08]
$\bar{c}_H$ or $\bar{c}_6 = 0.1$	[-0.08, +0.26]	[-0.05, +0.26]
$\bar{c}_{HB} = -0.005$	[-0.16, +0.18]	[-0.16, +0.15]
$\bar{c}_{HB} = 0.005$	[-0.22, +0.12]	[-0.10, +0.20]
$\bar{c}_{HW} = -0.001$	[-0.15, +0.18]	[-0.16, +0.15]
$\bar{c}_{HW} = 0.001$	[-0.21, +0.14]	[-0.12, +0.20]
$\bar{c}_W = -\bar{c}_B = -0.001$	[-0.14, +0.20]	[-0.18, +0.13]
$\bar{c}_W = -\bar{c}_B = 0.001$	[-0.22, +0.12]	[-0.10, +0.20]

TABLE D.1: Showing the one parameter reach corresponding to the 3σ limit with an integrated luminosity of 1000 fb^{-1} at center-of-mass energy of 500 GeV.

significantly improved, suggesting constructive interference in this case. Thus, precise measurement of the Higgs-gauge boson couplings elsewhere, including the sign of the couplings involved, is necessary to derive meaningful limits on the Higgs trilinear couplings. In fact, considering the apparently correlated influences of the different parameters, $\bar{c}_W$, $\bar{c}_{HW}$ and $\bar{c}_{HB}$ indicate that, it may be necessary to disentangle the effects of these parameters, in order to make precise statements regarding the hhh coupling.

Other Couplings	$\bar{c}_6$	$\bar{c}_H$
SM	[-3.00, +4.00]	[-1.80, +4.00]
$\bar{c}_W = -\bar{c}_B = 0.01$	[-8.50, +10.5]	[-6.00, +11.5]
$\bar{c}_W = -\bar{c}_B = -0.03$	[-4.00, +5.00]	[-4.00, +5.00]
$\bar{c}_{HB} = 0.05, \bar{c}_{HW} = 0.01$	[-8.00, +12.0]	[-6.50, +13.0]
$\bar{c}_{HB} = 0.05, \bar{c}_{HW} = -0.04$	[-11.0, +10.5]	[-10.5, +11.0]
$\bar{c}_{HB} = -0.05, \bar{c}_{HW} = 0.01$	[-7.00, +9.50]	[-6.00, +10.0]
$\bar{c}_{HB} = -0.05, \bar{c}_{HW} = -0.04$	[-2.00, +2.00]	[-2.00, +2.00]

TABLE D.2: Showing the two parameters reach corresponding to the 3σ limit with an integrated luminosity of 1000 fb^{-1} at center-of-mass energy of 500 GeV.

It is important to know the behaviour of the kinematic distributions, and how the anomalous parameters influence these, to derive any useful and reliable conclusions from the experimental results. This is so, even in cases where the fitting to obtain the reach of the parameters is done with the total number of events, as the reconstruction of events and the reduction of the background depend crucially on the kinematic distributions of the decay products. In the following we shall present some illustrative cases of distributions at the production level, in order to understand the effect of different couplings on these. The changes in the kinematic distributions at the production level will also be carried over to the distributions of their decay products. Presently we would like to be content with the analysis at the production level, considering the limited scope of this work. As mentioned earlier, we shall focus on an ILC running at a center-of-mass energy of 500 GeV for our study.

The normalized energy and angular distributions of the Z boson, and the invariant mass distribution of the hh pair are shown in Fig.D.5. The black solid curve corresponds to the SM case. We have found that the transverse momentum distribution of the Z boson behaves very similar to the energy distribution in different scenarios

considered. The distributions in the presence of $\bar{c}_6$ and $\bar{c}_H$ separately, and along with the other relevant couplings, $\bar{c}_W$, $\bar{c}_{HW}$ and $\bar{c}_{HB}$ are presented to understand the influence of these couplings on each other. Our analysis here is more of a qualitative nature, and therefore, we have fixed the values of $\bar{c}_6$ and $\bar{c}_H$ to be ± 1, and the values of other couplings to be the maximum allowed ones. The distributions are normalized, and therefore, only the deviation in the shape, indicating different functional dependence will be established through this. The case of $\bar{c}_W = -\bar{c}_B$, when considered alone coincides with that of the SM case, and therefore not shown. On the other hand, the case of $\bar{c}_6$ and $\bar{c}_H$ shows clear deviation from the SM case. Here, the combination $\bar{c}_6 \cdot \bar{c}_H = -1$ is considered, as from the analyses presented before shows that the other combination has insignificant effect. The figure on the left panel shows the case with $\bar{c}_W = -\bar{c}_B$ taking typical values along with $\bar{c}_6$ and $\bar{c}_H$, while the other parameters are set to zero, whereas the figure on the right considers $\bar{c}_{HW}$ and $\bar{c}_{HB}$ non-zero, while setting $\bar{c}_W = -\bar{c}_B$ to zero. The case with only $\bar{c}_6$ and $\bar{c}_H$ taking non-zero values, when compared with the SM case shows a perceivable change in the distribution with more number of events piling in the central region, and at higher energies and transverse momentum of the Z boson. Such an experimental observations could therefore be considered as an indication of the anomalous hhh coupling. We have considered only the opposite-sign combinations, for the same-sign combinations do not have much influence. At the same time, the presence of anomalous $\bar{c}_W$ and $\bar{c}_B$ couplings, when considered alone does not affect the distribution much, and therefore not presented. Presence of $\bar{c}_W$ and $\bar{c}_B$ with negative values when considered along with $\bar{c}_6$ and $\bar{c}_H$ do not have any influence. On the other hand, for positive values of $\bar{c}_W$ and $\bar{c}_B$, the distributions are affected when $\bar{c}_6 < 0$. The figure on the right consider the influence of $\bar{c}_{HW}$ and $\bar{c}_{HB}$ along with $\bar{c}_6$ and $\bar{c}_H$. When considered alone, different combinations of $\bar{c}_{HW}$ and $\bar{c}_{HB}$, except $\bar{c}_{HW} = -0.05$ and $\bar{c}_{HB} = -0.04$ have negligible deviation from the SM case, and therefore not presented. This combination with both the parameters taking negative values shows quite different $\cos\theta_Z$ dependence, indicating more $\cos^2\theta_Z$ component (cyan solid curve). Constructive interference of this case with the presence of $\bar{c}_6$ and $\bar{c}_H$ is seen in the cyan dotted curve. All other combinations of $\bar{c}_{HW}$ and $\bar{c}_{HB}$ have significant influence, when considered along with $\bar{c}_6 = -1$ and $\bar{c}_H = 1$ case to the extend that it coincides with the case of $\bar{c}_6 = 1$ and $\bar{c}_H = -1$. When considered along with $\bar{c}_6 = 1$ and $\bar{c}_H = -1$, only the combination of $\bar{c}_{HW} < 0$ shows significant deviation, as shown by the magenta curves. The above behaviours of the different scenarios change slightly in the case

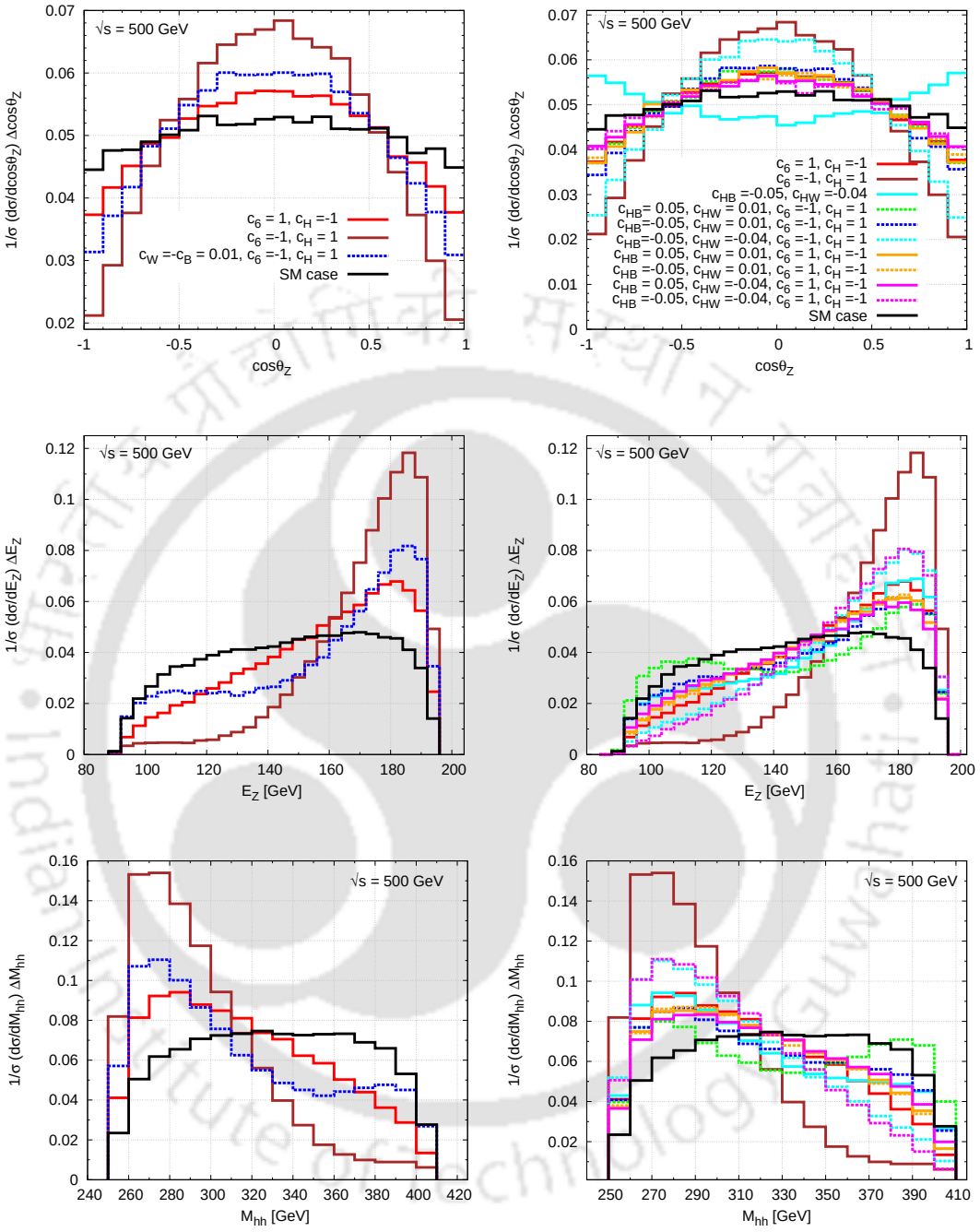

FIGURE D.5: Distributions of the $\cos\theta_Z$, energy of the Z boson and the invariant mass of the hh pair for the anomalous coupling values as in the inset, illustrating how the presence of $\bar{c}_W$ (first column), and $\bar{c}_{HW}$ and $\bar{c}_{HB}$ (second column) affect the influence of $\bar{c}_6$ and $\bar{c}_H$. A center-of-mass energy of 500 GeV is assumed. The colour coding is same in all figures as in the figures at top in respective columns.

of energy distribution. The same-sign combination of $\bar{c}_{HW}$ and $\bar{c}_{HB}$ has a distinct influence compared to their opposite-sign combination. The opposite-sign combination does not care about which of the parameter is negative. We have presented

only one of these illustrated by blue dotted curve. The case of both parameters being positive (green dotted curve) shows a distinct energy and M_{hh} distributions, when considered along with $\bar{c}_6 = -1$ and $\bar{c}_H = 1$, whereas for the opposite combination of $\bar{c}_6 = -1$ and $\bar{c}_H = 1$, no such clearly distinguishable feature is present. From this point of view, these two distributions are more suitable to distinguish different scenarios, compared to the $\cos\theta_Z$ distribution.

Bibliography

[1] W. Buchmuller and C. Ludeling. Field Theory and Standard Model. (DESY-06-151), 2006, hep-ph/0609174.

[2] M. Herrero. The Standard model. *NATO Sci.Ser.C*, 534:1–59, 1999, hep-ph/9812242.

[3] S. Dawson. Introduction to electroweak symmetry breaking. pages 1–83, 1998, hep-ph/9901280.

[4] Abdelhak Djouadi. The Anatomy of electro-weak symmetry breaking. I: The Higgs boson in the standard model. *Phys.Rept.*, 457:1–216, 2008, hep-ph/0503172.

[5] Peter W. Higgs. Broken symmetries, massless particles and gauge fields. *Phys.Lett.*, 12:132–133, 1964.

[6] Peter W. Higgs. Broken Symmetries and the Masses of Gauge Bosons. *Phys.Rev.Lett.*, 13:508–509, 1964.

[7] F. Englert and R. Brout. Broken Symmetry and the Mass of Gauge Vector Mesons. *Phys.Rev.Lett.*, 13:321–323, 1964.

[8] Georges Aad et al. Observation of a new particle in the search for the Standard Model Higgs boson with the ATLAS detector at the LHC. *Phys.Lett.*, B716:1–29, 2012, 1207.7214.

[9] Serguei Chatrchyan et al. Observation of a new boson at a mass of 125 GeV with the CMS experiment at the LHC. *Phys.Lett.*, B716:30–61, 2012, 1207.7235.

[10] ATLAS Collaboration, Report No. ATLAS-CONF-2013-029, 2013.

[11] ATLAS Collaboration, Report No. ATLAS-CONF-2013-011, 2013.

[12] ATLAS Collaboration, Report No. ATLAS-CONF-2013-010, 2013.

[13] ATLAS Collaboration, Report No. ATLAS-CONF-2013-030, 2013.

[14] ATLAS Collaboration, Report No. ATLAS-CONF-2013-034, 2013.

[15] ATLAS Collaboration, Report No. ATLAS-CONF-2013-031, 2013.

[16] ATLAS Collaboration, Report No. ATLAS-CONF-2013-009, 2013.

[17] ATLAS Collaboration, Report No. ATLAS-CONF-2013-012, 2013.

[18] Rodolfo Alexander Diaz. Phenomenological analysis of the two Higgs doublet model. 2002, hep-ph/0212237.

[19] Vernon Barger, Lisa L. Everett, Chris B. Jackson, Andrea D. Peterson, and Gabe Shaughnessy. Measuring the 2HDM Scalar Potential at LHC14. *Phys.Rev.*, D90:095006, 2014, 1408.2525.

[20] Rui Santos, P. M. Ferreira, Renato Guede, John F. Gunion, Howard E. Haber, et al. The CP-conserving 2HDM after the 8 TeV run. *PoS*, DIS2014: 127, 2014.

[21] Lei Wang. A simplified 2HDM with a scalar dark matter and the galactic center gamma-ray excess. 2014, 1406.3598.

[22] Stephen P. Martin. A Supersymmetry primer. *Adv.Ser.Direct.High Energy Phys.*, 21:1–153, 2010, hep-ph/9709356.

[23] R. Ahl Laamara, S. E. Ennadifi, and M. A. Loualidi. On Higgs-extended MSSM models. *J.Exp.Theor.Phys.*, 119:49–53, 2014.

[24] Beranger Dumont. Higgs coupling measurements and impact on the MSSM. *PoS*, DIS2014:128, 2014, 1407.0415.

[25] M. Maniatis. The Next-to-Minimal Supersymmetric extension of the Standard Model reviewed. *Int.J.Mod.Phys.*, A25:3505–3602, 2010, 0906.0777.

[26] Ulrich Ellwanger, Cyril Hugonie, and Ana M. Teixeira. The Next-to-Minimal Supersymmetric Standard Model. *Phys.Rept.*, 496:1–77, 2010, 0910.1785.

[27] H. Georgi and S. L. Glashow. Unity of All Elementary Particle Forces. *Phys. Rev. Lett.*, 32:438–441, 1974.

[28] A. J. Buras, John R. Ellis, M. K. Gaillard, and Dimitri V. Nanopoulos. Aspects of the Grand Unification of Strong, Weak and Electromagnetic Interactions. *Nucl. Phys.*, B135:66–92, 1978.

[29] Jogesh C. Pati and Abdus Salam. Unified Lepton-Hadron Symmetry and a Gauge Theory of the Basic Interactions. *Phys. Rev.*, D8:1240–1251, 1973.

[30] Harald Fritzsch and Peter Minkowski. Unified Interactions of Leptons and Hadrons. *Annals Phys.*, 93:193–266, 1975.

[31] Avadis Hacinliyan and Cihan Saclioglu. A List of Grand Unification Gauge Groups. *Phys. Rev.*, D19:2440, 1979.

[32] G. F. Giudice, C. Grojean, A. Pomarol, and R. Rattazzi. The Strongly-Interacting Light Higgs. *JHEP*, 0706:045, 2007, hep-ph/0703164.

[33] Scott Willenbrock and Cen Zhang. Effective Field Theory Beyond the Standard Model. 2014, 1401.0470.

[34] James Brau et al. ILC Reference Design Report: ILC Global Design Effort and World Wide Study. 2007, 0712.1950.

[35] D. M. Asner, T. Barklow, C. Calancha, K. Fujii, N. Graf, et al. ILC Higgs White Paper. 2013, 1310.0763.

[36] Gerald Aarons et al. International Linear Collider Reference Design Report Volume 2: Physics at the ILC. 2007, 0709.1893.

[37] E. M. Gregores, M. C. Gonzalez-Garcia, and S.F. Novaes. Discriminating new physics scenarios at NLC: The Role of polarization. *Phys.Rev.*, D56: 2920–2927, 1997, hep-ph/9703430.

[38] V.I. Telnov. Photon Collider Technology Overview. pages 73–82, 2009, 0908.3136.

[39] M. M. Muhlleitner and P. M. Zerwas. Elements of physics with a photon collider. *Acta Phys.Polon.*, B37:1021–1038, 2006, hep-ph/0511339.

[40] G. J. Gounaris, J. Layssac, and F. M. Renard. Signatures of anomalous couplings in boson pair production through gamma gamma collisions. *Z.Phys.*, C69:505–512, 1996, hep-ph/9505430.

[41] S. Abachi et al. Measurement of the $WW\gamma$ gauge boson couplings in $p\bar{p}$ collisions at $\sqrt{s} = 1.8$ TeV. *Phys.Rev.Lett.*, 75:1034–1039, 1995, hep-ex/9505007.

[42] S. Abachi et al. Measurement of the $ZZ\gamma$ and $Z\gamma\gamma$ couplings in $p\bar{p}$ collisions at $\sqrt{s} = 1.8$ TeV. *Phys.Rev.Lett.*, 75:1028, 1995, hep-ex/9503010.

[43] J. Alitti et al. Direct measurement of the W - gamma coupling at the CERN anti-p p collider. *Phys.Lett.*, B277:194–202, 1992.

[44] S. Abachi et al. Search for W boson pair production in $p\bar{p}$ collisions at $\sqrt{s} = 1.8$ TeV. *Phys.Rev.Lett.*, 75:1023–1027, 1995, hep-ex/9503012.

[45] Satendra Kumar and P. Poulose. Influence of anomalous VVH and VVHH on determination of Higgs self couplings at ILC. 2014, 1408.3563.

[46] Vernon Barger, Tao Han, Paul Langacker, Bob McElrath, and Peter Zerwas. Effects of genuine dimension-six Higgs operators. *Phys.Rev.*, D67:115001, 2003, hep-ph/0301097.

[47] J. Baglio, A. Djouadi, R. Gröber, M.M. Mühlleitner, J. Quevillon, et al. The measurement of the Higgs self-coupling at the LHC: theoretical status. *JHEP*, 1304:151, 2013, 1212.5581.

[48] G. S. Guralnik, C. R. Hagen, and T. W. B. Kibble. Global Conservation Laws and Massless Particles. *Phys.Rev.Lett.*, 13:585–587, 1964.

[49] Serguei Chatrchyan et al. Observation of a new boson with mass near 125 GeV in pp collisions at $\sqrt{s} = 7$ and 8 TeV. *JHEP*, 1306:081, 2013, 1303.4571.

[50] Georges Aad et al. Measurements of Higgs boson production and couplings in diboson final states with the ATLAS detector at the LHC. *Phys.Lett.*, B726:88–119, 2013, 1307.1427.

[51] Vardan Khachatryan et al. Observation of the diphoton decay of the Higgs boson and measurement of its properties. *Eur.Phys.J.*, C74(10):3076, 2014, 1407.0558.

[52] Georges Aad et al. Measurement of Higgs boson production in the diphoton decay channel in *pp* collisions at center-of-mass energies of 7 and 8 TeV with the ATLAS detector. *Phys.Rev.*, D90:112015, 2014, 1408.7084.

[53] Steven Weinberg. A Model of Leptons. *Phys.Rev.Lett.*, 19:1264–1266, 1967.

[54] Richard W. Schnee. Status of direct searches for WIMP dark matter. *AIP Conf.Proc.*, 903:8–15, 2007, astro-ph/0612565.

[55] Lars Bergstrom. Dark matter theory. *PoS*, EPS-HEP2011:012, 2011.

[56] Lars Bergstrom. Dark matter candidates: A status report. *AIP Conf.Proc.*, 1241:49–63, 2010.

[57] Lars Bergström. Cosmology and the Dark Matter Frontier. *Phys.Scripta*, T158:014014, 2013, 1309.7267.

[58] Andrew G. Cohen, A. De Rujula, and S. L. Glashow. A Matter - antimatter universe? *Astrophys.J.*, 495:539–549, 1998, astro-ph/9707087.

[59] Maxim Yu. Khlopov, Sergei G. Rubin, and Alexander S. Sakharov. Possible origin of antimatter regions in the baryon dominated universe. *Phys.Rev.*, D62:083505, 2000, hep-ph/0003285.

[60] K. M. Belotsky, Yu. A. Golubkov, M. Yu. Khlopov, R.V. Konoplich, and A.S. Sakharov. Antihelium flux signature for antimatter globular cluster in our galaxy. 1998, astro-ph/9807027.

[61] C. L. Bennett et al. First year Wilkinson Microwave Anisotropy Probe (WMAP) observations: Preliminary maps and basic results. *Astrophys.J.Suppl.*, 148:1–27, 2003, astro-ph/0302207.

[62] G. Gelmini and E. Roulet. Neutrino masses. *Rept.Prog.Phys.*, 58:1207–1266, 1995, hep-ph/9412278.

[63] M. C. Gonzalez-Garcia and Michele Maltoni. Phenomenology with Massive Neutrinos. *Phys.Rept.*, 460:1–129, 2008, 0704.1800.

[64] H. Aihara, T. Barklow, U. Baur, J. Busenitz, S. Errede, et al. Anomalous gauge boson interactions. 1995, hep-ph/9503425.

[65] Kaoru Hagiwara, R.D. Peccei, D. Zeppenfeld, and K. Hikasa. Probing the Weak Boson Sector in $e^+e^- \to W^+W^-$. *Nucl.Phys.*, B282:253, 1987.

[66] K. J. F. Gaemers and G. J. Gounaris. Polarization Amplitudes for $e^+e^- \to W^+W^- and e^+e^- \to ZZ$. *Z.Phys.*, C1:259, 1979.

[67] K. J. F. Gaemers and G. J. Gounaris. Bremsstrahlung Production of Higgs Bosons in e^+e^- Collisions. *Phys.Lett.*, B77:379, 1978.

[68] S Heinemeyer et al. Handbook of LHC Higgs Cross Sections: 3. Higgs Properties. 2013, 1307.1347.

[69] 1229968. Combined measurements of the mass and signal strength of the Higgs-like boson with the ATLAS detector using up to 25 fb^{-1} of proton-proton collision data. 2013.

[70] 1230214. Combination of standard model Higgs boson searches and measurements of the properties of the new boson with a mass near 125 GeV. 2013.

[71] C. P. Burgess, Stephen Godfrey, Heinz Konig, David London, and Ivan Maksymyk. Model independent global constraints on new physics. *Phys.Rev.*, D49:6115–6147, 1994, hep-ph/9312291.

[72] C. P. Burgess and David London. On anomalous gauge boson couplings and loop calculations. *Phys.Rev.Lett.*, 69:3428–3431, 1992.

[73] Tevatron Electroweak Working Group. 2012 Update of the Combination of CDF and D0 Results for the Mass of the W Boson. 2012, 1204.0042.

[74] Mathew Muether. Combination of CDF and DO results on the mass of the top quark using up to $8.7 fb^{-1}$ at the Tevatron. 2013, 1305.3929.

[75] Tevatron Electroweak Working Group. Combination of CDF and D0 results on the mass of the top quark using up to $9.7 fb^{-1}$ at the Tevatron. 2014, 1407.2682.

[76] S. Schael et al. Electroweak Measurements in Electron-Positron Collisions at W-Boson-Pair Energies at LEP. *Phys.Rept.*, 532:119–244, 2013, 1302.3415.

[77] S. Schael et al. Improved measurement of the triple gauge-boson couplings gamma W W and Z W W in e+ e- collisions. *Phys.Lett.*, B614:7–26, 2005.

[78] J. Abdallah et al. Measurements of CP-conserving Trilinear Gauge Boson Couplings WWV (V = gamma,Z) in e+e- Collisions at LEP2. *Eur.Phys.J.*, C66:35–56, 2010, 1002.0752.

[79] G. Abbiendi et al. Tests of the standard model and constraints on new physics from measurements of fermion pair production at 189-GeV to 209-GeV at LEP. *Eur.Phys.J.*, C33:173–212, 2004, hep-ex/0309053.

[80] M. Acciarri et al. Measurement of triple gauge boson couplings of the W boson at LEP. *Phys.Lett.*, B467:171–184, 1999, hep-ex/9910008.

[81] P. Achard et al. Measurement of triple gauge boson couplings of the W boson at LEP. *Phys.Lett.*, B586:151–166, 2004, hep-ex/0402036.

[82] C. J. C. Burges and Howard J. Schnitzer. Virtual Effects of Excited Quarks as Probes of a Possible New Hadronic Mass Scale. *Nucl.Phys.*, B228:464, 1983.

[83] Chung Ngoc Leung, S. T. Love, and S. Rao. Low-Energy Manifestations of a New Interaction Scale: Operator Analysis. *Z.Phys.*, C31:433, 1986.

[84] W. Buchmuller and D. Wyler. Effective Lagrangian Analysis of New Interactions and Flavor Conservation. *Nucl.Phys.*, B268:621–653, 1986.

[85] Roberto Contino, Margherita Ghezzi, Christophe Grojean, Margarete Muhlleitner, and Michael Spira. Effective Lagrangian for a light Higgs-like scalar. *JHEP*, 1307:035, 2013, 1303.3876.

[86] B. Grzadkowski, M. Iskrzynski, M. Misiak, and J. Rosiek. Dimension-Six Terms in the Standard Model Lagrangian. *JHEP*, 1010:085, 2010, 1008.4884.

[87] Adam Alloul, Benjamin Fuks, and Verónica Sanz. Phenomenology of the Higgs Effective Lagrangian via FEYNRULES. *JHEP*, 1404:110, 2014, 1310.5150.

[88] M. Baak, M. Goebel, J. Haller, A. Hoecker, D. Kennedy, et al. The Electroweak Fit of the Standard Model after the Discovery of a New Boson at the LHC. *Eur.Phys.J.*, C72:2205, 2012, 1209.2716.

[89] John Ellis, Veronica Sanz, and Tevong You. Complete Higgs Sector Constraints on Dimension-6 Operators. *JHEP*, 1407:036, 2014, 1404.3667.

[90] Benjamin W. Lee, C. Quigg, and H.B. Thacker. Weak Interactions at Very High-Energies: The Role of the Higgs Boson Mass. *Phys.Rev.*, D16:1519, 1977.

[91] B.L. Ioffe and Valery A. Khoze. What Can Be Expected from Experiments on Colliding e+ e- Beams with e Approximately Equal to $100 - GeV$. *Sov.J.Part.Nucl.*, 9:50, 1978.

[92] D.R.T. Jones and S.T. Petcov. Heavy Higgs Bosons at LEP. *Phys.Lett.*, B84:440, 1979.

[93] R.N. Cahn and Sally Dawson. Production of Very Massive Higgs Bosons. *Phys.Lett.*, B136:196, 1984.

[94] W Kilian, M Kramer, and P.M. Zerwas. Higgsstrahlung and W W fusion in e+ e- collisions. *Phys.Lett.*, B373:135–140, 1996, hep-ph/9512355.

[95] S. Dittmaier, M. Kramer, Y. Liao, M. Spira, and P.M. Zerwas. Higgs radiation off quarks in supersymmetric theories at e+ e- colliders. *Phys.Lett.*, B478:247–254, 2000, hep-ph/0002035.

[96] Sally Dawson, Andrei Gritsan, Heather Logan, Jianming Qian, Chris Tully, et al. Working Group Report: Higgs Boson. 2013, 1310.8361.

[97] Marcela S. Carena and Howard E. Haber. Higgs boson theory and phenomenology. *Prog.Part.Nucl.Phys.*, 50:63–152, 2003, hep-ph/0208209.

[98] J. Beringer et al. Review of Particle Physics (RPP). *Phys.Rev.*, D86:010001, 2012.

[99] Ties Behnke, James E. Brau, Philip N. Burrows, Juan Fuster, Michael Peskin, et al. The International Linear Collider Technical Design Report - Volume 4: Detectors. 2013, 1306.6329.

[100] Chris Adolphsen, Maura Barone, Barry Barish, Karsten Buesser, Philip Burrows, et al. The International Linear Collider Technical Design Report - Volume 3.II: Accelerator Baseline Design. 2013, 1306.6328.

[101] Chris Adolphsen, Maura Barone, Barry Barish, Karsten Buesser, Philip Burrows, et al. The International Linear Collider Technical Design Report - Volume 3.I: Accelerator & in the Technical Design Phase. 2013, 1306.6353.

[102] Howard Baer, Tim Barklow, Keisuke Fujii, Yuanning Gao, Andre Hoang, et al. The International Linear Collider Technical Design Report - Volume 2: Physics. 2013, 1306.6352.

[103] Ties Behnke, James E. Brau, Brian Foster, Juan Fuster, Mike Harrison, et al. The International Linear Collider Technical Design Report - Volume 1: Executive Summary. 2013, 1306.6327.

[104] Aharon Levy. CLICdp Overview: Overview of physics potential at CLIC. 2015, 1501.02614.

[105] K. Moning and J. Sekaric. *Eur. Phys. J C 38*, pages 427–436, 2005.

[106] Stanley J. Brodsky, Thomas G. Rizzo, and Ivan Schmidt. W Anomalous moments and the polarization asymmetry zero in $\gamma e \to W$ neutrino. *Phys.Rev.*, D52:4929–4935, 1995, hep-ph/9505441.

[107] Michael A. Doncheski, Stephen Godfrey, and K. Andrew Peterson. Single W boson production in high-energy $e\gamma$ collisions. 1997, hep-ph/9710299.

[108] Michael A. Doncheski, Stephen Godfrey, and K. Andrew Peterson. Measurement of the WWgamma coupling in the process egamma -gtnu qq bar off the W-boson resonance. *Phys.Rev.*, D59:117301, 1999.

[109] K. Ackerstaff et al. Measurement of triple gauge boson couplings from W^+W^- production at $S^{(1/2)}$ = 172-GeV. *Eur.Phys.J.*, C2:597–606, 1998, hep-ex/9709023.

[110] Eran Yehudai. Probing the $WW\gamma$ Vertex at a 1-tev e^+e^- Collider Using the Process $e\gamma \to W$ Neutrino. *Phys.Rev.*, D41:33, 1990.

[111] J. Alcaraz et al. A Combination of preliminary electroweak measurements and constraints on the standard model. 2006, hep-ex/0612034.

[112] V. M. Abazov et al. First study of the radiation-amplitude zero in $W\gamma$ production and limits on anomalous $WW\gamma$ couplings at $\sqrt{s}$ = 1.96- TeV. *Phys.Rev.Lett.*, 100:241805, 2008, 0803.0030.

[113] S. Atag and I. Sahin. Anomalous quartic WW gamma gamma and ZZ gamma gamma couplings in e gamma collision with initial beams and final state polarizations. *Phys.Rev.*, D75:073003, 2007, hep-ph/0703201.

[114] I. Sahin and A. A. Billur. Anomalous $WW\gamma$ couplings in $\gamma - p$ collision at the LHC. *Phys.Rev.*, D83:035011, 2011, 1101.4998.

[115] S. Y. Choi, J. S. Shim, H. S. Song, J. Song, and C. Yu. Single-photon events in e+ e- collisions. *Phys.Rev.*, D60:013007, 1999, hep-ph/9901368.

[116] Gilles Couture and Stephen Godfrey. Measurement of the W W gamma vertex through single photon production at e+ e- colliders. *Phys.Rev.*, D50: 5607–5612, 1994, hep-ph/9406257.

[117] J.A.M. Vermaseren. New features of FORM. 2000, math-ph/0010025.

[118] T. Hahn. CUBA: A Library for multidimensional numerical integration. *Comput.Phys.Commun.*, 168:78–95, 2005, hep-ph/0404043.

[119] Colin Kelley et al. Thomas Williams. Gnuplot. *http://www.gnuplot.info*.

[120] Georges Aad et al. Measurements of Higgs boson production and couplings in the four-lepton channel in pp collisions at center-of-mass energies of 7 and 8 TeV with the ATLAS detector. 2014, 1408.5191.

[121] Evidence for a particle decaying to W+W- in the fully leptonic final state in a standard model Higgs boson search in pp collisions at the LHC. (CMS-PAS-HIG-13-003), 2013.

[122] G. Moortgat-Pick, T. Abe, G. Alexander, B. Ananthanarayan, A.A. Babich, et al. The Role of polarized positrons and electrons in revealing fundamental interactions at the linear collider. *Phys.Rept.*, 460:131–243, 2008, hep-ph/0507011.

[123] H. Georgi. Effective field theory. *Ann.Rev.Nucl.Part.Sci.*, 43:209–252, 1993.

[124] Kaoru Hagiwara, S. Ishihara, R. Szalapski, and D. Zeppenfeld. Low-energy effects of new interactions in the electroweak boson sector. *Phys.Rev.*, D48: 2182–2203, 1993.

[125] Kaoru Hagiwara, R. Szalapski, and D. Zeppenfeld. Anomalous Higgs boson production and decay. *Phys.Lett.*, B318:155–162, 1993, hep-ph/9308347.

[126] S. Alam, S. Dawson, and R. Szalapski. Low-energy constraints on new physics revisited. *Phys.Rev.*, D57:1577–1590, 1998, hep-ph/9706542.

[127] Roberto Contino, Christophe Grojean, Mauro Moretti, Fulvio Piccinini, and Riccardo Rattazzi. Strong Double Higgs Production at the LHC. *JHEP*, 1005:089, 2010, 1002.1011.

[128] Roberto Contino. The Higgs as a Composite Nambu-Goldstone Boson. 2010, 1005.4269.

[129] R. Grober and M. Muhlleitner. Composite Higgs Boson Pair Production at the LHC. *JHEP*, 1106:020, 2011, 1012.1562.

[130] Martin B. Einhorn and Jose Wudka. The Bases of Effective Field Theories. *Nucl.Phys.*, B876:556–574, 2013, 1307.0478.

[131] F. Bonnet, M.B. Gavela, T. Ota, and W. Winter. Anomalous Higgs couplings at the LHC, and their theoretical interpretation. *Phys.Rev.*, D85:035016, 2012, 1105.5140.

[132] Tyler Corbett, O.J.P. Eboli, J. Gonzalez-Fraile, and M.C. Gonzalez-Garcia. Constraining anomalous Higgs interactions. *Phys.Rev.*, D86:075013, 2012, 1207.1344.

[133] We-Fu Chang, Wei-Ping Pan, and Fanrong Xu. Effective gauge-Higgs operators analysis of new physics associated with the Higgs boson. *Phys.Rev.*, D88(3):033004, 2013, 1303.7035.

[134] J. Elias-Miro, J.R. Espinosa, E. Masso, and A. Pomarol. Higgs windows to new physics through d=6 operators: constraints and one-loop anomalous dimensions. *JHEP*, 1311:066, 2013, 1308.1879.

[135] Shankha Banerjee, Satyanarayan Mukhopadhyay, and Biswarup Mukhopadhyaya. Higher dimensional operators and the LHC Higgs data: The role of modified kinematics. *Phys.Rev.*, D89(5):053010, 2014, 1308.4860.

[136] E. Boos, V. Bunichev, M. Dubinin, and Y. Kurihara. Higgs boson signal at complete tree level in the SM extension by dimension-six operators. *Phys.Rev.*, D89(3):035001, 2014, 1309.5410.

[137] Eduard Masso and Veronica Sanz. Limits on Anomalous Couplings of the Higgs to Electroweak Gauge Bosons from LEP and LHC. *Phys.Rev.*, D87 (3):033001, 2013, 1211.1320.

[138] Zhenyu Han and Witold Skiba. Effective theory analysis of precision electroweak data. *Phys.Rev.*, D71:075009, 2005, hep-ph/0412166.

[139] Tyler Corbett, O.J.P. Eboli, J. Gonzalez-Fraile, and M.C. Gonzalez-Garcia. Robust Determination of the Higgs Couplings: Power to the Data. *Phys.Rev.*, D87:015022, 2013, 1211.4580.

[140] Beranger Dumont, Sylvain Fichet, and Gero von Gersdorff. A Bayesian view of the Higgs sector with higher dimensional operators. *JHEP*, 1307: 065, 2013, 1304.3369.

[141] Alex Pomarol and Francesco Riva. Towards the Ultimate SM Fit to Close in on Higgs Physics. *JHEP*, 1401:151, 2014, 1308.2803.

[142] Hermes Belusca-Maito. Effective Higgs Lagrangian and Constraints on Higgs Couplings. 2014, 1404.5343.

[143] Rick S. Gupta, Alex Pomarol, and Francesco Riva. BSM Primary Effects. 2014, 1405.0181.

[144] Daniel Teyssier. LHC results and prospects: Beyond Standard Model. 2014, 1404.7311.

[145] A. De Rujula, M.B. Gavela, P. Hernandez, and E. Masso. The Selfcouplings of vector bosons: Does LEP-1 obviate LEP-2? *Nucl.Phys.*, B384:3–58, 1992.

[146] A. Gutierrez-Rodriguez, M.A. Hernandez-Ruiz, O.A. Sampayo, A. Chubykalo, and A. Espinoza-Garrido. The Triple Higgs Boson Self-Coupling at Future Linear e+e- Colliders Energies: ILC and CLIC. *J.Phys.Soc.Jap.*, 77:094101, 2008, 0807.0663.

[147] Yosuke Takubo. Analysis of Higgs Self-coupling with ZHH at ILC. 2009, 0907.0524.

[148] Junping Tian, Keisuke Fujii, and Yuanning Gao. Study of Higgs Self-coupling at ILC. 2010, 1008.0921.

[149] Marco Battaglia, Eduard Boos, and Wei-Ming Yao. Studying the Higgs potential at the e+ e- linear collider. *eConf*, C010630:E3016, 2001, hep-ph/0111276.

[150] Ryan Killick, Kunal Kumar, and Heather E. Logan. Learning what the Higgs boson is mixed with. *Phys.Rev.*, D88:033015, 2013, 1305.7236.

[151] A. Djouadi, W. Kilian, M. Muhlleitner, and P.M. Zerwas. Testing Higgs selfcouplings at e+ e- linear colliders. *Eur.Phys.J.*, C10:27–43, 1999, hep-ph/9903229.

[152] C. Castanier, P. Gay, P. Lutz, and J. Orloff. Higgs self coupling measurement in e+ e- collisions at center-of-mass energy of 500-GeV. 2001, hep-ex/0101028.

[153] Ramona Grober and Margarete Muhlleitner. Higgs pair production in the composite Higgs model. *PoS*, CORFU2011:021, 2011.

[154] Adam Alloul, Neil D. Christensen, Céline Degrande, Claude Duhr, and Benjamin Fuks. FeynRules 2.0 - A complete toolbox for tree-level phenomenology. *Comput.Phys.Commun.*, 185:2250–2300, 2014, 1310.1921.

[155] Fabio Maltoni and Tim Stelzer. MadEvent: Automatic event generation with MadGraph. *JHEP*, 0302:027, 2003, hep-ph/0208156.

[156] J. Alwall, R. Frederix, S. Frixione, V. Hirschi, F. Maltoni, et al. The automated computation of tree-level and next-to-leading order differential cross sections, and their matching to parton shower simulations. *JHEP*, 1407:079, 2014, 1405.0301.

[157] Johan Alwall, Pierre Artoisenet, Simon de Visscher, Claude Duhr, Rikkert Frederix, et al. New Developments in MadGraph/MadEvent. *AIP Conf.Proc.*, 1078:84–89, 2009, 0809.2410.

[158] Johan Alwall, Michel Herquet, Fabio Maltoni, Olivier Mattelaer, and Tim Stelzer. MadGraph 5 : Going Beyond. *JHEP*, 1106:128, 2011, 1106.0522.

[159] Celine Degrande, Claude Duhr, Benjamin Fuks, David Grellscheid, Olivier Mattelaer, et al. UFO - The Universal FeynRules Output. *Comput.Phys.Commun.*, 183:1201–1214, 2012, 1108.2040.

[160] I. F. Ginzburg, G. L. Kotkin, V. G. Serbo, and Valery I. Telnov. Colliding gamma e and gamma gamma Beams Based on the Single Pass Accelerators (of Vlepp Type). *Nucl.Instrum.Meth.*, 205:47–68, 1983.

[161] O. Kepka and C. Royon. Anomalous $WW\gamma$ coupling in photon-induced processes using forward detectors at the LHC. *Phys. Rev.*, D78:073005, 2008, 0808.0322.

[162] T. Jayaraman, G. Rajasekaran, and S. D. Rindani. VALIDITY OF THE EQUIVALENT PHOTON APPROXIMATION FOR THE PRODUCTION OF MASSIVE SPIN 1 PARTICLES. *Pramana*, 26:21–41, 1986.

[163] Florian Goertz, Andreas Papaefstathiou, Li Lin Yang, and José Zurita. Higgs boson pair production in the D=6 extension of the SM. 2014, 1410.3471.

Acronyms and Abbreviations

ALEPH	:	Apparatus for LEP PHysics
ALICE	:	A Large Ion Collider Experiment
ATLAS	:	A Toroidal LHC Apparatus
CDF	:	Collider Detector at Fermilab
CLIC	:	Compact Linear Collider
CMS	:	Compact Muon Solenoid
CL	:	Confidence Limit
CMF	:	Center-of-Mass Frame
DELPHI	:	Detector with Lepton-Photon and Hadron Identification
DM	:	Dark Matter
EFT	:	Effective Field Theory
EWSB	:	Electroweak Symmetry Breaking
FB	:	Forward Backward
FR	:	Feynman Rules
GeV	:	Giga electron Volt
ggF	:	gluon gluon Fusion
GUT	:	Grand Unified Theory
h.c.	:	Hermitian Conjugate
HEL	:	Higgs Effective Lagrangian
ILC	:	International Linear Collider
LEP	:	Large Electron-Positron Collider
LHC	:	Large Hadron Collider
LIA	:	Lorentz Invariant Amplitude
MG	:	Madevent Generator
MSSM	:	Minimal Supersymmetric Standard Model
NMSSM	:	Next-to-Minimal Supersymmetric Model
NWA	:	Narrow Width Approximation
OPAL	:	Omni-Purpose Apparatus for LEP

QCD	:	Quantum ChromoDynamics
QED	:	Quantum ElectroDynamics
QFT	:	Quantum Field Theory
SILH	:	Strongly Interacting Light Higgs
SLAC	:	Standford Linear Accelerator Center
SM	:	Standard Model
SSB	:	Spontaneous Symmetry Breaking
TeV	:	Tera electron Volt
TGC	:	Trilinear Gauge boson Couplings
2HDM	:	2 Higgs Doublet Model
VEV	:	Vacuum Expectation Value
VBF	:	Vector Bosons Fusion
UFO	:	Universal FeynRule Output
UV	:	Ultra Violet

Publications and Presentations

Publications

1. **Satendra Kumar and P. Poulose**, Pramana **79** (2012) 1247-1250.

2. **Satendra Kumar and P. Poulose**
XXI DAE-BRNS 2014 Proceedings (submitted).

3. **Satendra Kumar and P. Poulose**
(*Probing $WW\gamma$ coupling through $e^-\gamma \to \nu_e W^-$ at ILC*), arXiv:1501.01380v1 [hep-ph], submitted to EPJC.

4. **Satendra Kumar and P. Poulose**
(*Influence of anomalous VVH and VVHH on determination of Higgs self couplings at ILC*), arXiv:1408.3563v2 [hep-ph], submitted to PRD.

5. **Satendra Kumar, P. Poulose and Shibananda Sahoo**
(*Study of Higgs to gauge boson anomalous couplings through $e^-e^+ \to WWH$ at ILC*), Phys. Rev. D **91**, 073016 (2016), arXiv:1501.032831 [hep-ph].

Talks at Conferences

1. **2011 :** Lepton-Photon International Symposium 2011 at TIFR, Mumbai, India.

2. **2013 :** 20^{th} DAE-BRNS High Energy Physics Symposium 2013 held at Viswabharati University, Shantiniketan, India.

3. **2013 :** NC-HEPC 2013 National Conference on Contemporary Issues in HEP and Cosmology held at Gauahati University, Guwahati, India.

4. **2014 :** International Conference on New Trends in Field Theory, 2014, held at BHU, Varanasi, India.

5. **2014 :** 21^{th} DAE-BRNS High Energy Physics Symposium 2014 held at IIT Guwahati, Guwahati, India.

6. **2015 :** Asian Linear Collider Workshop 20-24 April 2015, KEK Tsukuba, Japan.

Schools and Workshops

1. **2010 :** SERC preparatory school in theoretical high energy physics, during Oct. 20 - Nov. 15, 2010, at BITs Goa, Goa, India.

2. **2011 :** Thinktank on physics@LHC 2011, during Dec. 05-09, 2011, Sariska, Rajasthan, India.

3. **2013 :** SERC main school in theoretical high energy physics, during Nov. 11 - 30, 2013, at IIT Kanpur, Kanpur, India.

4. **2014 :** Workshop on EWSB and flavours in the light of LHC, during Feb. 20 - 22, 2014, at IIT Guwahati, Guwahati, India.

Vitae

Mr. Satendra Kumar, born in Uttar Pradesh, India, received his B.Sc. degree with Mathematics and Physics as main subjects in 2006 from Y. D. College, Lakhimpur Kheri, Uttar Pradesh, and M.Sc. degree in Physics in 2008 from P. P. N. College, Kanpur, Uttar Pradesh. He joined IIT Guwahati for Ph.D. in 2009. He was awarded Junior Research Fellowship in 2009 and Senior Research Fellowship in 2011 by MHRD, India.